THE
PHYSICAL REVIEW
A Journal of Experimental and Theoretical Physics Established by E. L. Nichols in 1893
VOL. 58, NO. 9 NOVEMBER 1, 1940 SECOND SERIES

On the Production of Secondary Ionizing Particles by Non-Ionizing Agents in Cosmic Radiation

B. ROSSI,* L. JÁNOSSY, G. D. ROCHESTER AND M. BOUND
University of Manchester, Manchester, England
(Received September 4, 1940)

Previous experiments have shown that the number of coincidences recorded with a vertical counter arrangement is a few percent larger when some absorber is placed above the counters than with the same absorber between them. The effect is also present when the experimental conditions are such as to exclude the possibility of its being due to shower-production by photons. It had been, therefore, ascribed either to penetrating non-ionizing particles (neutrons, neutrettos) producing ionizing secondary rays, or to ordinary photons producing penetrating secondary particles (mesotrons). The present experiments show that a minor part, if any, of the observed influence of the position of the absorber can be due to the above processes. The major part of it arises from the interference of already known phenomena like scattering, knock-on showers, showers from the air, etc. This conclusion refers only to experiments performed near sea level.

I. INTRODUCTION

SEVERAL authors[1–6] have investigated the production of secondary particles by the non-ionizing component of cosmic rays with counter arrangements, which are, in principle, similar to those represented in Fig. 1. Two or more counters were placed vertically one above the other and the coincidences were recorded with an absorber s either above the whole system of counters (position s_1) or between the counters (position s_2). The counting rate was generally found to be larger in the former than in the latter position. This is what one would expect if ionizing particles were produced in s by non-ionizing agents.

When the absorber s has a comparatively small thickness and no other absorbers are present between the counters, the effect can easily be accounted for by cascade showers produced by photons. When, however, the absorber is thick enough to absorb the soft component of cosmic rays completely, the above interpretation is inadequate and, if the effect is to be accounted for by non-ionizing rays producing ionizing particles in the absorber, one must assume that either (a) the primary ionizing rays are more penetrating than photons (neutrons, "neutrettos,"[7] or (b) the secondary ionizing particles are more penetrating than electrons (mesotrons). If, finally, a difference is found by changing absorber s from s_1 to s_2, with an additional thick absorber S permanently between

* Now at Cornell University, Ithaca, New York.
[1] B. Rossi, Zeits. f. Physik **68**, 64 (1931).
[2] D. S. Hsiung, Phys. Rev. **46**, 653 (1934).
[3] H. Maass, Ann. d. Physik **27**, 507 (1936).
[4] M. Schein and V. C. Wilson, Phys. Rev. **54**, 304 (1939).
[5] F. R. Shonka, Phys. Rev. **55**, 24 (1939).
[6] M. Schein, W. P. Jesse and E. O. Wollan, Phys. Rev. **57**, 847 (1940).

[7] The possibility that "neutrettos," or neutral mesotrons, may be present in the cosmic radiation was first mentioned by N. Arley and W. Heitler [Nature **142**, 158 (1938)]. See also reference 5.

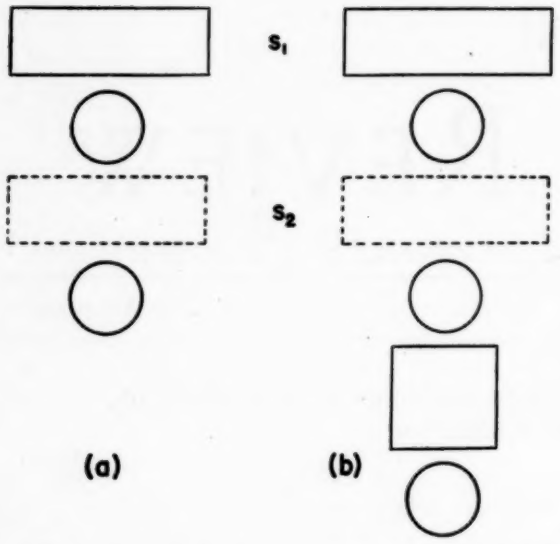

FIG. 1. Schematic arrangement of counters and absorbers for investigating the production of ionizing particles by non-ionizing rays.

the counters (see Fig. 1(b)), only hypothesis (b) is apparently left as a possible explanation.

As a matter of fact, the production of mesotrons by non-ionizing rays is the most likely interpretation of the large effects recently found by Schein and Wilson and by Schein, Jesse and Wollan in the high atmosphere with an arrangement similar to that represented in Fig. 1(b).[4,6] As for the much smaller differences found near sea level, however, the possibility cannot be ruled out that some spurious effects might have played an important role. We think especially of the following phenomena which have not always been taken adequately into consideration.

(c) *Knock-on showers.*—These contribute a number of extra counts, which is larger when s is in the upper than when it is in the lower position. This effect is likely to have influenced, for instance, the results of Rossi's experiments.[1]

(d) *Scattering.*—When the absorber is in the lower position an appreciable number of mesotrons may be removed from the beam by scattering. The scattering is much less effective when the absorber is above the counters for, in this case, the number of particles scattered out of the beam is approximately equal to the number of those scattered in. The effect of scattering depends largely upon the geometrical conditions and may have been quite appreciable, for instance, in the experiments of Maass.[3]

(e) *Side showers.*—Showers coming from the side, i.e., from the air or from whatever dense material may be present near the counters, give rise to coincidences, the number of which is likely to depend upon the position of s.

The purpose of the experiments described in the present paper is to determine whether the production of ionizing particles by non-ionizing rays (hypotheses (a) or (b)), or some more obvious effects (hypotheses (c), (d) or (e)) are responsible for the influence of the position of the absorber on the counting rate of a vertical counter arrangement near sea level.

II. EXPERIMENTAL ARRANGEMENTS

Part of the experiments were carried out with a set of nine Geiger-Müller counters, arranged as represented in Fig. 2. The five counters A and, similarly, the two counters D were connected in parallel. Counters A covered the full solid angle subtended by counters B, C, and D. Fourfold coincidences ($ABCD$) and threefold coincidences (BCD) were recorded simultaneously. Threefold coincidences (BCD) not accompanied by fourfold coincidences ($ABCD$) will be called *anticoincidences* ($BCD-A$). The arrangement is similar to that used by Jánossy and Rossi for investigating the photon component of cosmic rays.[8]

Some experiments were also performed with the arrangement represented in Fig. 3. The six counters A were connected in parallel and covered the whole solid angle subtended by counters B, C and D. The lead absorber Σ above the counters was 5.3 cm thick. The cloud chamber Ch was operated by anticoincidences ($BCD-A$), i.e., an expansion took place whenever a coinci-

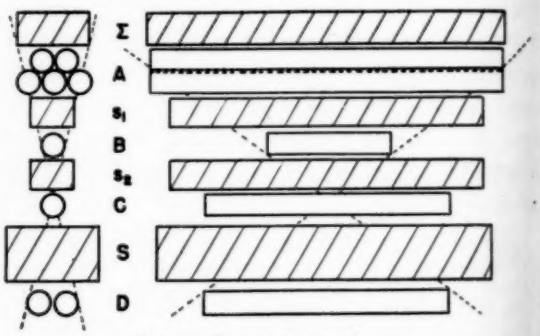

FIG. 2. Counter experiment.

[8] L. Jánossy and B. Rossi, Proc. Roy. Soc. 175, 88 (1940).

dence (BCD) occurred, which was not accompanied by a discharge in one of the counters A.

The anticoincidences were selected with the circuit represented in Fig. 4. The positive pulses from the output of an ordinary coincidence circuit connected with counters B, C and D set off the discharges of the thyratron T_1, while the pulses from a single stage amplifier connected with the counter battery A set off the discharges of the thyratron T_2. The pulses arising from the discharges of the thyratrons were transformed by the successive stages, as schematically represented in Fig. 5. Since the grid of V_2 was normally kept at a negative potential, a discharge of T_1 not accompanied by a discharge of T_2 gave rise to a positive pulse at the output of the anticoincidence circuit. When, however, T_1 and T_2 were discharged simultaneously, V_2 became conducting *before* the negative pulse from T_1 reached the grid of V_1', and resumed its initial nonconducting condition when this pulse was already over. Thus, the coincidence pulse could not be transmitted to the output.

The efficiency of the counter battery A was shown by control experiments to be greater than 99 percent in both arrangements. The anticoindidence circuit itself had 100 percent efficiency.

III. Search for Penetrating Particles Produced by Non-Ionizing Rays

In order to investigate whether penetrating ionizing particles are produced by non-ionizing rays (hypothesis (b)) measurements were taken with the counter arrangement represented in Fig. 2. A lead absorber 10 cm thick was permanently placed between C and D (position S), while a lead screen s, 5 cm thick, was placed alternately above counter B (position s_1) or between counters B and C (position s_2). No absorber was present above the counter battery A. Since 10 cm of lead are sufficient to stop the electron component of cosmic rays, a threefold coincidence (BCD) could only be produced by a penetrating particle. The experimental results are collected in Table I.

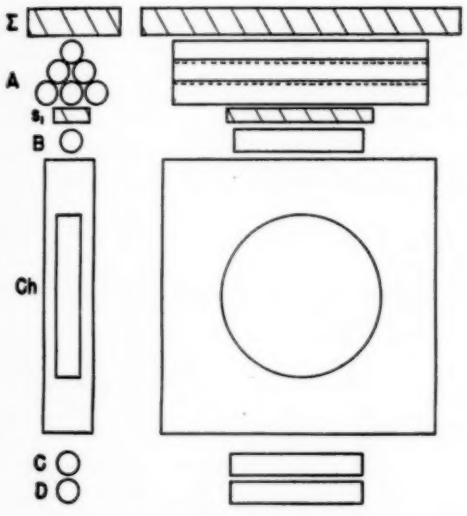

Fig. 3. Cloud-chamber experiment.

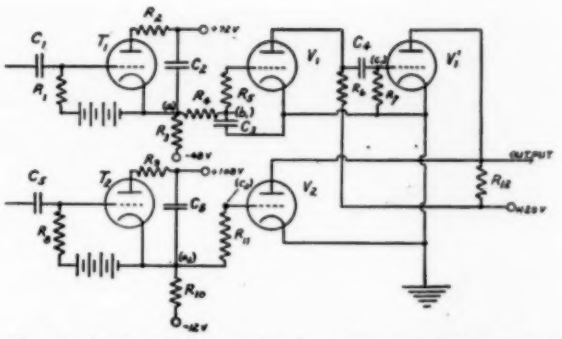

Fig. 4. Anticoincidence circuit. $R_1=R_8=0.2\text{M}\Omega$; $R_2=R_9=200\Omega$; $R_3=R_{10}=0.1\text{M}\Omega$; $R_4=1\text{M}\Omega$; $R_5=R_{11}=2\text{M}\Omega$; $R_6=R_7=2\text{M}\Omega$; $R_{12}=1\text{M}\Omega$; $C_1=C_5=0.0001\mu\text{f}$; $C_2=C_6=0.005\mu\text{f}$; $C_3=0.0005\mu\text{f}$; $C_4=0.01\mu\text{f}$.

Considering first the threefold coincidences (BCD) alone, it appears that their number is 1.6 ± 0.5 percent larger with the lead in s_1 than with the lead in s_2. This difference is of the same order of magnitude as that found by other authors under similar conditions, and could be interpreted as due to non-ionizing rays, like photons, producing in s penetrating ionizing particles like mesotrons. According to this assumption, however, the same difference which is found for the number of coincidences (BCD) should also be expected for the number of anticoincidences ($BCD-A$). On the contrary, the increase of anticoincidences ($BCD-A$) when the lead is moved from s_2 to s_1 is 8 times smaller than the increase of coincidences (BCD). We conclude that only a minor part, if any, of the 1.6 percent effect for threefold coincidences can be accounted for by the production of penetrating ionizing particles in the absorber s. The major part of it must be due to some disturbing phenomena like those described under (c), (d) and (e). For instance, with the lead in s_1, a

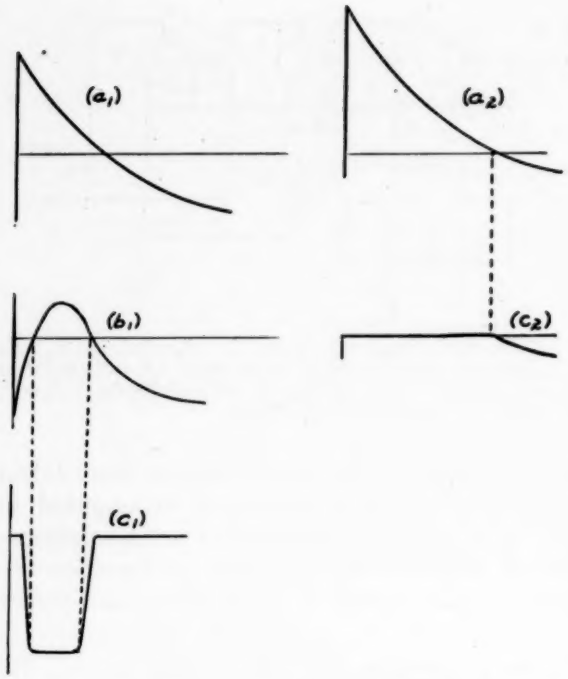

FIG. 5. Shape of the pulses at different points of the anticoincidence circuit Fig. 4.

mesotron traversing C, D and missing B can still give rise to a coincidence (BCD) by producing in s_1 a "knock-on" shower which discharges B. This, of course, cannot happen when the lead is in s_2. The effect of "knock-on" showers does not show when only anticoincidences ($BCD-A$) are recorded, because every particle going through the absorber s_1 and one of the counters D must also traverse one of the anticoincidence counters A.

TABLE I. *Arrangement Fig. 2. $S=10$ cm* Pb, $\Sigma=0$ *(s_1 and s_2 are in cm* Pb. *The errors are the standard statistical deviations).*

	TOTAL COUNTS		COUNTS PER HOUR			
	(a) $s_1=5$ $s_2=0$	(b) $s_1=0$ $s_2=5$	(a) $s_1=5$ $s_2=0$	(b) $s_1=0$ $s_2=5$	(a)−(b) C. PER HOUR	(a)−(b) % OF (BCD)
Coincidences (BCD)	87029	79359	328.8 ±1.1	323.5 ±1.2	5.3 ±1.6	1.6 ±0.5
Anticoincidences ($BCD-A$)	963	730	3.64 ±0.12	2.97 ±0.11	0.67 ±0.16	0.20 ±0.05

IV. SEARCH FOR IONIZING PARTICLES PRODUCED BY PENETRATING NON-IONIZING RAYS

The experiments referred to in the foregoing section show that no appreciable number of *penetrating* ionizing particles are generated by non-ionizing rays at sea level. In order to investigate whether *soft* ionizing particles (electrons) are generated by *penetrating* non-ionizing rays (hypothesis (a)), the counter arrangement represented in Fig. 2 was used again, with the only change that the absorber S was removed and a 5-cm thick lead absorber was placed above the counter battery A (position Σ). Under these conditions, photons coming from above cannot produce anticoincidences, since they have a negligibly small probability of traversing Σ without starting a shower which discharges A.[8] A penetrating non-ionizing agent, however, is likely to traverse Σ without encounter, and it can then give rise to an anticoincidence by producing a secondary ionizing particle in s_1.

Measurements were performed (a) with 5 cm of lead in s_1 and nothing in s_2, (b) with 5 cm of lead in s_2 and nothing in s_1, and (c) with no lead either in s_1 or in s_2. The experimental results are given in Table II.

The differences in the number of coincidences (BCD) are not very significant. The anticoincidences ($BCD-A$), however, are distinctly more frequent with the lead in s_1 than with the lead in s_2 or even than with no lead at all. This result is in agreement with hypothesis (a), but

TABLE II. *Arrangement Fig. 2. $S=0$, $\Sigma=5$ cm* Pb *(s_1 and s_2 are in cm* Pb. *The errors are the standard statistical deviations).*

	TOTAL COUNTS			COUNTS PER HOUR						
	(a) $s_1=5$ $s_2=0$	(b) $s_1=0$ $s_2=5$	(c) $s_1=0$ $s_2=0$	(a) $s_1=5$ $s_2=0$	(b) $s_1=0$ $s_2=5$	(c) $s_1=0$ $s_2=0$	(a)−(b) C. PER HOUR	(a)−(b) % OF (BCD)	(a)−(c) C. PER HOUR	(a)−(c) % OF (BCD)
Coincidences (BCD)	32110	28049	37681	350 ±2	347 ±2	366 ±2	3 ±2.8	0.86 ±0.80	−16 ±2.8	−4.6 ±0.8
Anticoincidences ($BCD-A$)	620	316	587	6.75 ±0.27	3.90 ±0.22	5.70 ±0.25	2.85 ±0.35	0.8 ±0.1	1.05 ±0.37	0.3 ±0.1

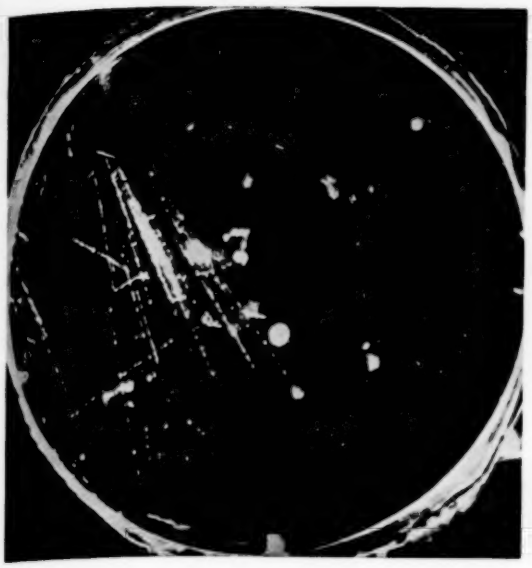

FIG. 6. Shower from the lead.

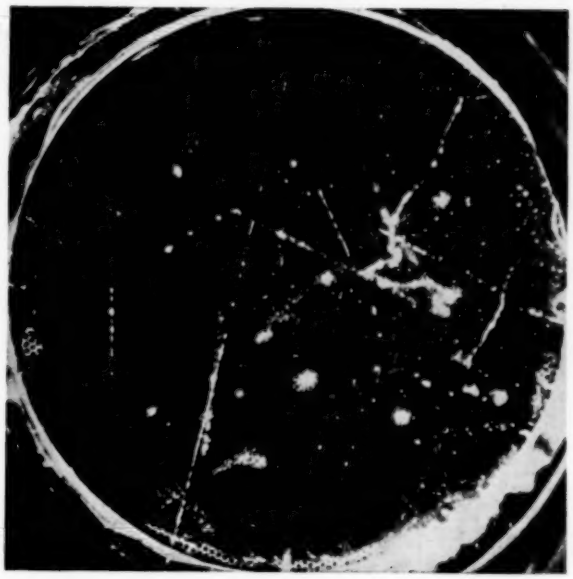

FIG. 7. Single particle accompanied by side shower.

could also be explained by the interference of some spurious effect.

In order to have some more definite information as to the origin of the observed differences, the arrangement represented in Fig. 3 was used. First, as a preliminary experiment, anticoincidences $(BCD-A)$ were recorded with and without a 1.5-cm thick lead absorber above counter B (position s_1). The results are given in Table III. In agreement with the previous results, the presence of the lead absorber between A and B was found to increase the number of anticoincidences. In the main experiment the anticoincidences $(BCD-A)$ were made to operate the cloud chamber *Ch*. A survey of the stereoscopic photographs obtained showed the results summarized in Table IV. The photographs are grouped under three main headings, namely, "blanks," i.e., no tracks due to cosmic-ray particles, "singles," i.e., one particle through B, C and D, and "showers," i.e., several associated particles. The "showers" are further subdivided into "showers from the lead," i.e., showers radiating from s_1, see Fig. 6, and "side showers," i.e., several particles crossing the chamber, presumably due to showers originating in the back of the cloud chamber, in the air, or in the walls of the building. Occasionally "side showers" occur with "singles" as shown in Fig. 7.

The "blanks" are equally frequent with and without the lead screen in s_1, and are mainly to be accounted for by chance coincidences between counters B, C and D. More than half of the remaining pictures exhibit showers coming from the side. All of these pictures and, possibly, some of the "blanks" are due to anticoincidences produced by side showers which discharge counters B, C and D without striking the counter battery A. The probability of such an

TABLE III. *Arrangement Fig. 3.* $\Sigma = 5.3$ *cm* Pb (s_1 *is in cm* Pb; *the errors are the standard statistical deviations*).

	TOTAL COUNTS		COUNTS PER HOUR		
	(a) $s_1=1.5$	(c) $s_1=0$	(a) $s_1=1.5$	(c) $s_1=0$	(a)−(c)
Anticoincidences $(BCD-A)$	151	82	0.70 ±0.06	0.35 ±0.04	0.35 ±0.07

TABLE IV. *Arrangement Fig. 3.* $\Sigma = 5.3$ *cm* Pb. *Cloud chamber operated by the anticoincidences* $(BCD-A)$. *For easier comparison of the data obtained with* $s_1=0$ *and* $s_1=1.5$ *cm* Pb, *the numbers of the events recorded in the first condition have been reduced to account for the difference in the time of observation (numbers in parenthesis).*

ABS. CM Pb	TIME (HR.)	PHOTOGRAPHS	BLANKS	SINGLES	SHOWERS		
					SIDE	Pb	TOTAL
$s_1=0$	136.15	58 (54)	29 (27)	8 (7.5)	21 (20)	0	21 (20)
$s_1=1.5$	127.42	89	29	19	30	11	41

event is apparently increased by the lead in s_1, since anticoincidences accompanied by side showers are more frequent with than without lead. This can be explained by the multiplication of shower particles in the lead.

Most of the "singles" observed without lead are probably due to a small lack of efficiency of the counter battery A. The "singles" obtained with lead in s_1 are more frequent than without lead, so that only part of them may be accounted for by lack of efficiency. The rest of the "singles" under lead and the "showers from the lead" are apparently due to secondary effects produced in the lead either by penetrating non-ionizing rays traversing the absorber Σ without encounter, or by photons missing the absorber Σ, or by electrons missing both the absorber Σ and the counter battery A. There is little doubt that the "singles" accompanied by side showers (see Fig. 7) are the result of secondary effects of electrons or photons. This is likely to be the case also for the remainder of the pictures, so that we do not find in our photographs any conclusive evidence for the existence of penetrating non-ionizing particles in the cosmic radiation. Furthermore these photographs show that most of the anticoincidences are due to spurious effects, especially to showers coming from the side.

The present experiments were initiated in the spring of 1939 in the Physical Laboratory of the University of Manchester, England, and were completed after the departure of the first-named author (B. R.) during the summer of the same year. The publication has been delayed by the recent European events. The writers express their appreciation to Professor P. M. S. Blackett for the facilities made available and for helpful discussions of the problem. One of us (B. R.) acknowledges with thanks the financial support granted to him by the Society for the Protection of Science and Learning.

NOVEMBER 1, 1940 PHYSICAL REVIEW VOLUME 58

The Mean Lifetime of the Mesotron from Electroscope Data

H. V. NEHER AND H. G. STEVER
Norman Bridge Laboratory of Physics, California Institute of Technology, Pasadena, California

(Received August 16, 1940)

In order to eliminate some experimental difficulties found in detecting the mesotron decay with Geiger counter apparatus, an experiment which consisted of the measurement of cosmic-ray intensity at various depths in two lakes of widely different altitude but of the same geomagnetic latitude was performed. One of our self-recording electroscopes which has been used in other cosmic-ray work was used. In the higher lake, about 12,000 ft. above the lower, readings were taken at depths of 4.9, 5.9 and 6.9 meters and in the lower lake at 1.3, 2.3 and 3.3 meters, the difference in depth being about equal in mass to the air between the lakes. On the basis of the most recent theory, air and water were assumed to be gram for gram equivalent absorbers for the mesotrons involved. The ratio of intensities at equivalent points in the two lakes was theoretically calculated and by matching this with the observed ratios a mean rest lifetime, τ_0, of 2.8×10^{-6} sec. was found for a rest mass of 160 times that of the electron.

I. INTRODUCTION

AT the Cosmic-Ray Symposium during the summer of 1939, B. Rossi[1] summarized the then existing evidence for the postulated decay of the mesotron. He pointed out that the temperature effect and the greater absorption of air compared with more dense materials resulted in a mean rest life of the order of 3.0×10^{-6} sec. Other experimental facts gave no evidence for mesotron disintegration although they were not contrary to such a theory. At that time no experiments showed that the mesotron was beta-radioactive. It was concluded that the disintegration evidence was incomplete.

Since the Symposium a number of experiments have been designed specifically to detect the

[1] B. Rossi, Rev. Mod. Phys. **11**, 296 (1939).

mesotron decay and to measure its mean rest life. As the first direct evidence that the mesotron was beta-radioactive, Williams and Roberts[2] published a cloud-chamber photograph of a positive mesotron at the end of its range emitting a positron with energy approximately half the rest energy of the mesotron. The mesotron lifetime obtained from the temperature effect is in the same range as the value from other experiments although the effect is not as clear. Blackett[3] first explained the negative temperature effect by assuming the formation level of the mesotrons is extended upwards for a warmer atmosphere so that there was a greater time for decay before reaching sea level. This view has been furthered by other observers although recently Hess[4] in analyzing five years of electroscope data concluded that the normal negative temperature effect was not completely explainable on the mesotron disintegration hypothesis.

The anomalous absorption of cosmic rays reported by Ehmert[5] and others, which was explained by Euler and Heisenberg[6] by the mesotron decay hypothesis, has been considerably investigated. Most results of this method lead to a mean lifetime of 2.6×10^{-6} sec. or higher. Rossi, Hilberry and Hoag[7] reported a lower value of 2.0×10^{-6} sec. for a mesotron rest mass of 160 times the electron rest mass. Fermi, in a pre-publication letter,[8] thought that the anomalous absorption could be explained by a correction in the absorption theory rather than by mesotron decay. When the effect of the field of the ionizing particle on surrounding electrons was taken into account the energy loss in dense materials was lessened. The order of magnitude of that correction was the same as that used to indicate mesotron decay. However, when the complete analysis[9] was published, Fermi indicated that only half or less of the anomalous absorption could be accounted for by this polarization effect.

All previous experiments to obtain the mesotron lifetime employed the Geiger counter cosmic-ray telescope as recording mechanism to compare the absorption of mesotrons in more dense materials such as lead, carbon, earth, to the absorption in air. In order to eliminate some of the corrections and inherent difficulties in Geiger counter measurements such as the correction for showers produced in the more dense absorber and the increased shower production in the air at higher altitudes, Professor J. R. Oppenheimer suggested the present experiment. The object was to compare the mesotron absorption in air and water by highly accurate electroscope data. For all points of measurement, the electroscope was surrounded by the same medium, water. Care was taken at all times to preserve the symmetry of the surroundings of the instrument.

Examining past experiments which compared the cosmic-ray absorption of air and water, those of Millikan and Cameron[10,11] stand out. In the first of these experiments, in 1926, these experimenters compared absorption curves in Arrowhead and Muir lakes with an altitude difference of about 2040 meters. The slight discrepancies from the mass absorption law for air and water were within the experimental error. In 1928, using more accurate pressure electroscopes, Millikan and Cameron performed a similar experiment in Arrowhead and Gem lakes, with an altitude difference of only 1200 meters. In this latter experiment the mass absorption law was found to hold.

II. Experimental Work

The experiment herein reported consisted in measurement of cosmic-ray intensities at various depths in two lakes of widely differing altitude. The intensities were measured by an accurate recording electroscope of the type used and described by Millikan and Neher.[12] Lake Tulainyo at 3921 meters above sea level was the higher lake and Kerchkoff Reservoir at 305 meters was the lower lake. These were chosen

[2] E. J. Williams and G. E. Roberts, Nature **145**, 102 (1940).
[3] P. M. S. Blackett, Phys. Rev. **54**, 973 (1938).
[4] V. F. Hess, Phys. Rev. **57**, 781 (1940).
[5] A. Ehmert, Zeits. f. Physik **106**, 751 (1937).
[6] H. Euler and W. Heisenberg, Ergeb. d. exakt. Naturwiss. (1938).
[7] B. Rossi, N. Hilberry and J. B. Hoag, Phys. Rev. **57**, 461 (1940).
[8] E. Fermi, Phys. Rev. **56**, 1242 (1939).
[9] E. Fermi, Phys. Rev. **57**, 485 (1940).
[10] R. A. Millikan and G. H. Cameron, Phys. Rev. **28**, 851 (1926).
[11] R. A. Millikan and G. H. Cameron, Phys. Rev. **31**, 921 (1928).
[12] R. A. Millikan and H. V. Neher, Phys. Rev. **50**, 15 (1936).

for their low horizon which was about 82° from the vertical in both cases. Since the intensity falls off approximately as $\cos^2\theta$, it is clear that not more than a small fraction of a percent of the total intensity was lost in either lake. Both lakes were at approximately 43° north geomagnetic latitude, well above the equatorial dip, and within 70 miles of each other longitudinally so that no difference of intensity due to the earth's magnetism entered. The instrument was placed well away from shore and from the bottom of the lakes. In Kerchkoff, measurements were made at depths 1.31, 2.31, and 3.31 meters below the surface; in Tulainyo at 4.88, 5.88, and 6.88 meters. The readings were taken first in Kerchkoff and then in Tulainyo after which the Kerchkoff readings were repeated. Table I gives a summary of the results. N, the number of ions per cubic centimeter per second, has been corrected for barometric pressure variation and for residual radioactivity of the instrument. The instrument had a negligible temperature coefficient for the range of temperatures encountered. Each N is an average of about 14 discharges of the electroscope which corresponds to 24 hours of measurement. The probable error of each reading was computed from the deviation from the mean of these 14 discharges. The 3.57 meters of water difference in depth of reading in the lakes corresponds approximately in stopping power to the 3.62×10^5-cm column of air at an average density 0.00094 g/cm³. In Fig. 1, the logarithm of N is plotted against the total absorber, both air and water, in meters of water equivalent. Air and water are taken as gram for gram equivalent in stopping power.

TABLE I. *Corrected readings for both lakes.*

Date	Lake Altitude in meters	Depth in Lake in meters	Total Absorber in M H_2O	Ions/cc/sec. N
Sept. 1	Kerchkoff	1.31	11.29	2.209±0.014
2	305	2.31	12.29	1.938±0.007
3		3.31	13.29	1.736±0.009
9	Tulainyo	4.88	11.38	2.501±0.007
10	3921	5.88	12.38	2.217±0.007
11		6.88	13.38	1.982±0.002
17	Kerchkoff	1.32	11.30	2.242±0.007
18	305	2.32	12.30	1.936±0.007
19		3.32	13.30	1.747±0.007

III. Relative Mesotron Stopping Power of Air and Water

Previous to the recent modification of the absorption theory by Fermi,[9] the energy loss per unit path in an absorber of n electrons per cubic centimeter by a high energy mesotron of energy E and velocity $v=\beta c$ was given by the Bethe-Bloch formula,[13,14]

$$-\frac{dE}{dy}=\frac{2\pi ne^4}{m_e c^2\beta^2}\operatorname{Log}\frac{m_e c^2\beta^2 W}{(13.5Z)^2(1-\beta^2)}, \quad (1)$$

where m_e is the rest mass of the electron and e is the electronic charge. W is the maximum energy which may be imparted to an electron in a direct collision with a mesotron of mass m.

$$W=\frac{E+2mc^2}{1+m_e c^2(1+m/m_e)^2/2E}.$$

Fermi subtracts from (1)

$$\frac{2\pi ne^4}{m_e c^2\beta^2}\operatorname{Log}\epsilon \quad \text{for} \quad \beta<\frac{1}{\sqrt{\epsilon}} \quad (2)$$

or

$$\frac{2\pi ne^4}{m_e c^2\beta^2}\left[\operatorname{Log}\frac{\epsilon-1}{1-\beta^2}+\frac{1-\epsilon\beta^2}{\epsilon-1}\right] \quad \text{for} \quad \beta>\frac{1}{\sqrt{\epsilon}}, \quad (3)$$

where ϵ is the effective dielectric constant for the polarization effect.

From the Bethe-Bloch formula, the ratio of the energy loss in one gram of air per square centimeter to the loss in a similar amount of water is about 0.9. When, however, the Fermi correction is applied to the case of water the ratio of energy losses is just 1.0 if an average mesotron energy of a few Bev and the value given by Fermi for ϵ are used. From these considerations it is concluded that points in the two lakes under equal masses of absorbing materials may be compared in intensity, the difference of intensity being just due to the mesotrons which have decayed in the 3.62×10^5-cm air column.

IV. Theory of Mean Lifetime Determination and Application to Experimental Results

Consider high energy mesotrons of velocity, $v=\beta c$, where $\beta\approx1$. In the coordinate system

[13] H. Bethe, *Handbuch der Physik*, Vol. 24, p. 1.
[14] F. Bloch, Zeits. f. Physik **81**, 363 (1933).

stationary with respect to the earth, the energy is given by $E=kmc^2$ where $k=1/(1-\beta^2)^{\frac{1}{2}}$ and the mean lifetime is $\tau=k\tau_0$ where τ_0 is the mean rest lifetime of the mesotron. Let P be the probability that a particle will survive for a time t so that the probability for disintegration in the time interval t to $t+dt$ is

$$-dP=Pdt/\tau. \tag{4}$$

For a mesotron incident at any angle θ from the vertical and having an energy, $E=kmc^2$, at $y=0$, where y is the vertical distance measured downward, with a uniform loss of energy, imc^2, per unit path, (4) may be written

$$-dP=\frac{Pdt}{\tau_0(k-iy\sec\theta)}=\frac{Pdy}{\beta c\tau_0(k/\sec\theta-iy)}. \tag{5}$$

Integrating (5) from $y=0$ to $y=y_0$, the probability, $P(E,\theta)$, that the mesotron will reach a vertical distance y_0 below $y=0$ is

$$P(E,\theta)=\left[\frac{E-imc^2y_0\sec\theta}{E}\right]^{1/i\beta c\tau_0}. \tag{6}$$

It is important to note that $P(E,\theta)=P(E',0)$ where $E'=E/\sec\theta$ or in words the probability that a particle of energy, E, traveling at an angle θ will reach a vertical distance, y_0, downward is the same as the probability that a particle of energy, $E/\sec\theta$, traveling vertically will reach y_0.

Assume that the energy distribution, $f(E)$, is of the form, B/E^γ for mesotrons above some minimum energy. This is a valid assumption for Blackett's[15] energy distribution curve at sea level is of that form with γ between 2 and 3. The total intensity incident at an angle θ at y_0 is

$$J_{y_0}(\theta)=\int_{E_0}^{\infty}P(E,\theta)\frac{B}{E^\gamma}dE, \tag{7}$$

where E_0 is the energy just sufficient to penetrate the air column and the layer of water above the instrument in the lower lake. By inserting a new variable $E'=E/\sec\theta$ in (7) it is seen that

$$J_{y_0}(\theta)=(\cos\theta)^{\gamma-1}J_{y_0}(0). \tag{8}$$

This last result shows that the total intensity,

[15] P. M. S. Blackett, Proc. Roy. Soc. **159**, 1 (1937).

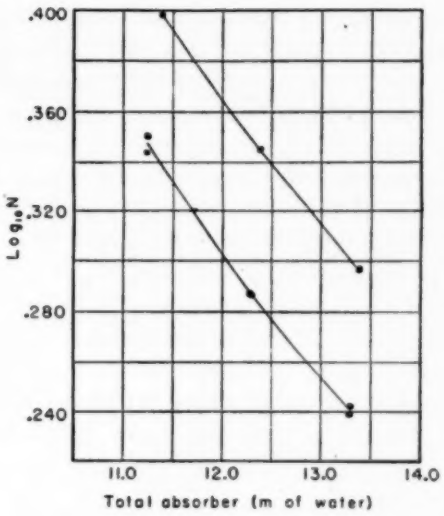

FIG. 1. The logarithm of N, the number of ions per cubic centimeter per second, is plotted against the total absorbing matter from the top of the atmosphere to the electroscope expressed in meters of water equivalent. The upper curve represents the absorption in the upper lake (elevation 3921 meters); the lower curve is the curve for the lower lake (elevation 305 meters).

N_{y_0}, which is the integral of (8) over the hemispherical solid angle, is just proportional to the vertical intensity, the constant of proportionality being the same for all y_0. With that in mind, the ratio of intensities at points in the two lakes under equal total absorber may be written

$$N_u/N_L=\int_{E_0}^{\infty}f(E)dE\Big/\int_{E_0}^{\infty}P(E,0)f(E)dE. \tag{9}$$

Since the energy distribution, $f(E)$, for the upper lake is not known, it is necessary to write an expression similar to (9) for the lower lake where Blackett's sea level energy curves hold to very good approximation, the lower lake being only 305 meters above sea level. It is to be remembered that the energy E in $P(E,\theta)$ in expression (6) is the energy at the upper lake. In terms of E', the energy at the lower lake, letting $f'(E')$ represent the lower lake energy distribution,

$$\frac{N_u}{N_L}=\int_{E_0'}^{\infty}\frac{f'(E')dE'}{P(E'+iy_0mc^2,0)}\Big/\int_{E_0'}^{\infty}f'(E')dE'. \tag{10}$$

E_0' is the energy necessary to penetrate to the instrument through the water in the lower lake. Expression (10) is integrated graphically for various values of m/τ_0 using Blackett's energy

distribution at sea level for $f'(E')$ and expression (6) for $P(E'+iy_0mc^2, 0)$. For the point at 3.3 meters under the surface of the lower lake E_0' has a value 0.75×10^9 ev. A value of 78 ion pairs per cm with 32 ev per ion pair in atmospheric air was used for the energy loss per unit path. The value of the ratio of mesotron intensities N_u/N_L from (10) is plotted against m/τ_0 and then the experimental value of N_u/N_L is used to find the experimental value of m/τ_0 from the plot. From Fig. 1 the experimental N_u/N_L is 1.15 which gives a value for m/τ_0 of 58 in m_e/microsecond units where m_e is the electron mass. Thus for a mass 160 times the electronic mass, the value of the mean rest lifetime is $\tau_0=2.8\times10^{-6}$ sec.

V. Discussion of Results and Sources of Errors

Experimentally the intensity, N, is made up of mesotrons, knock-on electrons, soft primary component and decay electrons. In the above determination of m/τ_0, it was assumed that the intensity measured by the electroscope was made up of mesotrons or a component proportional to the mesotron. Of the three soft components, the knock-on electrons are proportional to the mesotrons so they introduce no error. The soft primary component which is only 4 percent or 5 percent of the total intensity at sea level is negligible at the point in question 3 meters below sea level. In an accompanying paper, Mr. Nelson finds, using cascade theory, that at the lowest depth in the lower lake, the decay electrons are of negligible intensity. From these considerations it may be concluded that $N_u/N_L=1.15$ is the correct ratio of mesotron intensities.

It should be pointed out that, for the points at 1.3 and 2.3 meters below the surface of the lower lake and their corresponding points in the upper lake, the experimental ratios N_u/N_L are about the same as for the point at 3.3 meters. From expression (10), since E_0' is lower with a greater probability of decay, it might be expected that the ratio would be greater. However, the decay electron intensity is greater for the shallower depths in the lower lake so that the two effects approximately cancel. Nelson's quantitative results taking into account the decay electrons are in excellent agreement with the experimental intensities found. This is good evidence that the mesotron decay, detected in this and other experiments, is a beta-decay with the decay electron producing cascades.

The data herein presented were taken with well-tested dependable apparatus and the method used eliminated many errors inherent in other experiments. The chief error in the ratio m/τ_0 found here is not due to the experimental data but rather to the inaccuracies in the energy distribution and other approximations used in the derivation of expression (10). Naturally the value of τ_0 depends on an accurate mesotron mass determination, and until such is made the ratio m/τ_0 is the only constant determined by this experiment.

In conclusion appreciation for the funds used for this work is extended to the Carnegie Corporation of New York. Mr. T. Smith, Mr. H. Bradner and Mr. R. Hog generously assisted on location. Especially we thank both Professor Oppenheimer for pointing out several finer points in the results and Mr. Nelson for his accompanying article.

Note on the Neher-Stever Experiment

ELDRED NELSON
Department of Physics, University of California, Berkeley, California

(Received August 16, 1940)

Three problems important to the quantitative interpretation of experiments on the decay of the penetrating component of cosmic rays are discussed: (a) The correct treatment of the altitude effect in the energy distribution is found to be important in the determination of the decay constant of the mesotron; (b) the fraction of mesotrons decaying is shown to be independent of the zenith angle; (c) the absorption in water of cascades produced by decay electrons is calculated from the shower theory of Serber and is in agreement with the experimental results of Neher and Stever. This last point shows that one but not both of the decay products is shower producing.

THE experiment of Neher and Stever[1] on the relative stopping power of air and water for the penetrating cosmic rays indicates the presence of a component that decays. They immersed an ionization chamber in two neighboring lakes, differing in elevation by 3616 meters, to such depths that the total mass of absorber was approximately the same in both cases. The difference in the readings obtained should be a measure of the number of mesotrons decaying between the two lakes. In order to make a quantitative determination of the lifetime of the mesotron from their measurements, certain considerations must be met: (a) the variation of the energy distribution of the mesotrons with altitude; (b) the variation of the intensity of the mesotrons with the zenith angle; (c) the absorption of the soft component in the water. The soft component is composed chiefly of cascades from degraded primaries, knock-on secondaries, and decay electrons. Since the first of these will be approximately the same at corresponding depths in the two lakes[2] and the second will follow closely the absorption of the hard component, the main correction to the readings of the ionization chamber will come from the decayed mesotrons. Euler and Heisenberg[3] have calculated the energy distribution and the effect of decay of the mesotron; Bruins[4] has prepared extensive tables and graphs of this energy distribution for various altitudes and for several values of the decay constant; and Snyder[5] and Serber[6] have worked out the theory of multiplicative showers. With this material at hand, it is possible to give an adequate treatment to these problems.

Since the mesotrons are produced with an energy distribution $\sim E^{-2.93}$, lose energy in proportion to the amount of matter passed through, and decay spontaneously in a co-moving coordinate system, the probable number of mesotrons having an energy between E and $E+dE$ and decaying between l and $l+dl$ is[3,4]

$$N_0 dE dl = \frac{rN_0}{E(E+x-x_0)^{2.93}} \times \left(\frac{x_0}{x}\frac{E}{E+x-x_0}\right)^{rH/(E+x)} dE dl. \quad (1)$$

Here N_0 is the normalizing constant, $x-x_0$ is the energy loss of a mesotron produced at a height h above sea level,

$$x=\beta \sec\theta H e^{-(h-l)/H}, \quad x_0=\beta \sec\theta H e^{-h/H}.$$

H is the height of the homogeneous atmosphere, β is the energy loss per cm of the homogeneous atmosphere, θ is the zenith angle,

$$r=mc \sec\theta/\tau,$$

[1] H. V. Neher and H. G. Stever, Phys. Rev., this issue. The author wishes to express his appreciation to Dr. Neher and Mr. Stever for the use of their data.

[2] The intensity of the cascades from degraded primaries in addition to being the same in both lakes will be small compared to the intensity of the mesotrons and may be neglected.

[3] H. Euler and W. Heisenberg, Ergeb. d. exakt. Naturwiss. **17**, 1 (1938).

[4] E. M. Bruins, Proc. Kon. Ned. Akad. v. Wetensch. **42**, 54 (1939); **42**, 740 (1939); **43**, 75 (1940).

[5] H. Snyder, Phys. Rev. **53**, 960 (1938).

[6] R. Serber, Phys. Rev. **54**, 317 (1938).

m is the rest mass of the mesotron, τ its lifetime in the rest coordinate system, and c the velocity of light. The intensity of the penetrating cosmic rays (number of mesotrons) at a point l in the atmosphere is then

$$\int_{E_0}^{\infty} dE \int_{l}^{\infty} N_d dl = N_0 \int_{E_0}^{\infty} \frac{dE}{(E+x-x_0)^{2.93}} \times \left\{ \frac{x_0}{x} \frac{E}{E+x-x_0} \right\}^{\tau H/(E+x)}. \quad (2)$$

E_0 is the minimum energy detectable by the measuring apparatus. In this integrand,

$$(E+x-x_0)^{-2.93}$$

represents the initial energy distribution and

$$\left(\frac{x_0}{x} \frac{E}{E+x-x_0} \right)^{\tau H/(E+x)}$$

represents the effect of decay. It is important to use the value of x corresponding to the altitude at which the experiment is performed in both parts of the integrand, since the resultant distribution of energies and the intensity is sensitive to it. The use of sea level energy losses in the initial energy distribution or of sea level average energies in interpreting data obtained at higher altitudes will give a larger value of the decay constant m/τ than is consistent with Eqs. (1) and (2).

In regard to point (b) the fraction of mesotrons decaying is independent of the zenith angle if the absorbers in the apparatus have a plane surface (minimum energy $= E_0 \sec\theta$). This is readily seen by replacing E by $E' \sec\theta$ in Eqs. (1) and (2), the remaining dependence on θ being only the $\cos^{1.93}\theta$ of the initial energy distribution.[4]

$$\int_{E_0 \sec\theta}^{\infty} dE \int_{l}^{\infty} N_d dl = \cos^{1.93}\theta N_0 \int_{E_0}^{\infty} \frac{dE'}{[E'+\beta h e^{-h/H}(e^{l/H}-1)]^{2.93}} \times \left[\frac{E' e^{-l/H}}{E'+\beta h e^{-h/H}(e^{l/H}-1)} \right]^{\gamma} = \cos^{1.93}\theta \left\{ \int_{E_0 \sec\theta}^{\infty} dE \int_{l}^{\infty} N_d dl \right\}_{\theta=0},$$

where $$\gamma = \frac{mcH}{\tau(E'+\beta H e^{(l-h)/H})}.$$

The absorption of the soft component, however, depends on θ. This will be treated quantitatively in the discussion of point (c).

In the experiment of Neher and Stever the depths of immersion of their ionization chamber in the upper lake (4.88, 5.88, and 6.88 m) were so great that the contribution of the soft radiation is obviously negligible; in the lower lake the corresponding depths (1.31, 2.31, and 3.31 m) were small enough so that the showers of electrons were not entirely absorbed out. As pointed out in the first paragraph, a good estimate of this contribution may be obtained by treating only those cascades of charged particles produced by the electrons into which the mesotrons have decayed.[7]

Assuming that the mesotron decays into an electron and a neutrino, the probability that the decay electron has an energy between $\mathcal{E}$ and $\mathcal{E}+d\mathcal{E}$ is given by[7]

$$d\mathcal{E}/E \quad (3) \qquad \mathcal{E} \leqslant E.$$

According to Serber[6] the number of charged particles at a point l_2 in a shower produced by an electron of energy $\mathcal{E}$ at l is given by

$$\int_C dy e^{-k(l_2-l)\sec\theta} \mathcal{E}^y G(y). \quad (4)$$

$G(y)$ is a complicated function of the parameter y on which k also depends. The integration is carried out along the contour C parallel to the imaginary axis and to the right of the origin. Then from (1), (3), and (4) the number of charged particles at l_2 arising from a mesotron decaying between l and $l+dl$ is

$$N dl = \tau N_0 dl \int_0^{\infty} \frac{dE}{(E+x-x_0)^{2.93}} \times \left[\frac{x_0 E}{x(E+x-x_0)} \right]^{\tau H/(E+x)} \int_0^{E} \frac{d\mathcal{E}}{E} \times \int_C dy \mathcal{E}^y e^{-k(l_2-l)\sec\theta} G(y). \quad (5)$$

[7] A similar calculation was made by B. Feretti, Nuovo Cimento 15, 421 (1938) using the shower theory of Bhabha and Heitler to estimate the energy spectrum of the soft component at sea level.

TABLE I. *Results of calculation.*

Depth in Lower Lake	Ionization Due to Mesotrons	Ionization Due to Showers from Decay Electrons	Total Ionization	Observed Ionization
3.31 m	1.738	0.004	1.742	1.742
2.31 m	1.917	0.020	1.937	1.936
1.31 m	2.180	0.052	2.232	2.226

The integral over δ is readily done, but the integral over E in this form can apparently only be carried out numerically. However, since only high energy electrons contribute to the final result, (1) may be approximated by

$$\frac{N_0 r e^{-rl/E}}{E(E+x-x_0)^3} dEdl$$

and the integral over the energy

$$f=\int_0^\infty dE \frac{e^{-rl/E}E^{y-1}}{(E+x-x_0)^3}$$

may be carried out analytically. It can be expressed in terms of the Whittaker function.[8]

$$f=(rl)^{\frac{1}{2}(y-1)}(x-x_0)^{\frac{1}{2}(y-5)}\Gamma(3-y)e^{rl/2(x-x_0)} \times W_{\frac{1}{2}(y-5),\frac{1}{2}(-y)}[rl/(x-x_0)].$$

The y integral is then evaluated by the saddle point method. To obtain the total number of charged particles arising from decay electrons, (5) is integrated down to the surface l_1 of the lower lake, neglecting the mesotrons decaying in the lower lake as they are too few to give any appreciable contribution.

$$N_e=\int_0^{l_1} Ndl. \qquad (6)$$

This integral was done graphically.

As the absorption of the shower depends on the zenith angle, (6) must be averaged over all directions of the incident particles. This correction reduces (6) by approximately 40 percent.

[8] E. T. Whittaker and G. N. Watson, *Modern Analysis* (Cambridge University Press, fourth edition, 1935), p. 340.

In doing the numerical work the following values of the constants were used: $H=8\times10^5$ cm of air at standard conditions, $\beta=2.5\times10^8$ ev per cm of air at standard conditions, $h=18.4\times10^5$ cm (this corresponds to assuming that the mesotrons are produced at 0.1 atmosphere), and $mc^2/\tau=2.86\times10^{13}$ ev per sec. This decay constant corresponds to $\tau=2.8\times10^{-6}$ sec. and $m=160$ electron masses and is that obtained from the experimental results of Neher and Stever. Another choice of the lifetime, such as 2.4×10^{-6} sec., for the same mesotron mass would change the absorption in water only within the limits of experimental error but would lead to a significant discrepancy between the observed and calculated absorption in air. The results of this calculation are shown in Table I.

The intensity of the mesotrons was determined from Eq. (2) and the contribution of the decay electrons from Eq. (5) in both of which the normalization factor N_0 was chosen to fit the observed intensity at the 3.31 m depth. The correction due to the decay electrons at this depth is less than the probable error of the measurements and hence may be neglected. This also confirms the assumption that the ionization due to the decay electrons did not affect the readings taken in the upper lake. The ionization due to the showers from decay electrons is 15 percent at 1.3 m, 6 percent at 2.3 m, and 1.5 percent at 3.3 m of the ionization lost by mesotron decay. These figures would be little altered by any reasonable choice of the decay constant.

The agreement of the calculated and observed absorption in water of the cascades from decay electrons indicates that one but not both of the decay products, that is on the average only half of the mesotron energy, produces showers. This would contradict the hypothesis that the mesotron decays into a photon and an electron and tend to confirm Yukawa's original suggestion that it is β-radioactive, giving an electron and neutrino on decay.

The author wishes to thank Professor Oppenheimer for suggesting these problems and for many helpful discussions.

The Heat of Fission of Uranium

MALCOLM C. HENDERSON
*Palmer Physical Laboratory, Princeton, New Jersey**
(Received September 5, 1940)

The heat produced during slow neutron bombardment in a 13.36-g sample of metallic uranium was measured on a resistance thermometer. Simultaneously the number of fissions produced in a 54-microgram layer of uranium was counted by an ionization chamber and pulse amplifier. The two uranium samples were within one cm of each other and inside the same 1.5-cm lead shield and surrounded by 5 cm of paraffin. The source of neutrons was the Princeton cyclotron, using the Be–H reaction at 6.5 Mev. The 54-microgram layer gave 40.1±0.2 alpha-particles per min. into 2π solid angle and under slow neutron bombardment gave about 340 fissions per min. At the same time the heat output from the 13-gram sample was 40 microwatts. A method of calculation was developed that allows for the transient effects of fluctuations in the neutron output of the cyclotron. The weighted average of 13 runs, after various corrections that together amount to 3.8 percent, is 177 Mev per fission. The average deviation from this figure was 5 Mev and the result is believed to have a probable error of about 1 percent. The actual kinetic energy of recoil carried by the fission fragments is about 12 Mev less than this, ±50 percent, depending upon more precise knowledge of the fission mechanism.

INTRODUCTION

THERE have been several attempts to measure the total energy set free in the fission of the uranium nucleus.[1] So far, however, they have all depended upon the ionization process and an assumption that the total kinetic energy of the recoiling nuclei can be calculated from the total ionization. It seemed desirable to have a direct measurement and upon consideration of the approximate cross section for fission and of the number of neutrons available around cyclotrons it was found that the energy release in about 10 grams of uranium should be large enough to measure directly as heat. This approximate calculation has been justified.

The preliminary experiments were carried out in Berkeley in 1939 and a figure of 175 Mev per fission was published.[2] The results here described were obtained with the Princeton cyclotron, after modifying the measuring apparatus so that the measurements of the heat production and of the number of fissions were carried out simultaneously and in the same neutron atmosphere. A result of 180 Mev per fission was announced at the Pittsburgh meeting of the American Physical Society.[3] Reconsideration of various corrections now changes this figure to 177 Mev ±1 percent.

In Berkeley the neutron intensities were so great that "power from the atom" amounting to 350 microwatts was obtained. In Princeton the maximum was about 40 microwatts.

APPARATUS

The apparatus consisted of two closely adjacent but independent parts: a resistance thermometer to measure the rate of heat production in a 13.36-g sample of metallic uranium[4] and the usual combination of ionization chamber and pulse amplifier to measure the number of fissions occurring in a thin film of uranium containing 54.0×10^{-6} g.

The diagram, Fig. 1, indicates in cross section the relative size and arrangement of parts. The outer container of heavy copper had a paraffin lining nearly two inches thick. Fitting inside the paraffin was a rectangular lead shield which absorbed gamma-rays and acted, by its heat capacity and conductivity, as a stabilizing influence upon the internal temperature of the apparatus. The space inside the lead shield was a rectangular well, $6\times3\times20$ cm, and it accommodated both arms of the resistance thermometer

* Now at Dartmouth College, Hanover, New Hampshire.

[1] See L. A. Turner, Rev. Mod. Phys. **12**, 21 (1940) for a complete list to January 1940.

[2] M. C. Henderson, Phys. Rev. **56**, 703 (1939).

[3] M. C. Henderson, Phys. Rev. **58**, 200 (1940).

[4] The uranium was supplied by Metallic Hydrides, Inc. and was in granular form. Analysis by standard chemical procedures, carried out according to the advice of Professor Furman of the Princeton Chemistry Department, showed approximately a 2 percent impurity—probably largely oxygen—and the figure 13.36 g represents pure uranium with an accuracy of better than 1 percent. I am greatly indebted to Professor Furman for his advice and assistance.

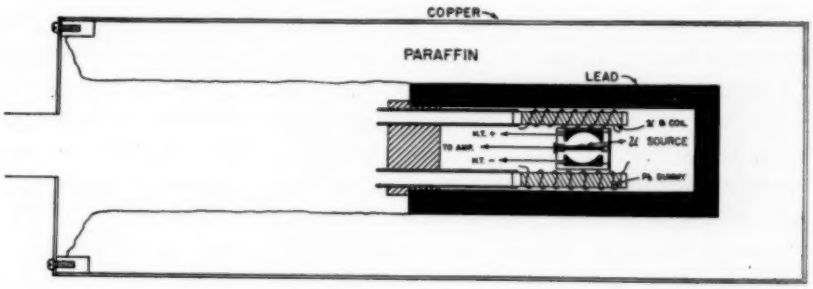

FIG. 1. Arrangement of apparatus.

and the ionization chamber in its own shielding case between them. The effective thickness of the lead was about 1.5 cm.

The rest of the space in the shield can contained the first tube of the pulse amplifier, sockets, connection plugs, lead-in wires and a brass shield connected to the lead shield but insulated from the copper can. All connections were made through plugs and the apparatus could be dismantled and reassembled quickly.

The thermometer was very similar to the one used by Watson and Henderson for measuring the heat production of various radioactive substances,[5] but was considerably larger. It consisted of two brass tubes, about 0.01 cm wall thickness, 0.7 cm diameter and 7.5 cm long. On each tube were wound, and shellacked in place, two coils of No. 46 ss copper wire, occupying 6 cm of their length. Copper wire was used to minimize thermal e.m.f.'s. The tubes were supported from one end by thin glass tubes which were cemented into the Lucite plug that closed the mouth of the well. Each coil had a resistance of 146 ohms. They were connected into a Wheatstone network with opposite arms of the net wound on the same tube, which method of connection doubles the sensitivity. They were also connected in such a manner as to make the magnetic flux intercepted by the bridge as a whole a minimum. This precaution avoids disturbances arising from changes in the magnetic field of the cyclotron.

The network was balanced as nearly as possible by adjusting the lengths of the wires and the residual lack of balance was compensated for by an opposing voltage in the galvanometer circuit. It is undesirable to balance by using a large external shunt resistance, since such a resistance introduces at least two sources of disturbance: thermal e.m.f.'s and a temperature coefficient different from that of the bridge.

The galvanometer was used at a sensitivity of about 2.5×10^{-10} amp./mm, an effective resistance of 1000 ohms and a half-equilibrium time at that resistance of 13 seconds. There was no disadvantage in the long time constant since the thermal half-equilibrium time of the bridge itself was 2.7 minutes. The temperature sensitivity was of the order of 10^{-4} deg./mm. The heat sensitivity, or better the power sensitivity, used was about 12 microwatts/cm throughout the work and was, of course, determined repeatedly. The bridge was operated directly from 4 dry cells in series-parallel.

The uranium heating sample, of gross weight 13.64 g, was sealed up with wax in a tube of copper foil that fitted snugly inside the thermometer tube. Enclosed with the uranium was a manganin heating coil of 49.0 ohms that was used in calibrating the bridge. Roughly $\frac{3}{4}$ of the heat capacity of the thermometer tube and contents was supplied by the uranium itself. A dummy source identical in dimensions, heat capacity and gamma-ray absorbing power was placed in the other tube. It consisted of a tube of copper foil loaded with lead. The dummy had an important part in compensating for possible heating from gamma-rays and in stabilizing the bridge thermally.

The connecting wires were brought out through six-wire microphone cable, which was in turn enclosed in tombac tubing leading to the control box.

The number of fissions produced was counted in the ionization chamber shown in the figure. The chamber was made double in order to compensate in part for the gamma-ray background that arises near every neutron source. The high

[5] S. W. Watson and M. C. Henderson, Proc. Roy. Soc. A118, 318 (1928).

tension electrodes were almost hemispheres with the uranium source at the center. Positive ions from gamma-rays and fissions were collected on one side and negative ions from gamma-rays alone on the other. In spite of this precaution the background disturbance was very large and the grid of the first tube was sometimes swung far enough positive to change the amplification. The source of fission particles was a 5-mm² piece of platinum foil on which some uranium had been sputtered. I am indebted to Dr. C. C. Van Voorhis for this uranium source.

The amount of uranium on the foil was determined by counting the number of alpha-particles emitted by it and using the figure given by Kovarik and Adams[6] for the number of alpha-particles per gram of uranium per second. The solid angle into which the particles were emitted was approximately 2π, but it is not necessary to know it even approximately since the fission particles and alpha-particles are emitted into exactly the same angle.

There is no evidence for a significant separation of isotopes in the evaporation process. Such a separation would, of course, invalidate the work described here.

The number of alpha-particles emitted by the foil as mounted was 40.15 per minute. A total of 23,336 particles was counted which corresponds to a probable error of $\frac{1}{2}$ percent. Determinations before and after the heating measurements agreed to better than the statistical probable error of each. If the solid angle into which the particles emerge was 2π, there was 54.00×10^{-6} g of uranium on the foil.

The amplifier used in counting the alpha-particles and fissions had four stages and was of standard design except for the use of "acorn" tubes in the first two stages and dry battery tubes in the third and fourth. All voltages were supplied by batteries and the entire amplifier, batteries and all except the first tube, fitted into a brass box $6''\times7''\times9''$. The third and fourth stages were shielded from the first two and were completely independent of them. It was found that three volts were ample for the cathodes of the acorn tubes, though rated at 6.3. A jack and plug was provided so that the tubes could be heated from an outside filament supply when conditions permitted.

The ionization-chamber potential was provided by a 4-mf condenser, charged occasionally by a battery or power pack. About 250 to 300 volts were used.

The output of the amplifier operated a thyratron scale-of-eight counter and a cathode-ray oscillograph. The output was visually monitored with the cathode-ray oscillograph at all times. There was enough feedback from the scale-of-eight into the oscillograph so that it was possible to tell by the shape of a pulse whether it had been counted or not, and this fact proved very useful.

The principal difficulty encountered was shielding the amplifier and thermometer from the intense radiofrequency fields of the unshielded cyclotron oscillator. By using tombac tubing and by making the shielding practically water tight and double nearly everywhere it was possible to get radiofrequency burns off the shielding and still have no trace of pick-up in either part of the apparatus. The entire system was left ungrounded.

A certain amount of 360-cycle ripple showed in the oscillograph trace because the cyclotron was driven by three-phase rectified power and the ion beam and neutron output were modulated by this ripple. It was, fortunately, small enough to be unimportant and, in fact, afforded a good check on the constancy of the output of neutrons.

No trouble was caused by the presence of the first amplifier tube inside the thermometer shield. If left running for an hour before a run it caused no further disturbance.

Procedure

In a normal day's run the cyclotron was started in the morning for some other research at about the same time that the bridge and amplifier were turned on. The thermometer was placed in position near the target and left undisturbed throughout the day. Extra paraffin blocks were piled around it. After about an hour the bridge had reached a reasonably steady rate of drift and a heat sensitivity determination was made. The beryllium target on a probe was then inserted between the dee's into the proton beam and the neutron output

[6] A. F. Kovarik and N. I. Adams, Jr., Phys. Rev. 40, 718 (1932).

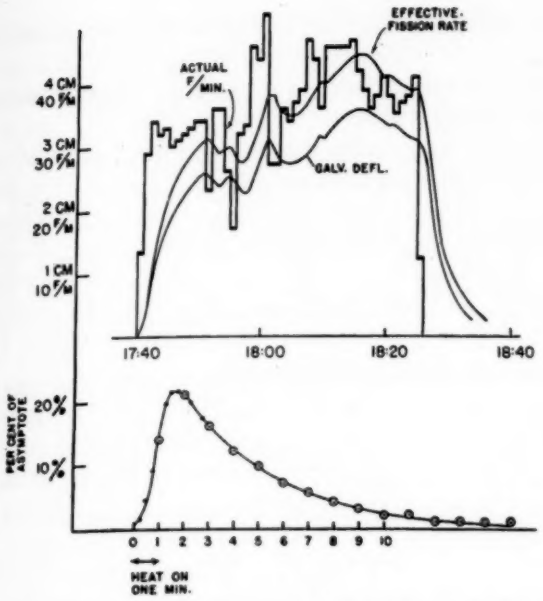

FIG. 2. Upper portion, actual and effective fission rates and corresponding galvanometer deflection. Lower curve, galvanometer response to a known input of heat energy.

was increased as far as possible. The proton energy was about 6.5 Mev, but the current to the probe was not measured.

The length of a run varied from a few minutes up to $\frac{3}{4}$ of an hour, depending upon the stability of the rate of drift and of the cyclotron output. To redetermine the rate of drift the neutron beam was turned off by detuning the cyclotron magnet slightly, leaving everything else running as before. This procedure was required because although no radiofrequency reached the bridge directly, the very considerable change in the heating of the room when the oscillator was turned off soon affected the rate of drift.

Galvanometer readings were taken every minute throughout the day and, when fissions were being produced, the number of counts on the scale-of-eight was read simultaneously. A plot of a typical run is shown in Fig. 2, after correction for the drift, which was always less than $\frac{1}{3}$ mm per minute. The histogram[7] gives the number recorded on the scale-of-eight in each minute.

The third curve represents what may be called the "effective rate of fission"; that is, a constant rate of fission that, if maintained from minus infinity to the time in question, would have produced the same galvanometer deflection as did the actual fluctuating number observed. It is a curve calculated from the histogram by a procedure based on the thermal characteristics of the thermometer.

In principle, the simplest procedure for calculating the heat evolved per fission, given a perfectly steady source of neutrons, would be to allow the bridge to come to approximate thermal equilibrium, read the galvanometer and the number of fissions per minute and divide one by the other, allowing for the ratio of masses of uranium in the two parts of the apparatus. In an actual experiment, the neutron output is far from steady, as may be seen from Fig. 2, and even if it were steady, the simple procedure wastes information, because each galvanometer reading is significant and can be used to determine the heat production. This is true because the galvanometer deflection at any instant is a consequence of the heat produced in all preceding minutes. The heat produced in each minute may be considered a "pulse" of heat and the sum of the effects of all pulses is the deflection. The effect of each pulse, however, dies away exponentially with time after an initial rise, independently of all the other pulses, in a manner depending upon the thermal characteristics of the thermometer.

The thermal characteristics in question can be measured by introducing a known quantity of heat in a time short compared to the half-equilibrium time of the bridge and noting the galvanometer deflections over twenty minutes or so. The lowest curve in Fig. 2 shows the result of such an experiment. The calibration heat was turned on for exactly one minute and the deflection was then followed back to equilibrium. The ordinates are expressed in percentage of the deflection that would have been reached asymptotically if the heat had been left on. The abscissas are minutes. The circles are the numbers taken from the curve and used as weighting factors in the calculation of the effective rate of fission. They differ from the exact values of the curve by less than $\frac{1}{2}$ percent of the asymptote. All but two were whole numbers, for ease in calculation, and their sum is of course 100 percent: 14, 21, 16, 12, 9.5, 7, 5.5, 4, 3,

[7] The ordinates in the figure should be multiplied by 8 to give the actual number of fissions per minute.

2, 2, 1, 1, 1, 1. After the first two, the ratio between successive numbers is approximately $2^{-1/2.7}=0.774$.

To carry out the calculation, the recorded number of fissions in each minute was considered to be proportional to the rate of heat production in that minute, which assumption is certainly in error only by the amount of the statistical fluctuation. Each recorded number was then multiplied by the weighting factor corresponding to its remoteness from the time of observation, i.e., the latest by 14 percent, the next by 21 percent, etc., and the sum of all the products taken. This sum is the "effective rate of fission" at the time of observation. Such a sum is then formed for the next minute and so on. The calculation is not as laborious as it sounds, and is lightened considerably by the fact that after the two proximate minutes the ratio of successive factors is 0.774. It was run off on a calculating machine.

The ratio of the galvanometer deflection at any moment to the effective fission rate at that moment is then a measure of the heat produced per fission. Since this is true point by point, the ratio of the areas under the curves is also such a measure and this ratio of areas is a properly weighted average of the ratios calculated from each point, because it weights the large deflections proportionately to their magnitude. Instead of actual areas, the sum of the ordinates was used; in practice, the parts of the curves where the galvanometer deflection was more than 1 cm was taken and the tails disregarded. From the ratio of the masses of uranium and the sensitivity of the galvanometer, the heat produced per fission can then be easily calculated.

Results

There were thirteen runs such as Fig. 2 that were satisfactory, as well as seven others in which the neutron output was too small to give an accurate result. The crude results were calculated from the formula:

$$\text{Mev per fission}=\frac{D\times S\times 1/13.64\text{ g}}{F\times 1/(54\times 10^{-6})\text{ g}}\times K, \quad (1)$$

where D/F is the ratio of the sums of ordinates over the useful parts of the curves, as described in the preceding section, S is the bridge sensitivity in microwatts per cm and K is a numerical factor to convert to the required units: $60\times 10/(1.6\times 10^{-6})$.

The values obtained, with the number of useful minutes in each run, are:

Mev	Min.	Mev	Min.	Mev	Min.
177	16	178	16	181	40
192	14	179	8	181	47
197	14	181	22	194	22
186	9	186	24	185	25
				182	20

The weighted average of these figures is 184.0 Mev/fission with the number of minutes as the weight, and the average deviation of the 13 runs is 5.0. This leads to a probable error of 1.4 Mev or $\frac{3}{4}$ percent, based on internal consistency only.

Corrections

There are a number of corrections to be applied to the result of the preceding section, the most important of which is caused by the difference in the neutron intensities falling on the two uranium samples.

To take the members of (1) in order:

The galvanometer deflection was of the order of 2 to 3 cm and nothing less than 1 cm was used. The spot could be read accurately to 0.2 mm, or better than 1 percent. The galvanometer scale was tested for linearity several times.

The heat sensitivity of the bridge was determined by producing a known joule heating in the coil buried in the uranium. The heating coil was measured on a laboratory standard Wheatstone bridge and found to be 49.0 ± 0.1 ohm. The current through the coil was calculated from the voltage of the new dry cell supplying it, measured against a potentiometer, and the total resistance of the circuit. Three different rates of heating were used: 21.6, 96.7, and 267 microwatts. The sensitivity was the same for all three.

The measurements of the masses have already been discussed. The calculation so far has been based on 13.64 g for the heating sample. Actually, 13.36 g was found on analysis, which raises the calculated heating by 2.1 percent.

The number of fissions was determined by counting on the scale-of-eight and monitoring the counting visually. It was found that if the

bias was set high enough to avoid spurious counts from switching surges, about one in forty of the fissions failed to be counted, or 2.5 percent. This degree of missing was determined repeatedly during the work and the determination was made easier by the characteristic shape of the fission surge. When the surge was counted by the scale-of-eight, a sharp spine appeared near the crest of the surge. Since there were more fissions than were counted, the heating result must be reduced by the 2.5 percent.

The method of calculating D/F has already been discussed. It assumes implicitly that the thermal characteristics of the bridge are the same for joule heating as for fission heating. This assumption is certainly true for the decaying part of the curve but there might be a difference in the rising part. In any case, the difference will be a second-order correction, since it applies only to the 14 percent contributed by the initial minute. The method also assumes a constant fission rate throughout the minute, which is of course far from true of a particular minute, but the differences will average out.

The last and most important correction to be made is for the effects of neutron absorption. Even though the two samples were as close together as possible they were unavoidably surrounded by different amounts of material, and in addition, the 13-g source will suffer some self-absorption, since its diameter was 7 mm. Scattering may be neglected entirely since the neutron atmosphere is approximately uniform.

The ionization chamber was built of 0.8-mm brass, the insulation was negligible and the collecting electrode was very thin, but the brass high tension electrodes together weighed 24.2 g, and were at an average radius of 1.2 cm from the uranium. They thus correspond to a spherical shell of 1.6-mm thickness, which, plus the 0.8 of the case, gives 2.4 mm. If the absorption is small, the reduction in neutron intensity may be calculated to be $1.9\times10^{24}\sigma$ percent. If it is assumed that the absorption coefficient for ordinary brass, 33 Zn 67 Cu, is the same as for copper only, 3.3×10^{-24},[8] the correction is then a 6.3 percent reduction in intensity, which reduces the calculated heat per fission.

The thermometer tube and copper foil around the 13-g source were together only about 0.25 mm thick, giving a correction of $+\frac{1}{2}$ percent approximately. The self-absorption in the uranium, which was a cylinder 7 mm in diameter and 5 cm long, with an actual density of 7.1 g/cc, looks troublesome to calculate. But, on assuming that the uranium is immersed in a uniform neutron atmosphere, an elliptic function of the second kind gives the average path of a neutron through the uranium before hitting an average atom, assuming also that the cylinder is infinitely long and that scattering is unimportant. Since the absorption is small, one may assume it to be linear with distance rather than exponential. The calculation then shows that the average neutron path is 1.3 times the radius of the cylinder, or 4.5 mm. From the actual density of the source, the absorption turns out to be 0.83σ percent, if σ is in 10^{-24} units. Taking σ to be 3×10^{-24}, we have a reduction in intensity of 2.4 percent and a total for the source, therefore, of 2.9 percent.

$$(+2.1)+(-2.5)+(-6.3)+(+2.9)=-3.8 \text{ percent.}$$

This correction amounts to 7.0 Mev and the corrected value is thus 177 Mev, with a probable error estimated at about 1 percent.

Discussion

The measurements made prior to December, 1939, have yielded values for the kinetic energy per fission that are well below that found here—mostly in the neighborhood of 125 Mev. Kanner and Barschall[9] however find about 160 Mev by measuring the energy of the individual members of the pairs of fission fragments. This value, according to a private communication, seems to be slightly too low, and 165 Mev is more accurate.

The available energy, from mass considerations alone, would seem to be about 200 Mev. Bohr and Wheeler[10] point out, however, that much of this must go to excite the residual nuclei and will not, therefore, appear as kinetic energy of recoil. This excitation energy will be dissi-

[8] M. Goldhaber and G. H. Briggs, Proc. Roy. Soc. A162, 127 (1937).

[9] M. H. Kanner and H. H. Barschall, Phys. Rev. 57, 372 (1940).

[10] N. Bohr and J. A. Wheeler, Phys. Rev. 56, 426 (1939).

pated by various processes, some of which will be registered by the thermometer used in this work and some not. The gamma-rays of more than 100 kev will practically all escape and only the softer x-rays will be recorded, but, unless there is a much larger number of them than has been noticed hitherto, they will not carry enough energy to affect the result found here. All the neutrons liberated in the fission process will of course escape, since the absorption coefficient is small and, even if the elastic scattering were large, the mass ratio is most unfavorable to the transfer of energy from neutron to nucleus.

Beta-rays, and positrons if any, will, on the other hand, be largely absorbed. A million-volt beta-ray will have much more than an even chance of being completely absorbed if liberated at random in the uranium. And, since the measurement of the heat production lasted in general about half an hour, all the delayed beta-particles produced by the numerous radioactive substances created in the fission process would also contribute to the total heating. If this contribution were very large, one might expect the apparent energy per fission to increase with time in the runs as taken. There was no evidence of this effect however. Most of the chemically identified activities that follow fission have, to be sure, a fairly long life. This is natural, since the body must live long enough for a chemical analysis to be carried out upon it. There are, however, many more bodies with half-lives of the order of seconds and minutes and these will all contribute in full to the heating. How many of these bodies there are, on the average, between the immediate products of fission and the final stable nucleus is not certain, but eight seems the most probable number. If, as seems likely at present, the fission is approximately: $_{92}U^{236} = {}_{56}Ba^{146,144} + {}_{36}Kr^{90,92}$ then there are needed four beta-ray activities for each nucleus to end in a stable form. If the split is to pairs of nuclei different from these, it seems likely that there will be more energy of excitation and less kinetic energy of the recoil particles, but the effect upon the measured heating will be small.

The emitted beta-particles will have to escape from the body of the uranium sample through a thickness that depends upon their point of liberation and their direction. The same method of calculation applies to them as to the absorption of neutrons as just discussed, and the average path of the beta-rays in the material of the source can be shown to be 4.5 mm. There is an error here, however, in that this calculation assumes the beta-particles to have an infinite range, but it nonetheless indicates that practically all the energy of the beta-particles will be absorbed. If the average energy of the beta-rays lies around 1.5 Mev, we would have a total of some 12 Mev from beta-ray heating to subtract from 177 to get the true recoil energy. This calculation cannot be an accurate one, but it indicates substantial agreement between the ionization measurements and the heat measurements, and the agreement justifies the implicit assumption underlying the ionization method: that as much energy goes to form a pair of ions whether produced by an alpha-particle or a fission fragment.

If, on the other hand, one uses the data to calculate the beta-ray energy available by assuming the validity of both sets of experiments, then $177-165=12$ Mev. This figure leaves a lot of energy, about 25 Mev, unaccounted for, and this energy will go to liberate neutrons and gamma-rays from the fission products. Without more detailed knowledge of the fission process it seems impossible to say more.

The neutrons used by Kanner and Barschall were D−D neutrons of full energy, while those effective in this work were largely slow neutrons from paraffin at room temperature. This fact was checked by placing a cadmium shield around the thermometer. There is no evident difference in the amounts of energy released by the two sorts of neutron.

Acknowledgments

I am much indebted to Professor E. O. Lawrence for permission to carry out some of this work in Berkeley. I am also indebted to Professor M. G. White for advice and cooperation throughout its completion in Princeton, and also to the rest of the cyclotron staff there.

New Lines and Terms in the Arc and First Spark Spectra of Molybdenum: Mo I and Mo II

SISTER M. ROSWITHA SCHAULS, O. S. F.* AND R. A. SAWYER
University of Michigan, Ann Arbor, Michigan

(Received September 3, 1940)

The spectrum of molybdenum, as excited in a hollow cathode discharge, has been photographed from 540A to 10,830A. The resonance triplet of Mo II, $^6S-{}^6P^0$, has been found, thus locating the lowest term, the $^6S_{5/2}$, at 11,783.70 cm^{-1} below the previously known lowest level, the $^6D_{1/2}$. Some 20 new lines have been classified and 7 new levels established. Two new multiplets, the $^6D-{}^6P^0$ and the $^6D-{}^6D^0$, have been arranged. Catalán's list of classified Mo I lines has been extended to include 36 additional lines. These lines were classified from levels previously determined by Catalán.

THE complete configuration of electrons for atomic molybdenum is $1s^2\,2s^2\,2p^6\,3s^2\,3p^6\,3d^{10}\,4s^2\,4p^6\,4d^5\,5s$. The lowest state[1] of singly ionized molybdenum is $4d^5\,{}^6S_{5/2}$ which is the limit for the $4d^5\,ms\,{}^5S$ and ^7S term of Mo I. Excitation of one of the five d electrons to an s state gives the configuration $4d^4\,5s$ with the low terms $4d^4(^5D)5s\,{}^4D$ and ^6D, while excitation of one d electron to a p state gives the configuration $4d^4(^5D)5p$ with the terms $^4P^0$, $^4D^0$, $^4F^0$, $^6P^0$, $^6D^0$ and $^6F^0$.

The first classifications in the Mo II spectrum were made by Meggers and Kiess.[2] Their investigation yielded five multiplets: $^4D-{}^4P^0$, $^4D-{}^4D^0$, $^4D-{}^4F^0$, $^6D-{}^6D^0$ and $^6D-{}^6F^0$, probably transitions between states of the low d^45s and d^45p configurations. The first, third and fifth multiplets mentioned above, as also the $^6D^0_{3/2}$ and $^6D^0_{1/2}$ terms of the fourth multiplet, were verified by Wilhelmy's[3] Zeeman-effect data. Wilhelmy also found a $^6D-{}^6P^0_{3/2}$ triad but was unable to complete the multiplet.

EXPERIMENTAL

The spectroscopic source used in this research was the hollow cathode discharge in an atmosphere of helium. The processes of excitation in this discharge are due to reactions between the neutral or metastable atoms of the metal and the metastable or ionized rare gas atoms.[4] Since the energy of ionization of helium is 198,308 cm^{-1}, and that of the lowest metastable state of molybdenum,[5] a^5S, is 46,432 cm^{-1}, the maximum energy available for the excitation of the Mo II spectrum is 151,876 cm^{-1} (659A). The source of power for the discharge was a d.c. generator operating to give 1500 volts. The discharge was run at 0.5 amp. and with about 9 mm pressure of helium. A molybdenum cathode was used.

The spectrum of the discharge was photographed from 540A to 10,830A. The region of wave-lengths shorter than 2078A was photographed with a concave grating vacuum spectrograph.[6] The grating (1 m radius, 14,400 lines per inch) gave a dispersion of about 17A/mm. Lines due to impurities in the discharge served as standards in the vacuum region. The region from 2078A–2506A was photographed with a Zeiss "Qu 24" quartz prism spectrograph, while for the region 2300A–4415A a Hilger E2 quartz prism spectrograph was used. The region of wave-lengths longer than 4415A was photographed with a Hilger E1 glass prism spectrograph. Iron arc comparison spectra were placed

TABLE I. *The resonance triplet $^6S-{}^6P^0$, together with two transitions from the $^6D^0$ levels. Intensities were taken from the lines on the vacuum plate. These lines also appeared on the spark plate, with the exception of the line 1972.15, which was out of its range.*

$4d^4\,5p$	$^6P^0_{7/2}$	693.81	$^6P^0_{5/2}$	568.03	$^6P^0_{3/2}$	$^6D^0_{7/2}$	127.74	$^6D^0_{5/2}$
$4d^5\,{}^6S_{5/2}$	50302.60(3) (1987.969) vac.		49608.79(3) (2015.118)		49040.76(4) (2038.462)	50706.08(1) (1972.15) vac.		50578.34(1) (1977.131) vac

* A member of the faculty of the College of Saint Teresa, Winona, Minnesota.

[1] C. C. Kiess and O. Laporte, Science **63**, 234–236 (1926).
[2] W. F. Meggers and C. C. Kiess, J. Opt. Soc. Am. **12**, 417 (1926).
[3] E. Wilhelmy, Ann. d. Physik **80**, 305 (1926).
[4] R. A. Sawyer, Phys. Rev. **36**, 44 (1930).
[5] M. A. Catalán and Pilar de Madariaga, Anal. Soc. Espan. Fis. Quim. **31**, 711 (1933).
[6] R. A. Sawyer, J. Opt. Soc. Am. **15**, 305 (1927).

TABLE II. *The $^6D-{}^6P^0$ and $^6D-{}^6D^0$ multiplets of molybdenum.*

	$^6D_{1/2}$	250.70	$^6D_{3/2}$	383.15	$^6D_{5/2}$	482.90	$^6D_{7/2}$	560.46	$^6D_{9/2}$
$^6P_{7/2}^0$					37885.24(5)	483.07	37402.17(5)	560.50	36841.67(2)
					(2638.765)		(2672.848)		(2713.515)
693.65					693.84		693.61		
$^6P_{5/2}^0$			37574.66(5)	383.26	37191.40(5)	482.84	36708.56(3)		
			(2660.578)		(2687.997)		(2723.355)		
568.03			568.05		568.05				
$^6P_{3/2}^0$	37257.33(4)	250.72	37006.61(4)	383.26	36623.35(2)				
	(2683.240)		(2701.420)		(2729.692)				
	$^6D_{1/2}$	250.70	$^6D_{3/2}$	383.15	$^6D_{5/2}$	482.90	$^6D_{7/2}$	560.46	$^6D_{9/2}$
$^6D_{9/2}^0$							36580.53(1)	560.40	36020.13(7)
−1224.55							(2732.887)		(2775.408)
							−1224.59		−1224.51
$^6D_{7/2}^0$					———		37805.12(5)	560.48	37244.64(6)
							(2644.357)		(2684.153)
127.99							128.19		
$^6D_{5/2}^0$			38543.37(4)		———		37676.93(4)		
			(2593.705)				(2653.355)		
385.62									
$^6D_{3/2}^0$	38408.61(2)		———		37774.63(4)				
	(2602.806)				(2646.491)				
242.57	242.57								
$^6D_{1/2}^0$	38166.04(2)	250.76	37915.28(3)						
	(2619.348)		(2636.674)						

on all plates throughout the quartz and glass regions.

In addition the spectrum from a 35,000-volt condensed-spark in air, covering the region 1944A–2200A, was photographed with a Bausch and Lomb quartz prism spectrograph. Copper and silver spark spectra were placed on these plates for comparison.

TABLE III. *New energy levels.*

CONFIGURATION	SYMBOL	J	TERM VALUE	$\Delta\nu$
$4d^5$	^6S	5/2	−11783.70	
$4d^4(^5D)5p$	$^6P^0$	3/2	37257.28[1]	
				568.03
		5/2	37825.31	
				693.65
		7/2	38518.96[2]	
$4d^4(^5D)5p$	$^6D^0$	5/2	38793.87	
				127.99
		7/2	38921.86[2]	
				−1224.55
		9/2	37697.31	

[1] Level given by Wilhelmy.
[2] Levels given by Meggers and Kiess, but differently assigned.

DATA AND CLASSIFICATION

In the absence of extensive Zeeman-effect data, the discovery of the $4d^5\ ^6S$ term, with transitions to $4d^4(^5D)5p\ ^6P^0$ and $^6D^0$, offers the best possibility for verification of these terms. Comparison with the Cr II spectrum indicated that these transitions should lie near 2000A. To bring out the $^6S-{}^6P^0$ and $^6S-{}^6D^0$ lines more strongly relative to the rest of the spectrum than in the hollow cathode discharge, a condensed spark plate was made in the region 2200A−1940A. Only a few lines having wave-lengths less than 2050A appeared on this plate, of which the three strongest form a $^6S-{}^6P^0$ resonance triplet, involving the $^6S-{}^6P_{3/2}^0$ term of Wilhelmy. A weaker line

TABLE IV. *Classified lines of* Mo II. *The letter n in column one indicates a new line. The symbols in column one have the following meaning: P—M. Puhlmann, Zeits. f. Wiss. Phot.* **17**, *7–131 (1917–1918); H—G. R. Harrison, M.I.T. Wavelength Tables (1939); E—F. Exner and E. Haschek, Tabellen der Bogenspektra (1911); S—new observation.*

AUTHORITY*	λ	I	ν	CLASSIFICATION	$\Delta\nu$	NOTE
n	1972.15	1	50706.1	$4d^5\ ^6S_{5/2} - 4d^45p\ ^6D_{7/2}^0$	−0.5	y
n	1977.13	1	50578.3	$4d^5\ ^6S_{5/2} - 4d^45p\ ^6D_{5/2}^0$	−0.7	y
n	1987.969	3	50302.60	$4d^5\ ^6S_{5/2} - 4d^45p\ ^6P_{7/2}^0$	+0.06	y
S	2015.118	3	49608.79	$4d^5\ ^6S_{5/2} - 4d^45p\ ^6P_{5/2}^0$	+0.22	
S	2038.462	4	49040.76	$4d^5\ ^6S_{5/2} - 4d^45p\ ^6P_{3/2}^0$	+0.22	
H	2593.705	4	38543.37	$4d^45s\ ^6D_{5/2} - 4d^45p\ ^6D_{5/2}^0$	−0.20	
P	2602.806	2	38408.61	$4d^45s\ ^6D_{1/2} - 4d^45p\ ^6D_{3/2}^0$	−0.10	x
P	2619.348	2	38166.04	$4d^45s\ ^6D_{1/2} - 4d^45p\ ^6D_{1/2}^0$	0	x
P	2636.674	3	37915.28	$4d^45s\ ^6D_{3/2} - 4d^45p\ ^6D_{1/2}^0$	+0.06	
P	2638.765	5	37885.24	$4d^45s\ ^6D_{3/2} - 4d^45p\ ^6P_{7/2}^0$	+0.13	x
P	2644.357	5	37805.12	$4d^45s\ ^6D_{1/2} - 4d^45p\ ^6D_{7/2}^0$	−0.01	
P	2646.491	4	37774.63	$4d^45s\ ^6D_{3/2} - 4d^45p\ ^6D_{3/2}^0$	+0.03	x
P	2653.355	4	37676.93	$4d^45s\ ^6D_{1/2} - 4d^45p\ ^6D_{3/2}^0$	+0.19	
P	2660.578	5	37574.66	$4d^45s\ ^6D_{3/2} - 4d^45p\ ^6P_{5/2}^0$	−0.04	
P	2672.848	5	37402.17	$4d^45s\ ^6D_{3/2} - 4d^45p\ ^6P_{7/2}^0$	+0.04	
P	2683.240	4	37257.33	$4d^45s\ ^6D_{1/2} - 4d^45p\ ^6P_{3/2}^0$	−0.05	y
P	2684.153	6	37244.64	$4d^45s\ ^6D_{5/2} - 4d^45p\ ^6D_{7/2}^0$	+0.01	
P	2687.997	5	37191.40	$4d^45s\ ^6D_{5/2} - 4d^45p\ ^6P_{5/2}^0$	+0.07	
P	2701.420	4	37006.61	$4d^45s\ ^6D_{3/2} - 4d^45p\ ^6P_{3/2}^0$	−0.03	y
P	2713.515	2	36841.67	$4d^45s\ ^6D_{5/2} - 4d^45p\ ^6P_{7/2}^0$	+0.08	
H	2723.355	3	36708.56	$4d^45s\ ^6D_{7/2} - 4d^45p\ ^6P_{5/2}^0$	+0.01	He
P	2729.692	2	36623.35	$4d^45s\ ^6D_{5/2} - 4d^45p\ ^6P_{3/2}^0$	+0.08	y
P	2732.887	1	36580.53	$4d^45s\ ^6D_{7/2} - 4d^45p\ ^6D_{5/2}^0$	+0.03	
P	2775.408	7	36020.13	$4d^45s\ ^6D_{9/2} - 4d^45p\ ^6D_{7/2}^0$	−0.03	

* The more accurate grating wave-length measurements of other observers were used for previously reported lines. The intensities are ours. y Vacuum wave-length. x Classified by Meggers and Kiess. y Zeeman effect by Wilhelmy. He Helium line superposed.

appears to be a $^6S-{}^6D_{5/2}{}^0$ transition. These transitions, together with a probable $^6S-{}^6D_{7/2}{}^0$ transition from the hollow cathode data, are given in Table I. The $^6D_{7/2}{}^0$ was previously assigned as $^6D_{9/2}{}^0$ by Meggers and Kiess. The corresponding $^6D-{}^6P^0$ multiplet is given in Table II. The intensities and the $^6P^0$ intervals fit the theoretical expectations as well as is to be anticipated for an element of this atomic number.

Some changes are necessary in the $^6D-{}^6D^0$ multiplet given by Meggers and Kiess, because their $^6D_{7/2}{}^0$ level has been reassigned as $^6P_{7/2}{}^0$, and because the combination of their $^6D_{9/2}{}^0$ term with $^6S_{5/2}{}^0$ has led to reassignment of this term as $^6D_{7/2}{}^0$. A revised $^6D-{}^6D^0$ multiplet is given in Table II. The $^6D_{5/2}{}^0$ and $^6D_{9/2}{}^0$ terms are new; the $^6D_{7/2}{}^0$ term, as noted, is a reassignment. The new and reassigned energy levels are given in Table III. All of the newly classified lines of Mo II are listed in Table IV.

In the course of this study of the molybdenum spectrum, a considerable number of lines were observed which appear to be previously unpublished transitions between levels of Mo I given by Catalán.[5] A list of these lines and their classification is given in Table V. The differences between the observed and calculated wave numbers in Tables IV and V is believed to be in all cases within the tolerance of accuracy of the respective measurements and wave-length standards. The authors are indebted to Professor O. Laporte for discussions of these spectra, and to Dr. H. B. Vincent for cooperation in obtaining the condensed spark spectrum with equipment in his laboratory.

TABLE V. *Classified lines of* Mo I. *This list supplements that of Catalán, reference 5. Lines were classified from levels as given by Catalán authorities as in Table IV.*

AUTHORITY	λ	I	ν	CLASSIFICATION	Δν	NOTES
"	1952.81 (vac.)	1	51209	$a^7S_3 - 49_3{}^0$	+0.80	
"	2026.54 (vac.)	1	49345	$a^7S_3 - 39_3{}^0$	+1.20	
"	2075.05 (vac.)	2	48192	$a^7S_3 - 32_4{}^0$	0	
H	2114.30	0	47281.94	$a^7S_3 - 26_2{}^0$	+0.06	
"	2128.98	0	46956.0	$a^7S_3 - 22_3{}^0$	−0.10	
H	2337.42	0	42969.08	$a^7S_3 - 12_3{}^0$	+0.02	
H	2387.18	0	41877.65	$a^5D_3 - 52_3{}^0$	−0.05	
H	2497.863	0	40022.16	$a^5D_1 - 48_2{}^0$	−0.16	
P	2601.96	1	38421.10	$a^5S_2 - 37_1{}^0$	+0.20	
"	2626.79	0	38057.9	$a^5G_3 - 56_2{}^0$	0	
H	2702.772	0	36988.10	$a^5G_4 - 52_5{}^0$	−0.20	
E	2737.3	1	36521.56	$a^3P_2 - 56_2{}^0$	+0.24	
H	2737.88	1	36513.82	$a^5S_2 - 26_2{}^0$	−0.12	
H	2884.590	0	34656.83	$a^5S_2 - 15_2{}^0$	−0.13	
H	2887.619	0	34620.48	$b^5D_1 - 56_2{}^0$	+0.12	
P	2892.812	3	34558.23	$b^5D_2 - 57_3{}^0$	−0.13	
"	2895.68	2	34524.1	$a^5G_2 - 48_2{}^0$	−0.40	
H	3057.88	3	32692.92	$a^5P_2 - 47_3{}^0$	−0.02	
H	3146.683	1	31770.32	$a^5P_3 - 45_3{}^0$	−0.12	
H	3173.777	0	31499.12	$a^5G_3 - 32_4{}^0$	−0.02	
H	3235.878	0	30894.63	$a^5G_3 - 28_3{}^0$	−0.03	
P	3266.283	1	30607.05	$a^5G_2 - 19_1{}^0$	−0.05	
H	3268.193	0	30589.16	$a^5G_3 - 26_2{}^0$	−0.06	
H	3383.981	3	29542.55	$a^5P_1 - 29_1{}^0$	+0.05	
H	3442.665	0	29039.17	$b^5D_1 - 36_1{}^0$	−0.17	
H	3445.411	2	28955.39	$a^5P_3 - 25_3{}^0$	+0.01	
H	3460.226	1	28891.60	$a^5P_2 - 19_1{}^0$	+0.10	*
P	3475.037	2	28768.47	$a^5P_1 - 19_1{}^0$	+0.13	*
H	3686.575	1	27117.76	$b^5D_1 - 19_1{}^0$	+0.14	*
H	3702.032	0	27004.54	$a^5G_3 - 58_3{}^0$	+0.06	
P	3707.170	2	26967.12	$b^5D_2 - 19_1{}^0$	+0.08	*
H	3885.508	0	25729.40	$a^5G_3 - 10_3{}^0$	+0.10	
E	4006.7	0	24951.17	$b^5D_1 - 14_2{}^0$	−0.37	
H	4078.381	0	24512.64	$a^5P_3 - 11_4{}^0$	+0.06	
H	4222.411	2	23676.46	$a^5P_1 - 9_1{}^0$	+0.14	
H	4981.827	0	20067.37	$b^5D_0 - 3_1{}^0$	−0.17	

* The symbol indicates that Catalán assigned these classifications to the wrong lines because of an arithmetical error of 1000 cm^{-1} in his level $19_1{}^0$.

On the Calculation of Force Fields from Scattering

FRANK C. HOYT AND WILLIAM E. FRYE
Ryerson Physical Laboratory, University of Chicago, Chicago, Illinois
(Received August 5, 1940)

A method is developed for calculating the field which gives an observed scattering under the assumption that the interaction can be represented by a central field and that the phase shifts can be calculated by the WKB approximation. Application to electronic and nuclear scattering is discussed.

FOR those scattering problems in which the interaction can be approximated by a central field, it should be possible to determine the form of the potential function of the field from the observed scattering. A method suggested by one of us[1] is applicable when the calculation can be made classically. It is here extended to the WKB approximation of quantum mechanics and illustrated by applications to electronic and nuclear scattering.

DESCRIPTION OF THE METHOD

When a two-body central field approximation is assumed, the scattering data may be analyzed by the Rayleigh-Faxèn-Holtsmark method to give the phase shifts at infinity of the radial wave functions with respect to those for a reference field (force-free field or Coulomb field). When the wave functions are calculated by the WKB method, the phase shift K_l for an angular momentum $l\hbar$ and an energy ϵ can be written in the form

$$K_l(\epsilon)=\int_a^\infty(\epsilon-u)^{\frac{1}{2}}dx-\int_{a_0}^\infty(\epsilon-u_0)^{\frac{1}{2}}dx. \quad (1)$$

The notation is as follows: $\epsilon=E/E_0$, $x=r(2mE_0)^{\frac{1}{2}}/\hbar$ where E is the energy in the center of gravity system, m the reduced mass, and E_0 is any conveniently chosen reference energy; $u=V(x)/E_0+\lambda^2/x^2$, $u_0=V_0(x)/x^2+\lambda^2/x^2$ where V and V_0 are the potentials for the scattering and reference fields, respectively, and $\lambda^2=l(l+1)$ or $(l+\frac{1}{2})^2$ according to the form judged to give the better WKB approximation. The classical turning point for the effective scattering potential (with inclusion of the centrifugal term) is at $x=a$, and that for the reference field at $x=a_0$. Equation (1) is, strictly speaking, valid only for energies giving a single turning point beyond which $\epsilon-u$ is positive. However, it differs inappreciably from the WKB first approximation for two or more turning points when a is taken as the largest and the intervals between the turning points are sufficiently great. It breaks down completely for energies near the top of a potential barrier.

The problem to be considered here is the determination of $u(x)$ from $K_l(\epsilon)$, and its solution can be made to depend on a simple form of integral equation first discussed by Abel[2] and used by Klein[3] in the determination of the potential curves of diatomic molecules from their band spectra, a problem which resembles the present one in many ways. The integral equation of Abel has the form

$$g(y)=\int_0^y\frac{f'(z)dz}{(y-z)^{\frac{1}{2}}}, \quad (2)$$

and its inversion is

$$f(z)=\frac{1}{\pi}\int_0^z\frac{g(y)dy}{(z-y)^{\frac{1}{2}}}+f(0). \quad (3)$$

The integral equation (1) will now be reduced to the form (2). The two integrals do not converge separately since $u(x)$ and $u_0(x)$ vanish at infinity, but their difference can be reduced to a single integral by changing the variable of integration to $\varphi=(\epsilon-u)^{\frac{1}{2}}$. Let the equations of the potential curves be written, respectively, in the forms $x=x(\varphi)$ and $x=x_0(\varphi)$. Equation (1) is then equivalent to[4]

$$K_l(\epsilon)=\int_0^{\sqrt{\epsilon}}[x_0(\varphi)-x(\varphi)]d\varphi$$

[1] F. C. Hoyt, Phys. Rev. **55**, 664 (1939).

[2] N. H. Abel, (1823), published in *Oeuvres Complètes* (Grøndahl and Søn, Oslo, 1881), Vol. I, p. 11.

[3] O. Klein, Zeits. f. Physik **76**, 226 (1932).

[4] The integrals of $x_0(\varphi)$ and $x(\varphi)$ converge separately only when the corresponding fields fall off at infinity more rapidly than a Coulomb field.

and a further change of variable from φ to u gives

$$K_l(\epsilon)=\int_0^{\epsilon}\frac{x_0(u)-x(u)}{2(\epsilon-u)^{\frac{1}{2}}}du, \qquad (4)$$

which has the Abelian form (2) with $y=\epsilon$, $z=u$ after setting

$$f'(u)=\tfrac{1}{2}[x_0(u)-x(u)], \quad f(0)=0. \qquad (5)$$

The inversion according to Eq. (3) is then

$$f(u)=\frac{1}{\pi}\int_0^{u}\frac{K_l(\epsilon)d\epsilon}{(u-\epsilon)^{\frac{1}{2}}}, \qquad (6)$$

which, together with (5), gives implicitly the effective radial potential for a given value of l.

The procedure used in applying the method is as follows. From values of the phase shift of a given order as a function of the energy from zero to u the integral in Eq. (6) is evaluated graphically for a number of different values of u. The resulting $f(u)$ is then plotted and differentiated graphically, which determines $x_0(u)-x(u)$ by Eq. (5). (The integral is improper and cannot be differentiated under the integral sign.) Since $x_0(u)$ is known analytically, this gives corresponding values of u and x for the effective potential corresponding to the l value used. The centrifugal term λ^2/x^2 is, of course, included in u and must be subtracted to give the true potential. Concordant results for the true potential should result from calculations for different l values.

Two types of reference field are of importance: the force-free field for which $x_0(u)=\lambda/u^{\frac{1}{2}}$ and the Coulomb field for which $x_0(u)=[\eta+(\eta^2+\lambda^2u)^{\frac{1}{2}}]/u$, with $\eta=zz'e^2(m/2E_0)^{\frac{1}{2}}$.

The method as outlined above can be expected to give the potential only in the interval from infinity to an eventual first maximum of the effective potential. For the determination of a point u, x on the curve depends on the phase shift as a function of energy from zero to u, and, as already pointed out, Eq. (1) breaks down near the top of a potential barrier. However, this fact does not necessarily exclude an energy range including a barrier in the actual potential, for the maximum will usually disappear from the effective potential for a sufficiently large l value because of the dominating centrifugal term. An accurate knowledge of the higher order phase shifts is then required, however.

Applications

Scattering of electrons by atoms

To illustrate the possibilities of the method for atomic scattering we have applied it to the scattering of 2- to 10-volt electrons in krypton, using the phase shifts obtained by Voss[5] from a phase shift analysis of the experimental data of Ramsauer and Kollath.[6] The resulting potential is shown in curve A of Fig. 1, and compared with the Hartree fields, with and without correction for polarization, as calculated by Holtsmark.[7] The agreement is better for the corrected Hartree potential, and the discrepancies at low energies may be partly attributable to neglect of exchange effects.

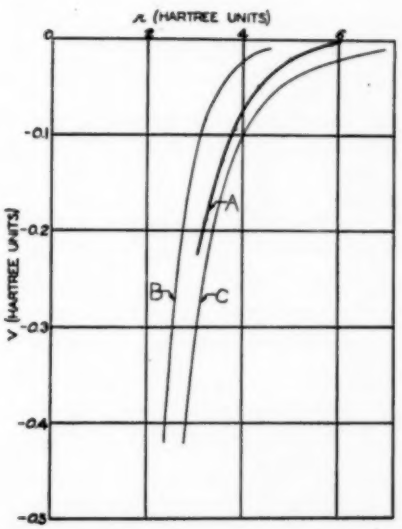

FIG. 1. Potential for the scattering of electrons by krypton. Curve A is calculated from third-order phase shifts deduced from the observed scattering. (The barrier is not removed for $l<3$.) Curves B and C are, respectively, the Hartree potentials for krypton without and with correction for polarization.

Nuclear scattering

Application of the method to nuclei is limited above all by the inadequacy of the central field approximation for the interaction. For s wave scattering of protons by protons, however, there

[5] W. Voss, Zeits. f. Physik **83**, 581 (1933).
[6] C. Ramsauer and R. Kollath, Ann. d. Physik **12**, 837 (1932).
[7] J. Holtsmark, Zeits. f. Physik **66**, 49 (1930).

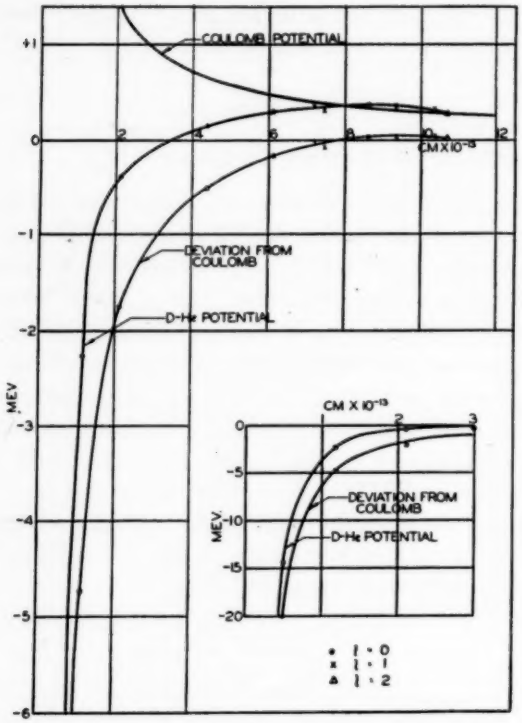

FIG. 2. The helium-deuteron interaction potential calculated from zero-, first- and second-order phase shifts.

seems to be at present no theoretical reason to expect deviations from a central field. Unfortunately we have so far been unable successfully to apply the procedure to this case, for, when the zero-order phase shifts are used, with $\lambda^2=\frac{1}{4}$, negative values of the radius are obtained. This behavior can reasonably be attributed to the occurrence of a potential barrier which is not eliminated by the centrifugal term $\frac{1}{4}x^2$. Of the five proton-proton potentials investigated by Hoisington, Share and Breit,[8] only the meson potential gives a barrier which would not have been eliminated, so that our result may be regarded as affording some slight evidence in favor of the meson potential. The meson potential barrier is removed for $l=1$, but the central field approximation is then doubtful and the p anomalies are not known accurately.

When the central field approximation is acceptable and there is a single turning point, the method can be expected to give fairly accurate results. An indication of the error resulting from use of the WKB approximation was obtained by applying the method with calculations of *exact* phase shifts for a potential $A/x-B/x^2$ made in this laboratory by Mr. S. J. Klapman. This potential, which has the general characteristics of nuclear potentials, was found to be reproduced to within about 2 percent over most of the range for a particular pair of values of A and B, although the error in the WKB phase shifts themselves is much larger than this.

For nuclear scattering processes in which the formation of a compound nucleus is of importance, the present method must be used with extreme caution and will probably prove to have only a limited applicability. Nevertheless it seems of interest to reproduce in Fig. 2 the result which it gives when applied uncritically to the phase shifts calculated by Mohr and Pringle[9] from their experiments on the scattering of α-particles by deuterium. The inner portion of the potential curve is probably without significance, since the central field approximation is certainly not valid in this region. At best the result can be relied on only beyond about 8×10^{-13} cm.

The possibility of application to nuclear scattering processes will be more thoroughly discussed in a second paper.

[8] Hoisington, Share and Breit, Phys. Rev. **56**, 884 (1939).

[9] C. B. O. Mohr and G. E. Pringle, Proc. Roy. Soc. **A160**, 191 (1937).

Products of Ionization by Electron Impact in Methyl and Ethyl Alcohol

CHARLES S. CUMMINGS, II* AND WALKER BLEAKNEY
Palmer Physical Laboratory, Princeton University, Princeton, New Jersey

(Received August 21, 1940)

Fourteen different ions were observed in methyl alcohol and twenty-five in ethyl alcohol. The appearance potentials of many of these were measured and the manner of dissociation in several cases was definitely established. The ionization potentials of the two molecules were found to be 10.8 volts for methyl and 11.3 volts for ethyl alcohol. In all cases subject to unambiguous interpretation that reaction occurred which required the least dissociation energy. The concept of localized charge on the oxygen atom in certain complex ions is supported by the results.

INTRODUCTION

SOME careful investigations have been made in the last few years of the products of ionization resulting from electron collisions in several of the simpler hydrocarbons. Methane was studied by L. G. Smith,[1] acetylene by Tate, P. T. Smith and Vaughan,[2] ethylene by Kusch, Hustrulid and Tate[3] and Delfosse and Hipple,[4] ethane by Hipple,[5] propane, propylene and allene by Delfosse and Bleakney.[6] It is the purpose of this paper to describe some results on methyl and ethyl alcohol, two close relatives of methane and ethane.

The apparatus used in this investigation was a mass-spectrograph which has been only briefly described. A more detailed report on this instrument will appear elsewhere. For the present it will be sufficient to say that this instrument is a demountable, all-metal design which may be baked at elevated temperatures to insure good vacuum conditions. The analyzer is of the familiar 180° type. In principle the apparatus is exactly the same as that in which most of the work in this field has been done. The yield of ions produced by electrons of controllable speed is studied as a function of this speed to determine the minimum energy required to produce an ion of a given type. The details of this procedure may be found in the references already cited.

The method of admitting the gas into the ionization chamber consisted in adjusting the pressure of the alcohol vapor behind a glass capillary leak. The vapor flowed continuously through the leak into the mass spectrograph and out through the pumps. There was some differential of pressure between the ionization chamber and the analyzer maintained by the pumps. It was found that the best stock chemicals were pure enough for the purposes in hand.

The first question which must be studied in an investigation of this kind is whether the ions actually observed are the result of single electron collisions. Several other processes may conceivably occur such as chemical reaction with residual impurities in the apparatus or with the walls, dissociation on the electron emitting filament, ionization through multiple collision or other changes suffered after the first electron impact. In the results to be described we are convinced that, with the possible exception of the mass 28 and mass 12 peaks in methyl alcohol, none of these disturbing processes played an important role. Experiments showed the results to be independent of pressure, electron current and filament temperature under the conditions of operation, and the values of the appearance potentials themselves indicate, as has been amply demonstrated in previous work, that we were observing the effect of single impacts.

It is convenient to represent the appearance potential of an ion as the sum of three quantities: (1) a dissociation energy, (2) an ionization energy, (3) the kinetic and excitational energy carried off by the products of the dissociation.

* Now at the Remington Arms Company, Bridgeport, Connecticut.

[1] L. G. Smith, Phys. Rev. **51**, 4 (1937).
[2] Tate, Smith and Vaughan, Phys. Rev. **48**, 523 (1935).
[3] Kusch, Hustrulid and Tate, Phys. Rev. **52**, 843 (1937).
[4] J. Delfosse and J. A. Hipple, Phys. Rev. **54**, 1060 (1938).
[5] J. A. Hipple, Phys. Rev. **53**, 530 (1938).
[6] J. Delfosse and W. Bleakney, Phys. Rev. **56**, 256 (1939).

This can be expressed algebraically as:

$$A(X^+)=P(X)+I(X)+W(X^+),$$

where: $A(X^+)\equiv$Appearance potential of the ion X^+; $I(X)\equiv$Ionization potential of molecule X; $W(X^+)\equiv$Excess energy (kinetic or excitational) appearing in the production of the ion X^+ from the parent molecule; $P(X)\equiv$Energy to produce neutral X from a parent molecule, all products being in their lowest state. In giving values for $P(X)$ the products as well as X must be stated.

TABLE I. *Heats of dissociation (ev). In all cases where source references are not given, values have been recalculated from data of Bichowsky and Rossini.*[8]

$D(H_2)$	4.48[7]	$D(CH_3)$	10.6[1]	$D(HCHO)$	13.68
$D(OH)$	4.31[7]	$D(C_2H_2)$	12.97	$D(CH_3OH)$	19.01
$D(CH)$	3.47[7]	$D(C_2H_4)$	19.31	$D(C_2H_5OH)$	29.27
$D(CH_4)$	15.16	$D(C_2H_6)$	25.17	$D(CH_3CHO)$	24.23
$D(H_2O)$	9.49[7]	$D(CH_2)$	7.0[1]		

With the present type of instrument there is no way of measuring the kinetic energy of the reaction nor of determining in what excited states the products are left. Hence, when we subtract the calculated dissociation energy from the appearance potential, we obtain a figure that is really $I(X)+W(X^+)$, i.e., an upper limit to the ionization potential. In most cases other evidence shows that $W(X^+)$ is a small quantity.

The calculation of the dissociation energy, and hence the determination of the ionization potential and process of formation, involves thermochemical data. The difficulty here is that practically all the molecules studied so far contain carbon, so that the heat of sublimation of carbon is involved in the thermochemical equations. This quantity is still subject to some uncertainty which is carried over into the calculated heats of dissociation. In this work we have adopted the value $L(C)=5.413$ electron volts as given by Herzberg.[7]

Table I lists the calculated heats of dissociation used in the analysis of the data. The values of the heats of formation involved in the calculations were taken from Bichowsky and Rossini.[8]

[7] G. Herzberg, *Molecular Spectra and Molecular Structure, I. Diatomic Molecules* (Prentice-Hall, Inc., 1939).

[8] F. R. Bichowsky and F. D. Rossini, *Thermochemistry of Chemical Substances* (Reinhold Publishing Corporation, New York, 1936).

Although the reactions induced by electron impact correspond thermochemically to reactions taking place at absolute zero, the correction of the heats of formation to their values at this temperature can be neglected.[1]

Experimental Results

Methyl alcohol

The methyl alcohol vapor was obtained from a bulb that contained several cubic centimeters of liquid alcohol at room temperature. The maximum available pressure behind the leak was the vapor pressure of the alcohol at room temperature. This was, however, more than adequate. After passing through the capillary leak into the mass spectrograph the vapor was subjected to electron bombardment under various conditions of pressure and electron energy and the product ions studied. A summary of the results and their interpretation is given in Tables II and III.

Table IV lists the energies of various combinations of one carbon, one oxygen and four hydrogen atoms with respect to the combination CH_3OH as zero.

Mass 32.—The appearance potential of the ion corresponding to this mass was $A(X^+)=10.8\pm0.2$ volts. This could have been only the molecular ion. Hence the reaction is uniquely determined:

$$CH_3OH\rightarrow CH_3OH^+ + e$$
$$I(CH_3OH)=A(CH_3OH^+)=10.8 \text{ volts}.$$

TABLE II. *Observed relative abundances for electron energy of 70 volts. No negative ions observed.*

Mass	Ion†	Ethyl Alcohol	Methyl Alcohol	Mass	Ion†	Ethyl Alcohol	Methyl Alcohol
46	$C_2H_5OH^+$	100.0		27	$C_2H_3^+$	272.0	
45	$C_2H_5O^+$	242.0		26	$C_2H_2^+$	110.0	
44	CH_3CHO^+	20.0		25	C_2H^+	23.5	
43	CH_3CO^+	56.4		24	C_2^+	4.8	
42	CH_2CO^+	24.4		19	H_3O^+	30.9	trace
41	$CHCO^+$	8.7		17	OH^+	3.9	0.5
40	C_2O^+	1.7		16	$CH_4^+ + O^+$	9.6	2.5
32	CH_3OH^+	11.3	100.0	15	CH_3^+	74.8	64.3
31	CH_2OH^+	986.0	176.0	14	CH_2^+	43.8	10.3
30	$HCHO^+$	56.5	16.1	13	CH^+	17.0	5.2
29	HCO^+	293.0*	134.7	12	C^+	18.7	6.0
29	$C_2H_5^+$			2	H_2^+	30.4	2.8
28	$C_2H_4^+$	390.0**		1	H^+	4.7	5.1
28	CO^+		81.5				

† For the purposes of this table, the designation of the ion is intended to indicate its components and not its structure.

* Either or both HCO^+ and $C_2H_5^+$.

** Appearance potential due to $C_2H_4^+$. Total peak may, however, contain a large fraction of CO^+.

According to Mulliken[9] the oxygen atom in CH_3OH (and also in C_2H_5OH) possesses four nonbonding orbitals, two of which are practically free from mixing and have the lowest ionization potentials of any of the electrons in the molecule. This implies that two of the electrons belong almost exclusively to the oxygen atom itself and are not very much involved in determining the structure of the molecule. Aside from the fact that their ease of removal should be somewhat modified by the fact that they are, after all, part of a molecular system they may be expected to behave very much as though they were outer electrons of a free oxygen atom.

Let us assume that it was one of these electrons that was removed and that the ionization potential of the molecule is the (modified) ionization potential of the oxygen atom and remains constant as long as the structure of the molecule is not radically altered. On this basis we shall assume 10.8 volts to be the energy necessary to remove one of these nonbonding electrons from the oxygen atom in the methyl alcohol molecule. This assumption will be justified by the following results.

Mass 31.—The appearance potential of the ion corresponding to this mass was $A(X^+)$

TABLE III. *Summary of results and interpretations.*

Ion	Appearance Potential: Ethyl Alcohol	Appearance Potential: Methyl Alcohol	Reaction: $C_2H_5OH\rightarrow$	Reaction: $CH_3OH\rightarrow$
$C_2H_5OH^+$	11.3±0.2		$C_2H_5OH^+$	
CH_3CHOH^+	11.0±0.1		CH_3CHOH^++H+e	
CH_3CHO^+	11.4±0.3		$CH_3CHO^++H_2+e$	
CH_2OH^+		10.8±0.2		CH_2OH^+
CH_3OH^+	11.3±0.2	11.8±0.1	$CH_3OH^++CH_3+e$	CH_3OH^++H+e
$HCHO^+$	12.8±0.2	12.4±0.1	$HCHO^++CH_4+e$	$HCHO^++H_2+e$
$C_2H_4^+$	11.3±0.2		$C_2H_4^++H_2O+e$	
$C_2H_3^+$	14.5±0.2		$C_2H_3^++H_2O+H+e$	
$C_2H_2^+$	14.1±0.2		$C_2H_2^++H_2O+H_2+e$	
H_2O^+	14.4±0.3	?		
HCO^+		14.2±0.2		
CH_2^+	15.5±0.3	14.0±0.5		
CH_3^+	16.5±0.5	15.4±0.5		

$=11.8\pm0.1$ volts. If we assume that the hydrogen atom came from the oxygen, the bond energy (dissociation energy) being roughly 4.6 volts,[10] we have the reaction:

$$CH_3OH\rightarrow CH_3O^++H+e,$$

which leads to the equation $I(CH_3O)\leqq 7.2$ volts,

[9] R. S. Mulliken, J. Chem. Phys. **3**, 506 (1935).
[10] N. Sidgwick, *The Covalent Link in Chemistry* (Cornell University Press, 1933).

TABLE IV. *Energies of various combinations of one carbon, one oxygen and four hydrogen atoms with respect to* CH_3OH *as zero. Concerning the accuracy of the various values the following remarks can be made: (1) This value is accurate to within the accuracy of the heat of sublimation of carbon and the heat of formation of methyl alcohol. (2) This is quite rough. It was estimated on the basis of the assumption that the* CH *bonds are, roughly, the same as the corresponding bonds in methane. That is, for the energy to remove this hydrogen atom, the difference between* $D(CH_4)$ *and* $D(CH_3)$ *was used. (3) This was calculated on the basis of the strength of the* O−H *link in alcohol as given by Sidgwick.*[10] *(4) Accurate to within the accuracy of the heat of sublimation of carbon and the heat of formation of formaldehyde. (5) Same as (4) plus* $D(H_2)$. *(6) Estimated in same manner as (2) and hence quite rough. (7) Same as (6) plus* $D(H_2)$.

(1) C+O+4H	19.01 ev	(5) $HCHO+H_2$	0.85 ev
(2) CH_3OH+H	4.56	(6) HCOH+2H	8.16
(3) H_3CO+H	4.60	(7) $HCOH+H_2$	3.68
(4) HCHO+2H	5.33	(8) CH_3OH	0.00

a rather unlikely figure. If it is assumed that the ion results from the breaking of a C−H bond without further change, the situation is equally bad.

There is, however, another alternative. It must be remembered that O^+ is trivalent and that the C−O− in the molecule can become C=O⁺− in the ion, assuming, of course, the localization of the charge on the oxygen atom as discussed above. This allows us to postulate the reaction:

$$CH_3OH\rightarrow CH_2OH^++H+e,$$

where the bond between C and O is now double and is quite consistent with the postulate that the electron removed in the ionization process came from the oxygen atom. Further, the change from single to double bond gives us back some of the energy ordinarily required to break a C−H bond. Using the figure 10.8 volts for the (modified) ionization potential of the oxygen atom as justified in the discussion of mass 32 and basing our calculation on the above reaction, we should be able to estimate the appearance potential of the mass 31 ion and get some idea concerning the reasonableness of our assumptions.

For the difference between the C−O and C=O bonds we shall use the value 3.65 volts.[10] For the energy to break the C−H bond we shall use the value 4.56 volts (Table IV). We then have:

$$A(X^+)_{\text{est}}=10.8+4.56-3.65=11.7 \text{ volts}.$$

This is to be compared with the experimental value of 11.8 volts. The agreement is much better than the accuracy of the data would lead one to expect and for this reason should not be taken too seriously. However, it definitely favors our postulated reaction and the idea of the "independence" and localization of the nonbonding orbital. It may seem remarkable that all this readjustment in the structure of the molecule takes place during the time of a single electron collision, but throughout this investigation the evidence allows no other conclusion. Such phenomena have been suggested before in the case of cyanogen[11] and benzene.[12]

Mass 30.—The appearance potential of the ion corresponding to this mass was $A(X^+)=12.4\pm0.1$ volts. Depending upon whether the two hydrogen atoms are considered to have come from the carbon or one from the carbon and one from the oxygen we have a choice of the following four reactions:

$$(1)\ CH_3OH\rightarrow HCHO^+ + 2H + e$$
$$(2)\ CH_3OH\rightarrow HCHO^+ + H_2 + e$$
$$(3)\ CH_3OH\rightarrow HCOH^+ + 2H + e$$
$$(4)\ CH_3OH\rightarrow HCOH^+ + H_2 + e.$$

The ionized molecule in the first two reactions is of course the formaldehyde molecule. On the basis of the energies given in Table I the following values for the upper limit of the ionization potential are obtained: (1) 7.1 volts, (2) 11.5 volts, (3) 4.3 volts, (4) 8.8 volts. Of these, reaction (2) is the most reasonable. However, to assist in determining the actual reaction, formaldehyde was admitted to the apparatus and its ionization potential measured directly. For this the value 11.4 ± 0.2 volts was obtained. This indicates strongly that reaction 2 was the one that actually occurred. Jewitt[13] has obtained the value 11.3 ± 0.5 volts for the directly measured value of the ionization potential of the formaldehyde molecule. This is in very good agreement with the values reported here.

Mass 19.—This ion was present in sufficient quantity to be detected, but not to allow its appearance potential to be measured. The ion must be identified as H_3O^+. This is in accord with the concept of a trivalent O^+.

Mass 28 and mass 12.—The ions corresponding to these masses must have been CO^+ and C^+, respectively. Changing the gas pressure or the filament temperature over a limited range gave no indication that this was true, but their appearance potentials indicate very strongly that these ions were to some extent produced from free CO due to thermal decomposition of the alcohol on the filament. This is seen from the fact that the observed appearance potentials were 14.0 and 22.6 volts, respectively. For the appearance potentials of CO^+ and C^+ from CO Vaughan[14] gives 13.9 and 22.5 volts, respectively. The agreement is too close to be ignored.

Ethyl alcohol

Vapor of absolute ethyl alcohol was admitted to the apparatus and studied in the same manner as the methyl alcohol discussed above. Time did not permit quite such a thorough investigation of ethyl alcohol. Not all of the appearance potentials were measured, nor of those which were determined was the accuracy as good as in the case of methyl alcohol. However, the most important measurements were made with sufficient accuracy for all those reactions which offered some hope of a unique identification. The results obtained in the case of this molecule are summarized in Tables II and III. The energies of the most important combinations of two carbon, one oxygen and six hydrogen atoms referred to the molecule C_2H_5OH as zero are listed in Table V.

Mass 46.—The appearance potential of this ion was 11.3 ± 0.2 volts. Since this must correspond to the molecular ion we have the unique reaction

$$C_2H_5OH\rightarrow C_2H_5OH^+ + e.$$

This gives $I(C_2H_5OH)=A(C_2H_5OH^+)=11.3$ volts. Following the argument put forth in the discussion of the methyl alcohol molecule we shall assume that ionization represents the removal of a nonbonding electron from the oxygen atom in the molecule and that 11.3 volts is its ionization potential. This is 0.5 volt higher

[11] Bleakney, Condon and Smith, J. Phys. Chem. **41**, 197 (1937).
[12] Hustrulid, Kusch and Tate, Phys. Rev. **54**, 1037 (1938).
[13] T. N. Jewitt, Phys. Rev. **46**, 616 (1934).
[14] A. L. Vaughan, Phys. Rev. **38**, 1687 (1931).

TABLE V. *Energies of various combinations of two carbon, one oxygen and six hydrogen atoms with respect to* C_2H_5OH *as zero. In addition to the uncertainty in the heat of sublimation of carbon the numbered items in this table depend on the following quantities: (1) Heat of formation of ethyl alcohol. (2) Heat of formation of acetaldehyde. (3) Same as (1) plus* $D(H_2)$. *(4) Heat of formation of ethane. (5) Heats of formation of formaldehyde and methane. (6) Heats of formation of ethylene and water. (7) The error here lies chiefly in the value assumed for the strength of the first* C−H *bond in ethylene. It was obtained by interpolation between the heats of dissociation of acetylene and ethylene. (8) Same as (7) plus* $D(H_2)$. *(9) Same as (7) plus* D(OH). *(10) Same as (9) plus* $D(H_2)$. *(11) Same as (7) plus* $D(H_2O)$. *(12) Heats of dissociation of acetylene, water and hydrogen.*

(1) $2C+O+6H$	29.27 ev
(2) $CH_3CHO+2H$	5.04
(3) CH_3CHO+H_2	0.56
(4) C_2H_6+O	4.10
(5) $HCHO+CH_4$	0.43
(6) $C_2H_4+H_2O$	0.47
(7) C_2H_3+O+3H	13.10
(8) $C_2H_3+O+H_2+H$	8.62
(9) $C_2H_3+OH+2H$	8.79
(10) $C_2H_3+OH+H_2$	4.31
(11) $C_2H_3+H_2O+H$	3.61
(12) $C_2H_3+H_2O+H_2$	2.33
(13) C_2H_5OH	0.00

than the corresponding potential in methyl alcohol.

Mass 45.—The ion corresponding to this mass appeared at 11.0±0.1 volts. For the production of this ion we shall assume a reaction analogous to that deduced for the production of mass 31 in methyl alcohol:

$$C_2H_5OH \rightarrow CH_3CHOH^+ + H + e.$$

In a similar manner we should be able to predict an appearance potential for this ion. For the energy to remove the hydrogen atom we shall use the value 2.90 volts assumed to be the strength of the first C−H bond in ethane.[5] For the difference between the C−O and C=O bonds in ethyl alcohol we have the value 3.61 volts.[10] For the ionization potential of the oxygen atom we shall use the value 11.3 volts found for the molecular ion. We then have

$$A(X^+)_{est} = 11.3 + 2.9 - 3.6 = 10.6 \text{ volts.}$$

This is to be compared with the experimental value 11.0 volts and, in view of the roughness of the assumed values for the various bond strengths, can be considered fairly good agreement. Any other mechanism leads to quite unreasonable results.

Mass 44.—The appearance potential of this ion was 11.4±0.3 volts. This is about 3 volts below $I(CO_2)$. The most reasonable assumption is that this peak represents the acetaldehyde ion produced according to one of the reactions:

$$C_2H_5OH \rightarrow CH_3CHO^+ + 2H + e$$
$$C_2H_5OH \rightarrow CH_3CHO^+ + H_2 + e.$$

The first gives us $I(CH_3CHO) \leq 6.4$ volts and the second ≤ 10.7 volts. The latter is a very reasonable value and is in good accord with the values obtained for methyl and ethyl alcohol and formaldehyde as is to be expected from the Mulliken picture.

Mass 31.—The appearance potential of this ion was 11.3±0.2 volts. This was by far the most abundant ion. A straightforward and unique explanation of the nature of this ion and the reaction involved in its production cannot be made. However, on the basis of some not unreasonable assumptions a rather interesting case can be made. Let us assume that the ion is the same as the ion that we have concluded corresponded to mass 31 in methyl alcohol and that the reaction involved is

$$C_2H_5OH \rightarrow CH_2OH^+ + CH_3 + e.$$

On this basis let us try to estimate its appearance potential. Recognizing the fact that the ions are not produced in "steps" we can, nevertheless, for the sake of energy considerations, break this reaction down into the following chain:

(a) $C_2H_5OH \rightarrow CH_3OH + CH_2$
(b) $CH_3OH + CH_2 \rightarrow CH_2OH^+ + CH_2 + H + e$
(c) $CH_2OH^+ + CH_2 + H + e \rightarrow CH_2OH^+ + CH_3 + e.$

The appearance potential will then be the algebraic sum of the energies involved in the three steps. From Table V the energy required for (a) is 3.26 volts. From our data on methyl alcohol the energy required for (b) is 11.8 volts. According to Smith[1] the energy required for (c) is −3.6 volts. Hence:

$$A(X^+) = 11.8 + 3.3 - 3.6 = 11.5 \text{ volts.}$$

This is in very close agreement with the experimental value 11.3 volts. It is scarcely necessary to add, however, that this result simply makes the postulates plausible and is in no sense proof. Some alternative process may exist that will

give just as good agreement, although it is not obvious just what it would be. The low appearance potential demands some way in which energy can be saved as in the formation of the double bond. Any process not based on this concept seems most unlikely.

Mass 30.—This ion appeared at 12.8±0.2 volts. For this mass we have not only a choice of several reactions to produce one ion but also a choice of two ions, namely $C_2H_6^+$ and $HCHO^+$. For the first we have $C_2H_5OH \rightarrow C_2H_6^+ + O + e$. This gives $I(C_2H_6) \leq 8.7$ volts, much lower than the directly measured value 11.6 volts found by Hipple.[5] The only reasonable alternative is that the ion is $HCHO^+$. The only reaction consistent with the value 11.4 volts for the directly measured ionization potential of HCHO is

$$C_2H_5OH \rightarrow HCHO^+ + CH_4 + e.$$

This gives $I(HCHO) \leq 12.4$ volts, and requires an excess energy of about 1 volt.

Mass 28.—The appearance potential of this ion was 11.3±0.2 volts. On the basis of mass this could have been due to either CO^+ or $C_2H_4^+$. The first is at once ruled out, since the directly measured ionization potential of CO is 13.9 volts.[12] The ion must have been $C_2H_4^+$ produced by the reaction

$$C_2H_5OH \rightarrow C_2H_4^+ + H_2O + e.$$

This gives $I(C_2H_4) \leq 10.8$ volts in complete agreement with the directly measured value 10.80 volts.[3]

Mass 27.—The appearance potential of the ion corresponding to this mass was 14.5±0.2 volts. This could have been only the $C_2H_3^+$ ion. The processes by which the ion could have been formed are limited to the following:

(1) $C_2H_5OH \rightarrow C_2H_3^+ + O + 3H + e$
(2) $C_2H_5OH \rightarrow C_2H_3^+ + O + H_2 + H + e$
(3) $C_2H_5OH \rightarrow C_2H_3^+ + OH + 2H + e$
(4) $C_2H_5OH \rightarrow C_2H_3^+ + OH + H_2 + e$
(5) $C_2H_5OH \rightarrow C_2H_3^+ + H_2O + H + e.$

Corresponding to these reactions we have the following upper limits for $I(C_2H_3)$: (1) 1.4 volts, (2) 5.9 volts, (3) 5.7 volts, (4) 10.2 volts, (5) 10.9 volts. The value obtained on the basis of reaction (5) is in very good agreement with the 11.0 volts given by Kusch, Hustrulid and Tate.[3] (The value 11.0 volts given by them was not changed by a recalculation on the basis of the thermochemical data used in the present paper.)

Mass 26.—The appearance potential of the ion corresponding to this mass was 14.1±0.2 volts. This peak must have been due to the acetylene ion $C_2H_2^+$. The only reaction leading to a reasonable ionization potential is:

$$C_2H_5OH \rightarrow C_2H_2^+ + H_2O + H_2 + e.$$

This gives $I(C_2H_2) \leq 11.8$ volts. The directly measured value is 11.2 volts.[2] The extra 0.6 volt can be very reasonably accounted for as excess energy.

Mass 19.—This peak must be identified with H_3O^+. Its appearance potential was 14.4±0.3 volts. Because of the great number of possible configurations involved and our lack of accurate data concerning the energies of most of them, no inference can be made as to the reaction responsible for the production of this ion.

Conclusion

The work reported here can be summarized briefly in the following way.

Ions were produced from methyl and ethyl alcohol by electron impact and their abundances and appearance potentials measured. In all cases subject to analysis the reactions giving the most reasonable interpretations were those requiring the lowest dissociation energy. The concept of "localized" ionization and the nonmixing of the nonbonding orbitals is supported by the results obtained from these substances. In fact, unless this picture is adopted we are led to unreasonably low ionization potentials and very unsatisfactory interpretations of the results.

In conclusion we should like to express our appreciation to Mr. Ralph Osborne for construction of the apparatus and to the Research Corporation for financial assistance.

The Directional Dependence of Electrical Conductivity*

E. M. Baroody†
Cornell University, Ithaca, New York
(Received July 23, 1940)

An attempt is made to apply the theory of conductivity to the question of directional dependence. The first section reviews the usual theory, developing the basic equations in the somewhat generalized form necessary for the problem. The next section discusses the nature of the electron-lattice interaction in some detail. This seems desirable since a number of very significant points—notably the polarization of the lattice waves, and the role of strictly transverse waves when these actually occur—seem to have received much too causal attention in the past. In a third section the directional dependence is calculated for several simple models. No very serious attempt is made to relate the theoretical results with experimental data.

Introduction

THE conductivity of a general metallic crystal is adequately specified when conductivities along three principal conductivity axes are given. This means that the conductivity is completely described by a second-order symmetric tensor, and that by proper choice of axes this tensor can be diagonalized. The effect of an arbitrary electric field may be determined by considering the components along the principal axes. Each component of the current density is obtained by multiplying the field component by the appropriate conductivity. In general, of course, the resultant current is not in the direction of the field.

What has been said indicates that the conductivity of a cubic crystal is isotropic, an anisotropy first entering for tetragonal, hexagonal and trigonal crystals. These have two principal conductivities—parallel and perpendicular to the axis of maximum symmetry. The directional dependence of the conductivity can be indicated by the ratio of these two. For some common metals at room temperature:

$$\sigma_{\parallel}/\sigma_{\perp}=1.21\ (\text{Mg});\quad 0.93\ (\text{Zn});\quad 0.83\ (\text{Cd});\quad 0.69\ (\text{Sn}).$$

The first three are hexagonal close-packed; the last is tetragonal.

The general equations of the theory of conductivity include the factors from which the directional dependence arises, but, since in most applications this dependence is not of interest, simplifying assumptions are introduced which lead to an isotropic result. In the present investigation it is proposed to return to the general equations and consider the way in which anisotropy enters for certain models. Some attention will be given to application to real metals, but it will be seen that any serious attempt to make such application is premature.

(1) General Theory[1]

A calculation of the conductivity requires the determination of the slight modification produced in the distribution function of the electrons by an external field. The modified distribution may be assumed to be:

$$f(\mathbf{K})=f_0(E)+g(\mathbf{K}). \tag{1}$$

This gives the probability that the state $\mathbf{K}$ in wave vector space is occupied. In the absence of the field it reduces to the Fermi function, $f_0(E)$. The assumed distribution is more definitely determined by substitution into the stationary state equation:

$$\left(\frac{\partial f}{\partial t}\right)_{\text{lattice}}=+\frac{e}{\hbar}\frac{df_0}{dE}\operatorname{grad}_K E\cdot\mathbf{F}, \tag{2}$$

which states that the distribution is unchanging, the effect of the external field, $\mathbf{F}$ being just balanced by transitions arising from the interaction of the electrons with the lattice.

The effect of the electron lattice interaction is

* This report is based upon the thesis submitted by the author to the faculty of the Graduate School of Cornell University for the degree of Doctor of Philosophy.

† Now at North Dakota Agricultural College, Fargo, N. D.

[1] This section is based on the treatment of Sommerfeld and Bethe (*Handbuch der Physik*, Vol. 24/2). Very slight modifications have been made to fit the treatment to the present purpose.

calculated by the usual perturbation methods. The probability that $\mathbf{K}'$ is occupied at some finite time as a result of the transition $\mathbf{K}\rightarrow\mathbf{K}'$, $\mathbf{K}$ having been occupied and $\mathbf{K}'$ empty at zero time is:

$$\frac{|U(\mathbf{K},\mathbf{K}')|^2}{\hbar^2}\Omega(x) \equiv \frac{|U(\mathbf{K},\mathbf{K}')|^2}{\hbar^2}\frac{2[1-\cos(xt/\hbar)]}{(x/\hbar)^2}. \quad (3)$$

Here: $x=E_{K'}-E_K\pm\hbar\omega$ ($\hbar\omega$ is the energy of the lattice quantum involved), and $U(\mathbf{K},\mathbf{K}')$ is the matrix element of the perturbation. (Departure of the lattice potential, $V(\mathbf{r})$ from periodicity.)

The probable transitions are those in which energy is conserved and for which:

$$\mathbf{K}'=\mathbf{K}\pm\mathbf{q}+2\pi\mathbf{g}. \quad (4)$$

$\mathbf{q}$ is the propagation vector of the lattice wave; $\mathbf{g}$ a vector in the reciprocal lattice. The plus sign corresponds to absorption of a lattice quantum; the negative to emission. The matrix element to be associated with a given transition is:

$$U(\mathbf{K},\mathbf{K}')=\left(\frac{N_{qj}+1}{2M\omega_{qj}}\right)^{\frac{1}{2}}K_j \quad \text{(emission)}$$
$$\text{or } U(\mathbf{K},\mathbf{K}')=\left(\frac{N_{qj}}{2M\omega_{qj}}\right)^{\frac{1}{2}}K_j \quad \text{(absorption)}. \quad (5)$$

(j indicates the polarization of the lattice wave.)

$$N_{qj}=(\exp[\hbar\omega_{qj}/kT]-1)^{-1} \quad (6)$$

gives the probability that the wave is excited.

$$K_j=\int_{\text{unit cell}} u_K(\mathbf{r})(\partial V/\partial s_j)u_{K'}^*(\mathbf{r})d\tau, \quad (7)$$

$\partial V/\partial S_j$ being the component of grad V in the direction of polarization of the wave, and $u_K(\mathbf{r})$ the periodic part of the electron wave function.

The contribution to $(\partial f(\mathbf{K})/\partial t)_{\text{lattice}}$ arising from interaction with states of higher energy is:

$$\sum_{K',j}\frac{K_j^2\Omega(E_K-E_{K'}+\hbar\omega_{qj})}{2\hbar^2M\omega_{qj}}\{(N_{qj}+1)f(\mathbf{K}')(1-f(\mathbf{K}))-N_{qj}f(\mathbf{K})(1-f(\mathbf{K}'))\}, \quad (8)$$
$$\mathbf{K}-\mathbf{K}'=\pm\mathbf{q}.$$

The $\mathbf{K}'$ summation may be replaced by an integral if we introduce:

$$\text{Density of states}=1/8\pi^3,$$
$$\text{Volume element}=(dE_{K'}/|\text{grad}_{K'}\,E|)dS', \quad (9)$$

where dS' is an element of area lying in the constant energy surface. As is always the case in this type of problem the energy integration can be carried out. One finally has for $(\partial f/\partial t)_{\text{lattice}}$ due to exchange of electrons with states near $\mathbf{K}'$ of higher energy:

$$\frac{K_j^2dS'}{8\pi^2\hbar M\omega_{qj}|\text{grad}_{K'}\,E|}\{(N_{qj}+1)f(\mathbf{K}')(1-f(\mathbf{K}))-N_{qj}f(\mathbf{K})(1-f(\mathbf{K}'))\}, \quad (10)$$
$$E_{K'}=E_K+\hbar\omega_{qj}.$$

The interaction with states of lower energy leads to a similar expression:

$$\frac{K_j^2dS'}{8\pi^2\hbar M\omega_{qj}|\text{grad}_{K'}\,E|}\{N_{qj}f(\mathbf{K}')(1-f(\mathbf{K}))-(N_{qj}+1)f(\mathbf{K})(1-f(\mathbf{K}'))\}, \quad (11)$$
$$E_{K'}=E_K-\hbar\omega_{qj}.$$

At *high temperatures* ($T\gg\theta_D$), $\hbar\omega_{qj}/kT\ll1$ for all lattice waves, so that:

$$N_{qj}\doteq N_{qj}+1\doteq kT/\hbar\omega_{qj} \text{ and } f(\mathbf{K}'), \text{ at } E_K+\hbar\omega_{qj}\doteq f(\mathbf{K}'), \text{ at } E_K-\hbar\omega_{qj};\ f_0(E_K)\doteq f_0(E_K\pm\hbar\omega_{qj}). \quad (12)$$

Both emission and absorption terms simplify and when combined lead to the following condition for the stationary state:

$$\frac{kT}{4\pi^2M\hbar^2}\int_{S'}\sum_j\left(\frac{K_j}{\omega_{qj}}\right)^2\{g(\mathbf{K}')-g(\mathbf{K})\}\frac{dS'}{|\text{grad}_{K'}\,E|}=\frac{e}{\hbar}\frac{df_0}{dE}\text{grad}_K\,E\cdot\mathbf{F}. \quad (13)$$

The substitution:

$$g(\mathbf{K}) = -(df_0/dE)g(\vartheta, \varphi) \tag{14}$$

is convenient. Here $g(\vartheta, \varphi)$ is independent of the energy, ϑ and φ being coordinates which fix the point on a surface of constant energy in K-space. For present purposes the high temperature equation can be written:

$$\int_{S'} \Sigma_j \left(\frac{K_j}{\omega_{qj}}\right)^2 \{g(\vartheta', \varphi') - g(\vartheta, \varphi)\} \frac{dS'}{|\text{grad}_{K'} E|} = \text{constant} \frac{\partial E}{\partial K_{\text{field}}}. \tag{15}$$

At *low temperatures* ($T \ll \theta_D$), $\hbar\omega_{qj}/kT \gg 1$ for most lattice waves. The energy difference between initial and final states is important and specific values of N_{qj} and $N_{qj}+1$ must be considered. $(\partial f/\partial t)_{\text{lattice}}$ is found to be proportional to:

$$\frac{1}{|\text{grad}_K E|} \Sigma_j \int_0^{q_{\max}} dq \int_0^{2\pi} d\beta \frac{N_{qj} C_j^2 q^3}{\omega_{qj}} \{g(\vartheta', \varphi') - g(\vartheta, \varphi)\} \{f_0(E+\hbar\omega)e^{\hbar\omega/kT} + f_0(E-\hbar\omega)\}. \tag{16}$$

Since only small q are significant, K_j has been taken proportional to q ($K_j = C_j q$) (justification later) and $dS = q dq d\beta$ where β is the azimuthal angle of a polar coordinate system with axis along $\text{grad}_K E$.

It is desirable to expand in powers of q the difference entering the stationary state equation. The linear term is found to give zero on integration over β, so that the approximation is:

$$g(\vartheta', \varphi') - g(\vartheta, \varphi) \doteq q^2 \delta(\vartheta, \varphi, \beta). \tag{17}$$

It is convenient in the low temperature calculations to treat ω as the independent variable rather than q. Since for low frequencies q is proportional to ω, this can be done by setting:

$$q_j(\omega, \Theta, \Phi) = F_j(\Theta, \Phi)\omega/\bar{u}_j, \tag{18}$$

where $\bar{u}_j$ is an average velocity of the lattice wave of polarization j, and $F_j(\Theta, \Phi)$ takes into account the dependence of the velocity on the direction of propagation. Further, the range of the ω (or q) integral may be extended indefinitely. Finally the double integral becomes:

$$\int_0^\infty \frac{f_0(E+\hbar\omega)e^{\hbar\omega/kT} + f_0(E-\hbar\omega)}{e^{\hbar\omega/kT} - 1} \omega^4 d\omega \int_0^{2\pi} \Sigma_j \left(\frac{C_j F_j^3}{\bar{u}_j^3}\right)^2 \delta(\vartheta, \varphi, \beta) d\beta. \tag{19}$$

In the approximation used here the second integral does not depend on the energy. Its value is to be determined for $E = \zeta$. With $E = \zeta$, the first integral may be easily evaluated. This brings in the T^5 variation of the resistance, but is of no particular interest here. For present purposes the stationary state equation can be written:

$$\int_0^{2\pi} \Sigma_j \left(\frac{C_j F_j^3}{\bar{u}_j^3}\right)^2 \delta(\vartheta, \varphi, \beta) d\beta = \text{constant} \left(|\text{grad}_K E| \frac{\partial E}{\partial K_{\text{field}}} \right)_{E=\zeta}. \tag{20}$$

Solutions of the equations

If one assumes (1) that the surfaces of constant energy are spheres, and (2) that the "interaction function" ($\Sigma_j (K_j/\omega_{qj})^2$ or $\Sigma_j (C_j F_j^3/\bar{u}_j^3)^2$) does not depend on the direction of propagation of the lattice wave the stationarity equations are readily solved. It is found that the modification in the distribution function is proportional to the cosine of the angle between **K** and the electric field, and that the coefficient does not depend on the direction of the field. This means that the distribution is shifted bodily without distortion, and that the amount of the shift is independent of the field direction. If either assumption fails, the solution becomes more complicated. The center of gravity of the distribution is shifted and the shape slightly altered, both the magnitude of the shift and the nature of the distortion depending on the direction of the field. In Section (3) the equations will be solved for several simple models.

Calculation of the current from the distribution function

The current density in the zth direction is:

$$j_z=\frac{2e}{8\pi^3\hbar}\int_0^\infty -\frac{df_0}{dE}dE\int_S \frac{g(\vartheta,\varphi)(\partial E/\partial K_z)}{|\mathrm{grad}_K E|}dS. \tag{21}$$

The functions in the second integral are all taken independent of E and written for $E=\zeta$, since the integrand in the first integral has a sharp maximum at this value. Evaluating the first integral:

$$j_z=\frac{e}{4\pi^3\hbar}\int_S \frac{g(\vartheta,\varphi)(\partial E/\partial K_z)}{|\mathrm{grad}_K E|}dS. \tag{22}$$

For a metal with general axial symmetry and a spherical Fermi surface of radius K this gives:

$$j_{\|}=\frac{eK^2}{2\pi^2\hbar}\int_0^\pi g(\vartheta)\cos\vartheta\sin\vartheta d\vartheta$$

(field parallel to axis) (23)

$$j_\perp=\frac{eK^2}{4\pi^3\hbar}\int_0^{2\pi}d\varphi\int_0^\pi d\vartheta g(\vartheta,\varphi)\sin^2\vartheta\cos\varphi.$$

(field perpendicular to axis).

If the energy depends on the wave vector as:

$$E(\mathbf{K})=\zeta\left(\frac{K_x^2+K_y^2}{a^2}+\frac{K_z^2}{c^2}\right), \tag{24}$$

we get an ellipsoidal Fermi surface:

$$(K_x^2+K_y^2)/a^2+K_z^2/c^2=1, \tag{25}$$

which may be represented parametrically:

$$K_x=a\sin\vartheta\cos\varphi,\quad K_y=a\sin\vartheta\sin\varphi,\ K_z=c\cos\vartheta.$$

(ϑ is the usual parametric angle—not the polar angle. In the limiting case of the sphere the distinction disappears.) For this ellipsoid:

$$dS=a\sin\vartheta(a^2\cos^2\vartheta+c^2\sin^2\vartheta)^{\frac{1}{2}}d\vartheta d\varphi \tag{26}$$

$$\partial E/\partial K_x=(2\zeta/a)\sin\vartheta\cos\varphi,\quad \partial E/\partial K_y=(2\zeta/a)\sin\vartheta\sin\varphi,\quad \partial E/\partial K_z=(2\zeta/c)\cos\vartheta, \tag{27}$$

so that for field along z:

$$j_{\|}=\frac{ea^2}{2\pi^2\hbar}\int_0^\pi g(\vartheta)\cos\vartheta\sin\vartheta d\vartheta, \tag{28}$$

while for field along x:

$$j_\perp=\frac{eac}{4\pi^3\hbar}\int_0^{2\pi}d\varphi\int_0^\pi d\vartheta g(\vartheta,\varphi)\sin^2\vartheta\cos\varphi. \tag{28'}$$

In addition to altering $g(\vartheta,\varphi)$, the change in the form of $E(\mathbf{K})$ causes the electron velocity to vary with position on the Fermi surface, multiplying $\sigma_{\|}/\sigma_\perp$ by the factor a/c.

(2) Electron Lattice Interaction

This section considers in some detail the nature of the interaction functions:

$$\begin{array}{ll}\sum_j(K_j/\omega_{q_j})^2 & \text{(high temperatures),}\\ \sum_j(C_jF_j^3/\bar{u}_j^3)^2 & \text{(low temperatures).}\end{array} \tag{29}$$

This seems advisable since the published work in explicit calculations treats only spherical distributions and spherically symmetric wave functions, and assumes that the lattice waves can be treated as longitudinal and transverse. If this assumption is false the sum over three lattice waves must be retained in any case. If, further, general wave functions are admitted, even strictly transverse waves have importance. It is found in what follows that for the hexagonal metals at low temperatures, it is this last point which is significant. That is, the elastic waves are found to be essentially longitudinal and transverse, but both types contribute to the resistance. It seems likely that the transverse waves are the more important for most metals, particularly at low temperatures.

If by use of the wave equation the potential energy is eliminated from K_j [Eq. (7)], the following is obtained:[2]

$$K_j=\frac{\hbar^2}{2m}\mathbf{q}\cdot\int\{2i\,\text{grad}\,u_K+(\mathbf{K}+\mathbf{K}')u_K\}\frac{\partial u_{K'}{}^*}{\partial s_j}d\tau. \tag{30}$$

This simplifies if E is a function of $|\mathbf{K}|$, ($|\mathbf{K}|=|\mathbf{K}'|$), or if u has certain symmetry properties (see below).

$$K_j=\frac{\hbar^2 i}{m}\mathbf{q}\cdot\int\text{grad}\,u_K\left(\frac{\partial u_{K'}}{\partial s_j}\right)d\tau. \tag{30'}$$

In general at low temperatures ($\mathbf{q}$ small, $\mathbf{K}\approx\mathbf{K}'$) it has the form:

$$K_j=\frac{\hbar^2}{m}\mathbf{q}\cdot\int(i\,\text{grad}\,u_K+\mathbf{K}u_K)\frac{\partial u_K}{\partial s_j}d\tau. \tag{30''}$$

"Hexagonal metal"

We here assume that the scattering depends upon:

$$K_j=\frac{\hbar^2 i}{m}qC_j\equiv\frac{\hbar^2 i}{m}q\int\frac{\partial u}{\partial q}\frac{\partial u}{\partial s_j}d\tau, \tag{31}$$

where $\partial u/\partial q$ denotes the component of grad u along $\mathbf{q}$. The assumption implies that u is real and independent of $\mathbf{K}$, and that the second term in the integrand of the matrix element [Eq. (30)] can be neglected.

Let $\mathbf{q}$ make an angle Θ with the hexagonal axis and lie in the $\Phi=0$ plane. The unit polarization vectors are essentially:

$S_1\sim\sin\Theta,$	$0,$	$\cos\Theta$	(longitudinal)
$S_2\sim 0,$	$1,$	0	(transverse $\perp$ plane)
$S_3\sim-\cos\Theta,$	$0,$	$\sin\Theta.$	(transverse in plane)

If we then take $u(\mathbf{r})=u(r,\vartheta)$ we have:

$$\begin{aligned}
C_1&=\int\left\{\cos^2\Theta\left(\frac{\partial u}{\partial z}\right)^2+\sin^2\Theta\left(\frac{\partial u}{\partial x}\right)^2\right\}d\tau=C_z\cos^2\Theta+C_x\sin^2\Theta,\\
C_2&=0,\\
C_3&=\int\sin\Theta\cos\Theta\left\{\left(\frac{\partial u}{\partial z}\right)^2-\left(\frac{\partial u}{\partial x}\right)^2\right\}d\tau=(C_z-C_x)\sin\Theta\cos\Theta.
\end{aligned} \tag{32}$$

[2] See A. Sommerfeld and H. A. Bethe, reference 2, p. 512.

Integrals for p state symmetric about z axis

Let us now calculate the C_j for the wave function:

$$u(r, \vartheta)=v(r)\cos\vartheta. \tag{33}$$

For this function:

$$\frac{\partial u}{\partial x}=\sin\vartheta\cos\vartheta\left\{\frac{\partial v}{\partial r}-\frac{v(r)}{r}\right\}\cos\varphi, \quad \frac{\partial u}{\partial z}=\frac{\partial v}{\partial r}\cos^2\vartheta+\frac{v(r)}{r}\sin^2\vartheta.$$

For a spherical atomic volume the integration over angles can be carried out, giving:

$$C_x=\frac{4\pi}{15}\int\left\{\left(\frac{\partial v}{\partial r}\right)^2+\left(\frac{v}{r}\right)^2-2\frac{\partial v}{\partial r}\frac{v(r)}{r}\right\}r^2dr,$$
$$C_z=\frac{4\pi}{15}\int\left\{3\left(\frac{\partial v}{\partial r}\right)^2+8\left(\frac{v}{r}\right)^2+4\frac{\partial v}{\partial r}\frac{v(r)}{r}\right\}r^2dr. \tag{34}$$

It is to be noted that for this wave function the neglected term in the matrix element vanishes. Also, unless the integral of the cross-term, $(\partial v/\partial r)(v/r)$ is large and negative, $C_z \gg C_x$. Actually this integral should be small since the radial function and its derivative would be expected to change sign alternately. The assumed form of K_j [Eq. (31)] is reasonable then, and the C_j become [cf. Eq. (32)]:

$$C_z\cos^2\Theta, \quad 0, \quad C_z\sin\Theta\cos\Theta. \tag{35}$$

As was to be anticipated the angular dependence of the wave function has given importance to the transverse waves. (If u were a function of φ, C_2 would also be finite.) At low temperatures the scattering depends upon:

$$C_z^2\cos^2\Theta\{\cos^2\Theta(F_1/\bar{u}_1)^6+\sin^2\Theta(F_3/\bar{u}_3)^6\}. \tag{36}$$

Now $\bar{u}_3\approx\bar{u}_1/2$ and $F_1\approx F_3\approx 1$. This means that for a spherical electron distribution the second (transverse) term is more important than the first. At high temperatures the low velocity of the transverse wave exerts less influence since the second rather than the sixth-power enters. It is to be noted that the nature of the approximate matrix element to be used in a calculation would depend very markedly on the shape of the electron distribution since this determines which Θ's are of importance.

Propagation of elastic waves in hexagonal crystals[3]

An investigation of the propagation of plane waves in an elastic medium leads to the following secular equation for the allowed velocities:

$$\begin{vmatrix}(a-\lambda) & h & g\\ h & (b-\lambda) & f\\ g & f & (c-\lambda)\end{vmatrix}=0 \tag{37}$$

$\lambda=\rho u^2$, where ρ is the density of the medium, and $u(\alpha, \beta, \gamma)$, the velocity as a function of the direction cosines of the propagation vector. For tetragonal and hexagonal crystals:

$$\begin{aligned} a&=\alpha^2a_{11}+\beta^2a_{66}+\gamma^2a_{44}, & f&=(a_{13}+a_{44})\beta\gamma,\\ b&=\alpha^2a_{66}+\beta^2a_{11}+\gamma^2a_{44}, & g&=(a_{13}+a_{44})\gamma\alpha,\\ c&=\alpha^2a_{44}+\beta^2a_{44}+\gamma^2a_{33}, & h&=(a_{12}+a_{66})\alpha\beta. \end{aligned} \tag{38}$$

For hexagonal crystals the roots of the secular equation depend only on γ. For these crystals:

$$2a_{66}=a_{11}-a_{12} \tag{39}$$

and expansion of the determinant shows that α and β enter the coefficients of the cubic only in the combination $\alpha^2+\beta^2$. This conclusion can be reached without explicit reference to Eq. (39) by turning directly to symmetry considerations. The coefficients in the cubic show complete or tetragonal symmetry about the unique axis. Hexagonal symmetry is achieved only by *removal* of the tetragonal terms. Without loss of generality waves propagated in the $\Phi=0$ plane may be studied. With $\beta=0$, $\alpha=(1-\gamma^2)^{\frac{1}{2}}$ the

[3] For a discussion of elastic waves in crystals, see K. Forsterling, Ann. d. Physik **61**, 549 (1920). For curves showing the directional dependence of wave velocities in Cd and Zn, see E. Grüneisen and E. Goens, Zeits. f. Physik **26**, 235 (1924). This paper does not give analytical expressions for solutions of the secular equation, however, and arbitrarily labels the waves longitudinal and transverse.

secular equation becomes:

$$\begin{vmatrix} (a_0-\lambda) & 0 & g_0 \\ 0 & (b_0-\lambda) & 0 \\ g_0 & 0 & (c_0-\lambda) \end{vmatrix}=0 \qquad (37')$$

with the roots:

$$\begin{aligned} \lambda_1&=\tfrac{1}{2}(a_0+c_0)+\tfrac{1}{2}[(a_0-c_0)^2+4g_0^2]^{\frac{1}{2}},\\ \lambda_2&=b_0,\\ \lambda_3&=\tfrac{1}{2}(a_0+c_0)-\tfrac{1}{2}[(a_0-c_0)^2+4g_0^2]^{\frac{1}{2}}. \end{aligned} \qquad (40)$$

The polarization of the waves can be determined from the amplitude equations. The first wave is nearly longitudinal, the second strictly transverse, the third nearly transverse.

The directional dependence of the velocity may be approximated by expressions of the form:

$$u_j(\gamma)=\bar{u}_j(1-\alpha_j P_2(\gamma)). \qquad (41)$$

The results shown in Table I are obtained for three common hexagonal close-packed metals.

The above discussion was intended to point out some important aspects of the electron-lattice interaction and to indicate some of the things to be borne in mind if a calculation of an interaction function is attempted. The discussion of elastic waves would have direct applicability only at low temperatures. In addition to playing a part in emphasizing the importance of transverse waves, the calculation can provide the basis of an estimate of directional dependence in the conductivity brought about by anisotropy in the lattice vibrations alone. This will be mentioned again in (3, b).

(3) Directional Dependence for Certain Models

(a) Ellipsoidal constant energy surfaces

We treat here a model characterized by an isotropic interaction function and the energy function of Eq. (24):

$$E(\mathbf{K})=\zeta\left(\frac{K_x^2+K_y^2}{a^2}+\frac{K_z^2}{c^2}\right).$$

Table I. *Values of* $\bar{u}$ *(in units of* 10^5 *cm/sec.) and* α *for* Mg, Zn, *and* Cd.

	$\bar{u}_1$	$\bar{u}_2$	$\bar{u}_3$	α_1	α_2	α_3
Mg	5.7	3.1	3.2	0.00	0.00	0.00
Zn	4.34	2.80	2.12	0.19	0.14	0.14
Cd	3.17	1.80	1.36	0.23	0.18	0.00

From the relations (26) and (27) it is seen that:

$$\frac{dS}{|\mathrm{grad}_K E|}=\frac{a^2c}{2\zeta}\sin\vartheta d\vartheta d\varphi,$$

so that the *high temperature* equations are:

$$\int_{-1}^{+1}\{g(\eta')-g(\eta)\}d\eta'=G\frac{\eta}{c} \qquad (42)$$

(parallel field)
(η has been written for $\cos\vartheta$)

and

$$\int_0^{2\pi}d\varphi'\int_{-1}^{+1}d\eta'\{g(\eta',\varphi')-g(\eta,0)\}=2\pi G\frac{(1-\eta^2)^{\frac{1}{2}}}{a}. \qquad (42')$$

(perpendicular field—along $\varphi=0$).

These have the very simple solutions:

$$-(G/2c)\eta, \quad -(G/2a)(1-\eta^2)^{\frac{1}{2}}\cos\varphi, \qquad (43)$$

corresponding to the conductivity ratio:

$$\sigma_{\parallel}/\sigma_{\perp}=(a/c)^2. \qquad (44)$$

This is just the result implied in the discussion of the "effective number of free electrons" by Mott and Jones.[4] Its simplicity is associated with the fact that the problem can be treated without specific reference to the exclusion principle in terms of a surface density of states, $dS/8\pi^3|\mathrm{grad}_K E|$, giving the number of states of energy between E and $E+dE$ in the neighborhood of the element dS of the Fermi surface. This treatment is possible because the breadth of the Fermi surface ($\sim kT$) is large compared to the energy of all scattering quanta. At low temperatures the exclusion principle plays a more positive role. The directional dependence no longer arises only from variations in the velocity and effective mass of the electrons.

In treating the low temperature case it is convenient to write the condition for the stationary state as a differential equation. The function $\delta(\vartheta,\varphi,\beta)$ which was introduced in Eq. (17) is the second-degree coefficient in a Taylor expansion of $g(\vartheta',\varphi')$ in terms of q. When the interac-

[4] N. F. Mott and H. Jones, *Theory of Metals and Alloys* (Oxford, 1936), p. 96.

tion function is assumed independent of the direction of $\mathfrak{q}$, integration over β leads to the Laplacian of $g(\vartheta, \varphi)$ for the ellipsoid. The differential equations are:

$$\frac{1}{a\sin\vartheta(a^2\cos^2\vartheta+c^2\sin^2\vartheta)^{\frac{1}{2}}}\frac{\partial}{\partial\vartheta}\left(\frac{a\sin\vartheta}{(a^2\cos^2\vartheta+c^2\sin^2\vartheta)^{\frac{1}{2}}}\frac{\partial g}{\partial\vartheta}\right)+\frac{1}{a^2\sin^2\vartheta}\frac{\partial^2 g}{\partial\varphi^2}$$

$$=\text{constant}\,\frac{(a^2\cos^2\vartheta+c^2\sin^2\vartheta)^{\frac{1}{2}}}{ac}\times\begin{cases}\cos\vartheta/c\ (\|)\\ \sin\vartheta/a\ (\perp).\end{cases}\tag{45}$$

Nearly spherical distribution.—

$$a/c=1+\epsilon\quad|\epsilon|\ll 1.\tag{46}$$

The equations for the stationary state in terms of $\eta=\cos\vartheta$ to first order in ϵ are:

$$\frac{\partial}{\partial\eta}\left((1-\eta^2)\frac{\partial g}{\partial\eta}\right)+\epsilon\left\{\frac{1-3\eta^2}{3}\frac{\partial}{\partial\eta}\left((1-\eta^2)\frac{\partial g}{\partial\eta}\right)+\frac{\partial}{\partial\eta}\left((1-\eta^2)^2\frac{\partial g}{\partial\eta}\right)\right\}=-\frac{D}{M}\eta\left\{1+\epsilon\left(\frac{3\eta^2+1}{3}\right)\right\}$$

and

$$\frac{\partial}{\partial\eta}\left((1-\eta^2)\frac{\partial g}{\partial\eta}\right)+\frac{1}{1-\eta^2}\frac{\partial^2 g}{\partial\varphi^2}+\epsilon\left\{\frac{1-3\eta^2}{3}\frac{\partial}{\partial\eta}\left((1-\eta^2)\frac{\partial g}{\partial\eta}\right)+\frac{\partial}{\partial\eta}\left((1-\eta^2)^2\frac{\partial g}{\partial\eta}\right)-\frac{2}{3(1-\eta^2)}\frac{\partial^2 g}{\partial\varphi^2}\right\}$$

$$=-\frac{D}{M}(1-\eta^2)^{\frac{1}{2}}\left(1+\epsilon\frac{3\eta^2-2}{3}\right).\tag{47}$$

Solutions to first order in ϵ are:

$$\begin{aligned}&D\eta(1+\tfrac{2}{3}\epsilon\eta^2)/2M,\\ &D(1-\eta^2)^{\frac{1}{2}}(1+(\epsilon/3)(2\eta^2-1))\cos\varphi/2M.\end{aligned}\tag{48}$$

The ratio of conductivities is:

$$\frac{\sigma_{\|}}{\sigma_{\perp}}=\frac{a}{c}\cdot\frac{1+2\epsilon/5}{1-\epsilon/5}=1+\frac{8\epsilon}{5}=\left(\frac{a}{c}\right)^{1.6}\tag{49}$$

(slightly closer to unity than the corresponding ratio at high temperatures).

Very flat ellipsoid.—

$$a/c\gg 1.\tag{50}$$

We are here concerned with the equation:

$$\Delta g=\text{const.}\,|\text{grad}_K E|\,\partial E/\partial K_{\text{field}},\tag{51}$$

where Δ is the Laplacian for a very flat ellipsoid of revolution. For points away from the edges of the distribution ($\tan\vartheta\ll a/c$) the equation can be written:

$$\frac{\partial^2 g}{\partial K_x^2}+\frac{\partial^2 g}{\partial K_y^2}=\text{constant}\,\frac{\partial E}{\partial K_z}\frac{\partial E}{\partial K_{\text{field}}}.\tag{52}$$

For parallel field this becomes:

$$\frac{1}{\rho}\frac{\partial}{\partial\rho}\left(\rho\frac{\partial g}{\partial\rho}\right)=\mp\frac{A}{a^2c^2}(a^2-\rho^2);\quad\rho^2=K_x^2+K_y^2=a^2\sin^2\vartheta.\tag{53}$$

(sign changes when ϑ goes through $\pi/2$)

The solution which is well-behaved at $\rho=0$ and vanishes at $\rho=a$ is:

$$g(\rho)=(\pm A/16a^2c^2)(a^2-\rho^2)(3a^2-\rho^2).\tag{54}$$

This is the significant solution of the stationary state equation for parallel field. Its range of validity covers most of the distribution, and includes the region where $g(\rho)$ and the contribution of a given electron to the current are large. It is incorrect only in the exact way in which it goes to zero near the edges of the ellipsoid.

For perpendicular field the ρ equation for $\tan\vartheta \ll a/c$ has the form:

$$\frac{1}{\rho}\frac{\partial}{\partial\rho}\left(\rho\frac{\partial g}{\partial\rho}\right)-\frac{g(\rho)}{\rho^2}=\frac{A}{a^3c}(a^2-\rho^2)^{\frac{1}{2}}\rho. \tag{53'}$$

(complete solution $g(\rho)\cos\varphi$)

The function:

$$\frac{Aa}{15c}\frac{(1+x^2)-(1-x^2)^{5/2}}{x};\quad x=\rho/a \tag{54'}$$

is a solution and satisfies the required boundary conditions (behaves like x for small x, and has a derivative which vanishes at $x=1$).

Since for perpendicular field $g(\rho)$ and the contribution to the current from a given electron are greatest near the edge of the ellipsoid, it seems advisable to investigate the behavior of g for large $\tan\vartheta$. By introducing $y=\cos\delta$ (δ being the angle between the normal to the ellipsoid and the z axis) a simple equation for the range $\tan\vartheta\approx a/c$ to $\vartheta=\pi/2$ can be obtained:

$$\frac{\partial}{\partial y}\left((1-y^2)\frac{\partial g}{\partial y}\right)-\frac{g(y)}{1-y^2}\left(\frac{c}{a}\right)^4=A\left(\frac{c}{a}\right)^4\frac{1}{(1-y^2)^{\frac{1}{2}}}. \tag{55}$$

Keeping in mind that $c/a\ll 1$, we see that the solution is essentially constant in this range, that is, there is no abrupt change in the behavior of $g(\rho)$ near the edges of the distribution. The solution given above [Eq. (54')] can, therefore, be used for the whole range of θ.

A computation of the conductivity ratio gives:

$$\frac{\sigma_{\parallel}}{\sigma_{\perp}}=\frac{a^4}{24c^2}\Big/\frac{a^2}{20}=\frac{5}{6}\left(\frac{a}{c}\right)^2, \tag{56}$$

slightly smaller than for high temperatures.

(b) Anisotropic interaction function

We now consider the anisotropy in the conductivity when the electron distribution is spherical and the interaction function of the form:

$$M(\Theta)=M_0(1+\mu\cos^2\Theta),\quad |\mu|\ll 1. \tag{57}$$

Low temperatures.—If as before η is written for $\cos\vartheta$, the differences entering the equation for the stationary state are:

Parallel field:

$$g(\eta')-g(\eta)=\frac{\partial g}{\partial\eta}(\delta\eta)+\frac{1}{2}\frac{\partial^2 g}{\partial\eta^2}(\delta\eta)^2. \tag{58}$$

Perpendicular field: (58)

$$g(\eta',\varphi')-g(\eta,0)\approx\frac{\partial g}{\partial\eta}(\delta\eta)+\frac{1}{2}\frac{\partial^2 g}{\partial\eta^2}(\delta\eta)^2+\frac{1}{2}\frac{\partial^2 g}{\partial\varphi^2}(\delta\varphi)^2,$$

where

$$\delta\eta=-\frac{q^2}{2K^2}\eta-\frac{q}{K}\cos\beta(1-\eta^2)^{\frac{1}{2}},\quad \delta\varphi=\frac{q}{K}\frac{\sin\beta}{(1-\eta^2)^{\frac{1}{2}}}.$$

(In the perpendicular equation the terms which would finally give zero on integration over β have been omitted.)

To sufficient approximation:

$$\cos\Theta = -(1-\eta^2)^{\frac{1}{2}}\cos\beta. \tag{59}$$

The differential equations obtained are:

$$\frac{\partial}{\partial\eta}\left((1-\eta^2)\frac{\partial g}{\partial\eta}\right)+\mu(1-\eta^2)\left(\frac{3}{4}(1-\eta^2)\frac{\partial^2 g}{\partial\eta^2}-\eta\frac{\partial g}{\partial\eta}\right)=-\frac{D}{M_0}\eta$$

and

$$\left\{\frac{\partial}{\partial\eta}\left((1-\eta^2)\frac{\partial g}{\partial\eta}\right)-\frac{g(\eta)}{(1-\eta^2)}\right\}+\mu(1-\eta^2)\left\{\frac{3}{4}(1-\eta^2)\frac{\partial^2 g}{\partial\eta^2}-\eta\frac{\partial g}{\partial\eta}-\frac{1}{4}\frac{g(\eta)}{(1-\eta^2)}\right\}=-\frac{D}{M_0}(1-\eta^2)^{\frac{1}{2}}. \tag{60}$$

(complete solution $g(\eta)\cos\varphi$)

For small μ these equations have the solutions:

$$\begin{aligned} g_{\parallel}(\eta) &= (D/2M_0)\eta[1+(\mu/12)(\eta^2-3)], \\ g_{\perp}(\eta) &= (D/2M_0)(1-\eta^2)^{\frac{1}{2}}[1+(\mu/12)(\eta^2-5)]. \end{aligned} \tag{61}$$

Introducing

$$\bar{M}=\int_0^1 M(\cos\Theta)d\cos\Theta = M_0(1+\mu/3), \tag{62}$$

the complete solutions for small μ are:

$$(D/2\bar{M})\eta[1+(\mu/12)(\eta^2+1)],\quad (D/2\bar{M})(1-\eta^2)^{\frac{1}{2}}[1+(\mu/12)(\eta^2-1)]\cos\varphi. \tag{63}$$

The ratio of conductivities is:

$$\frac{\sigma_{\parallel}}{\sigma_{\perp}}=\frac{1+2\mu/15}{1-\mu/15}=1+\frac{\mu}{5}. \tag{64}$$

High temperatures.—The following are stationary state equations for the model at high temperatures:

$$\begin{aligned} \frac{1}{2\pi}\int_0^{2\pi}d\varphi'\int_{-1}^{+1}d\eta'(1+\mu\cos^2\Theta)\{g(\eta')-g(\eta)\} &= -\frac{2D}{M_0}\eta, \\ \frac{1}{2\pi}\int_0^{2\pi}d\varphi'\int_{-1}^{+1}d\eta'(1+\mu\cos^2\Theta)\{g(\eta',\varphi')-g(\eta,0)\} &= -\frac{2D}{M_0}(1-\eta^2)^{\frac{1}{2}}, \end{aligned} \tag{65}$$

where

$$\cos^2\Theta = \tfrac{1}{2}(\eta'-\eta)^2/\{(1-\eta\eta')-(1-\eta^2)^{\frac{1}{2}}(1-\eta'^2)^{\frac{1}{2}}\cos\varphi'\}. \tag{66}$$

Solutions correct to first order in μ.—If the function:

$$B(\eta+bP_3(\eta))$$

is substituted into the parallel equation it becomes (to first order):

$$2\eta+2bP_3(\eta)-\frac{\mu}{2\pi}\int_{-1}^{+1}d\eta'\int_0^{2\pi}d\varphi'(\eta'-\eta)\cos^2\Theta = \frac{2D}{BM_0}\eta.$$

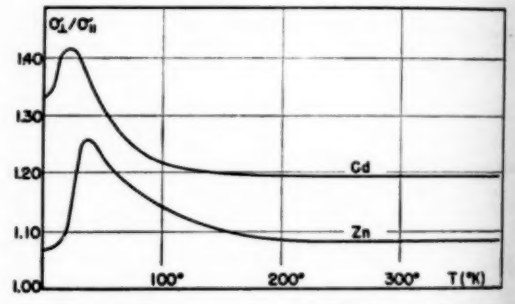

FIG. 1. Variation of $\sigma_{\perp}/\sigma_{\parallel}$ as a function of temperature (data of Grüneisen and Goens).

The φ' integral is:

$$\frac{1}{2}\int_0^{2\pi}\frac{d\varphi'}{(1-\eta\eta')-(1-\eta^2)^{\frac{1}{2}}(1-\eta'^2)^{\frac{1}{2}}\cos\varphi'}=\frac{\pi}{|\eta-\eta'|}.$$

This gives for the μ term:

$$-\frac{\mu}{2}\int_{-1}^{+1}d\eta'\frac{(\eta'-\eta)^3}{|\eta-\eta'|}=\mu\eta(\tfrac{1}{3}\eta^2+1)$$

and the equation becomes:

$$1+\tfrac{1}{2}b(5\eta^2-3)+\tfrac{1}{2}\mu(\tfrac{1}{3}\eta^2+1)=D/BM_0.$$

If we choose:

$$b=-\frac{\mu}{15},\quad B=\frac{D}{M_0}\left(1-\frac{3\mu}{5}\right)=\frac{D}{\bar{M}}\left(1-\frac{4\mu}{15}\right),$$

the equation is solved. The solution:

$$\frac{D}{\bar{M}}\left(1-\frac{4\mu}{15}\right)\left(\eta-\frac{\mu}{15}P_3(\eta)\right)$$

can be written:

$$D/\bar{M}\eta[1-(\mu/6)(\eta^2+1)]. \qquad (67)$$

In a similar way a first-order solution of the perpendicular equation can be obtained:

$$(D/\bar{M})(1-\eta^2)^{\frac{1}{2}}[1-(\mu/6)(\eta^2-1)]\cos\varphi. \qquad (67')$$

These correspond to the conductivity ratio:

$$\frac{\sigma_{||}}{\sigma_\perp}=\frac{1-4\mu/15}{1+2\mu/15}=1-\frac{2\mu}{5}. \qquad (68)$$

It is to be noticed that the ratios for low and high temperatures lie on different sides of unity. Something of this sort might well be expected since entirely different lattice waves may be of importance for the two cases. For example, consider the scattering of electrons near the pole of the distribution. At low temperatures electrons are exchanged directly only with neighboring points on the sphere. Waves traveling at right angles to the symmetry axis are responsible for the transitions. At high temperatures transitions to or from all points of the surface are possible, involving lattice waves propagated in all directions.

If the anisotropy of the interaction function is assumed to arise solely from anisotropy of the lattice waves one has:

$$M(\Theta)=\bar{M}F_1^6(\Theta) \quad \text{(low temperatures)}$$
$$M(\Theta)=\bar{M}F_1^2(\Theta). \quad \text{(high temperatures)}$$

If the anisotropy is assumed small these become:

$$M(\Theta)=\bar{M}(1+6\alpha_1P_2(\cos\Theta))$$
$$M(\Theta)=\bar{M}(1+2\alpha_1P_2(\cos\Theta)),$$

the corresponding μ's being:

$$9\alpha_1 \quad \text{and} \quad 3\alpha_1$$

and the conductivity ratios:

$$\sigma_{||}/\sigma_\perp=1+9\alpha_1/5 \quad \text{(low temperatures)}$$
$$\sigma_{||}/\sigma_\perp=1-6\alpha_1/5. \quad \text{(high temperatures)}$$

The values of α_1 for cadmium and zinc (0.23 and 0.19) are not small enough to justify the use of these expressions except for extremely rough estimates. Results of their use are listed below. For comparison experimental values from data due to Grüneisen and Goens are written alongside in parenthesis.

	Cadmium	Zinc
$\sigma_{||}/\sigma_\perp$	1.41(0.71)	1.34(0.90) (low)
	0.72(0.83)	0.77(0.92) (high).

It is seen that although the calculated values are in accidental agreement with experiment in the high temperature case, the necessity for very serious attention to other sources of anisotropy is indicated by the low temperature data. In this connection we note that magnesium has a rather anisotropic conductivity, while the lattice waves seem to be isotropic at low temperatures.

The value 0.72 for cadmium at high temperatures agrees with that obtained by Houston[8] in an early paper on the theory of conductivity ($\sigma_{||}/\sigma_\perp=1/1.4$). Houston treated the scattering of the electrons by use of an expression derived by Debye for x-rays. This gives the probability of scattering in a given direction in terms of the binding constants of the lattice atoms, these in turn being computed from the elastic constants of the metal.

Further remarks

It is clear that the directional dependence is an essentially complex effect so that it would be futile to make estimates for serious comparison

[8] W. V. Houston, Zeits. f. Physik **48**, 449 (1928).

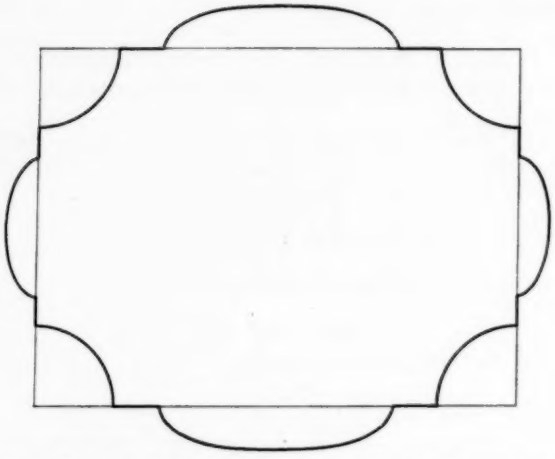

FIG. 2. Suggested distribution of electrons in K space for a metal with a unique axis.

with experiment without having available much more quantitative information than we do about electronic wave functions and energy surfaces for real metals. It is desirable, however, to make some further reference to measurements and to point out more or less how these fit with theoretical ideas. The following data plotted in Fig. 1 for cadmium and zinc are due to Grüneisen and Goens:[6]

	T(°K)	373	273	195	130	82	20
$\sigma_\perp/\sigma_\parallel$	Zinc	1.086	1.082	1.078	1.107	1.170	1.108
	Cadmium	1.189	1.191	1.194	1.200	1.230	1.406

As would be expected the ratio is independent of temperature at high temperatures—each conductivity following the $1/T$ law. (A similar behavior would be expected at low temperatures—each conductivity following the $1/T^5$ law.) As one moves from high to low temperatures a definite fluctuation seems to begin at a point well below the Debye temperature (Zn $\approx$ 235°K, Cd $\approx$ 168°K). This means that the temperature indicating the transition from high to low temperature conditions depends upon the field direction. For a complex distribution there are a variety of reasons for expecting this. For cadmium and zinc the transition evidently begins at a higher temperature for perpendicular field.

The shape of the K space electron distribution is of course very important for the directional effects. Unfortunately little is known at present about the distribution for multivalent metals. In general, however, it is to be expected that the Fermi surface will overlap the first Brillouin zone. A suggested picture for a metal with a unique axis is given in Fig. 2. The overlapping electrons fall into very flat ellipsoids of revolution. At high temperatures transitions between various parts of the distribution would be expected. If overlapping occurred at all places, as indicated, the anisotropy in the conductivity need not be large. At low temperatures the distribution would be equivalent to a number of independent parts, the observed current being the superposition of contributions from various parts. Again a comparatively small anisotropy would be understandable. On the other hand, it is entirely possible that for some metal the conducting electrons might lie principally in a single very flat ellipsoid, so that a large anisotropy would result.

In concluding the report, the author wishes to express his appreciation to Professor Bethe for suggesting the problem, and for many helpful consultations throughout the course of the work.

[6] E. Grüneisen and E. Goens, Zeits. f. Physik **26**, 250 (1924).

Properties of Rochelle Salt. IV [1]

HANS MUELLER
Massachusetts Institute of Technology, Cambridge, Massachusetts

(Received September 12, 1940)

A new class of effects in crystals, called morphic effects, is considered. They arise when elastic strains alter the symmetry of the structure. This necessitates the introduction of new coefficients, proportional to the acting strains, into the matrix of the coefficients which characterize the linear effects. The new coefficients give rise to a series of new quadratic effects in crystal physics. These morphic effects play a role in the photoelasticity of cubic crystals. They are especially large in the crystals of Rochelle salt, where they are responsible for the so-called Kerr effects and a new type of irreversible piezoelectric effects. The existence of this new effect has been verified. It creates irreversible normal strains when the crystal is polarized in the *a* direction, and spontaneous contractions occur when the crystal is cooled to below the Curie point. The spontaneous normal strains are responsible for the anomalous thermal expansion of Rochelle salt and for a series of other anomalies. It is suggested that these strains may also be the cause for the existence of the lower Curie point.

THE KERR EFFECT OF ROCHELLE SALT

IN 1893, in the course of his classical investigation of the relation between the piezoelectric, photoelastic and electro-optical properties of crystals, Pockels[2] discovered in Rochelle salt an irreversible electro-optical effect for electric fields parallel to the *a* axis. In 1930 the writer, unaware of Pockels' work, rediscovered this so-called Kerr effect and, in collaboration with Miss Groat,[3] studied its dependence on field intensity and temperature for various light directions. In contrast to all other crystals, for which the Kerr effect is too small to be observed, the quadratic change of birefringence in Rochelle salt is about a million times larger than the electro-optical double refraction in most liquids. It appears, therefore, improbable that it could be explained on the basis of the Langevin-Born theory for the Kerr effect in gases and liquids, and a lattice theory of the phenomenon cannot be attempted as long as the crystal structure of Rochelle salt is not known. Jaffé[4] has proposed an explanation based on the laws of classical crystal physics. He pointed out that at temperatures between the Curie points the crystal is not rhombic but monoclinic hemimorphic. Crystals of the latter class have, for electric fields in direction of the polar axis, a linear electro-optical effect which gives rise to the same kind of optical changes as are observed in the Kerr effect of Rochelle salt. According to this theory the Kerr effect is really a linear effect. It is not reversed by a reversal of the field because such a reversal also inverts the direction of the polar axis by the process of orientation-twinning. Although the suppositions of Jaffé's theory are correct, his explanation is not adequate, because it implies that the effect should vanish at the Curie points, while actually it is largest at these temperatures and it also exists above the upper Curie point, where the crystal is rhombic. A more satisfactory theory is obtained by the following modification of Jaffé's argument:

For crystals of the rhombic hemiedric class an electric field E_x in the *a* direction produces a linear electro-optical effect which is given by the equations

$$a_{11}=1/n_a^2, \quad a_{22}=1/n_b^2, \quad a_{33}=1/n_c^2,$$
$$a_{23}=r_{41}P_x, \quad a_{31}=a_{12}=0. \qquad (1)$$

n_a, n_b, n_c are the principal refractive indices of the unpolarized crystal, P_x is the electric polarization and r_{41} is an electro-optical constant.[5] The polarization constants a_{ik} determine the

[1] This is the last of a series of four papers on this subject. The previous articles, Phys. Rev. **47**, 175 (1935); **57**, 829 (1940) and **58**, 565 (1940) are referred to as papers I, II and III, respectively.

[2] F. Pockels, Abhand. d. Ges. d. Wiss. zu Göttingen, Math. Phys. Klasse **39**, 1 (1893).

[3] L. M. Groat, M. S. Thesis, 1932. Massachusetts Institute of Technology, see paper I.

[4] H. von R. Jaffé, Phys. Rev. **51**, 43 (1937).

[5] To avoid confusion with the piezoelectric constants e_{ik} we denote the electro-optical constants by r_{ik}, instead of by e_{ik}, as customary after F. Pockels, *Lehrbuch d. Kristalloptik* (Leipzig, 1905).

optical index ellipsoid $\Sigma a_{ik}yz=1$ of the polarized crystal. Equations (1) would be valid for Rochelle salt above the upper Curie point if the piezoelectric effect were small. However, since this effect is unusually large, it becomes necessary to enlarge the classical theory. The piezoelectric action of the field E_x is to create a shearing deformation $y_s=-f_{14}P_x/c_{44}$ (from Eq. (2a), III), which alters the symmetry of the crystal from rhombic hemiedric to monoclinic hemimorphic with the a axis as polar axis. For crystals of the latter class the equations for the linear electro-optical effect, for fields in the a direction[6] are

$$\begin{aligned} &a_{11}-1/n_a^2=r_{11}P_x, \qquad a_{22}-1/n_b^2=r_{21}P_x, \\ &a_{33}-1/n_c^2=r_{31}P_x, \qquad a_{23}=r_{41}P_x, \\ &\qquad a_{31}=a_{12}=0. \end{aligned} \tag{2}$$

Since the appearance of the three new constants r_{11}, r_{21}, r_{31} is the result of the piezoelectric deformation y_s, these parameters are proportional to the strain and, therefore, also to the polarization P_x. Whence $r_{11}=s_1P_x$, $r_{21}=s_2P_x$, $r_{31}=s_3P_x$, and the final equations for the electro-optical effects in Rochelle salt for fields in the a direction take the form

$$\begin{aligned} &a_{11}-1/n_a^2=s_1P_x^2, \qquad a_{22}-1/n_b^2=s_2P_x^2, \\ &\qquad a_{33}-1/n_c^2=s_3P_x^2, \end{aligned} \tag{3a}$$

$$a_{23}=r_{41}P_x, \qquad a_{31}=a_{12}=0. \tag{3b}$$

Equations (3b) describe the ordinary linear electro-optical effect which is observed when the light direction does not coincide with a crystallographic axis. If the light traverses the crystal along the b or c axis only the optical changes described by Eqs. (3a) are observed. They represent an irreversible or quadratic electro-optical effect. Since $a_{11}=1/(n_a+\delta n_a)^2$, where δn_a is the change of the refractive index, the changes of the birefringence are

$$\Delta_a=\delta(n_b-n_c)/\lambda=k_aP_x^2, \tag{4a}$$

$$\Delta_b=\delta(n_c-n_a)/\lambda=k_bP_x^2, \tag{4b}$$

$$\Delta_c=\delta(n_a-n_b)/\lambda=k_cP_x^2, \tag{4c}$$

where $k_a=(n_c^3s_3-n_b^3s_2)/2\lambda$, etc., $k_a+k_b+k_c=0$, and λ is the wave-length of the light. (4b) and (4c) represent the transversal Kerr effects for light traveling in the b or c direction, (4a) gives the longitudinal Kerr effect for light parallel to the field. These equations account for the curious field and temperature dependence of the electro-optical double refraction. From the Curie-Weiss law $\kappa_1=C/(t-t_c)$ and Eq. (3a), III, it follows that for temperatures above the Curie point

$$E_x=P_x(t-t_c)/C+BP_x^3. \tag{5}$$

By substitution of $P_x=(\Delta/k)^{\frac{1}{2}}$, from Eq. (4), we arrive at the empirically verified relation (Fig. 12, I)

$$E_x/\Delta^{\frac{1}{2}}=R(t-t_c)+Q\Delta, \tag{6}$$

where $R=1/Ck^{\frac{1}{2}}$ and $Q=B/k^{\frac{1}{2}}$, whence

$$Q/R^3=BC^3. \tag{7}$$

The experimental values are[7] $k_a=1.7\times10^{-7}$, $k_b=-6.4\times10^{-7}$, $k_c=4.7\times10^{-7}$, $R_b=6.9\pm0.2$, $Q_b=150\pm20$, $R_c=10.1\pm0.2$, $Q_c=307\pm10$. These data give $Q_b/R_b^3=4.5\pm1.0$, $Q_c/R_c^3=3.0\pm0.4$. The latter value is based on more accurate data and agrees quite well with the results of the dielectric measurements which give $C=178$, $B=5.8\pm0.7\times10^{-8}$, whence $BC^3=3.3\pm0.4$. The electro-optical measurements lead therefore to the same value of B as derived in paper III from the dielectric and elastic saturation effects.

Between the Curie points the spontaneous polarization P_x^0 creates a spontaneous Kerr effect $\Delta^0=kP_x^{0^2}$. This gives rise to the anomalous temperature variation of the birefringence near the two Curie points (Figs. 18 and 19, I). The full curve in Fig. 1 presents the observed variation of $(n_a-n_c)/\lambda$ with temperature. By subtracting from these data the values of Δ_b^0, as calculated from k_b and the values of P_x^0 from Table II in paper III, we obtain the dotted curve which represents the change of birefringence of the clamped crystal. This curve has no anomalies at the Curie points, but the slope changes markedly in the range between $-5°$ and 0°C. Although the change is gradual and appears at a somewhat lower temperature than the minimum of the $\chi_1(t)$ curve, we suspect that it is caused by the peculiar type of transition

[6] We follow Jaffé's suggestion of designating the polar axis by a and not by c, as is customary in monoclinic crystals.

[7] From paper I. k is identical with ρf^2. The equation on page 189 of paper I (Phys. Rev. 47) should read $\rho_c f^2=4.7\pm1.0\times10^{-7}$.

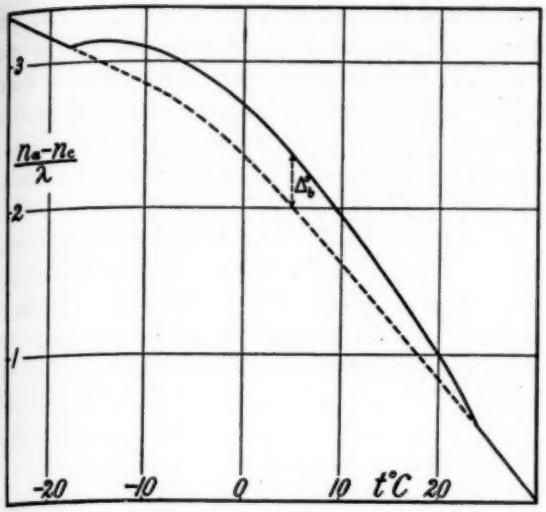

FIG. 1. Temperature dependence of the birefringence of the free crystal (full curve) and the clamped crystal (dotted curve) of Rochelle salt.

which the clamped crystal undergoes in this temperature range.

The irreversible electro-optical effect in the ferroelectric temperature range can be explained, as Jaffé proposed, as a linear effect of the monoclinic structure, but to obtain quantitative agreement with the observations it is necessary to correlate the change of birefringence with the electric polarization, and not with the field E or the inner field F. If the applied field E_x is larger than the coercive field, but not large enough to produce dielectric saturation, one can assume that it changes the polarization from P_x^0 to $P_x^0+\delta P_x$, where $P_x^0 \gg \delta P_x$ and where P_x^0 has the same direction as the applied field. The change of birefringence is, in first approximation,

$$\Delta = k(P_x^0+\delta P_x)^2 - \Delta^0 = 2kP_x^0\delta P_x = 2kP_x^0\kappa_1^0 E_x, \quad (8)$$

where κ_1^0 is the susceptibility of the free crystal in the ferroelectric state. Although P_x^0 vanishes at the Curie points, the Kerr effect does not become zero, because, as was shown in paper III, κ_1^0 increases near these temperatures at the same rate as $1/P_x^{0^2}$. Hence the electro-optical effects are larger at the Curie points than at any other temperature. Theory and observations furnish at the Curie points $\Delta = (E_x/Q)^{\frac{1}{2}}$. At temperatures between, but not too close to the Curie points, Δ is proportional to the field. However, it does not reverse its sign when E_x is reversed, because the product $P_x^0 E_x$ is always positive, except for small fields where the $\Delta(E_x)$ curve represents a quadratic hysteresis loop (Fig. 23, I). In strong fields the change of birefringence tends toward saturation in the same manner as P_x^2. The smallest Kerr effect in the ferroelectric range occurs at the transition temperature of the clamped crystal near 5°C. Since all conclusions agree with the facts there can be little doubt that the fundamental relations (3) are correct. From the values of k, c_{44} and f_{14} one finds by a rough estimate that the electro-optical constants r_{11}, r_{21} and r_{31} reach the same order of magnitude (of about 10^{-7}) as the ordinary constant r_{41} when the shearing strain y_z is of the order of 10^{-3}. This means that, from the phenomenological point of view, a crystal of Rochelle salt must be considered to be monoclinic when the angle between the b and c axes differs from 90° by only a few minutes.

MORPHIC EFFECTS IN CRYSTAL PHYSICS

The above discussion shows that the Kerr effect in Rochelle salt belongs to a new class of effects in crystal physics which, as far as the writer knows, have not been discussed previously[8] and which we propose to call "morphic" effects. They occur when the symmetry of a crystal is altered by elastic strains. The change of symmetry calls for a change in the matrix of the coefficients which determine the linear effects. New coefficients, which were zero in the undeformed crystal, may appear, or coefficients which had originally identical values become different. Morphic effects are of higher order, but their properties can be derived from the theory of the linear effects. They are linear effects with variable coefficients. The theory of these effects is not covered by the theory of the ordinary second order effects (electrostriction, etc.), because, as is seen form the examples given below, the morphic effects do not follow the same laws of superposition which hold for quadratic effects. Since a deformation usually will not create new symmetry elements but rather reduce their number, the morphic effects can not occur in

[8] A similar type of effect for isotropic solids has been considered by L. Brillouin, Proc. Indian Acad. Sci. 8, 251 (1938). The name "morphic" was suggested by Dr. J. F. G. Hicks.

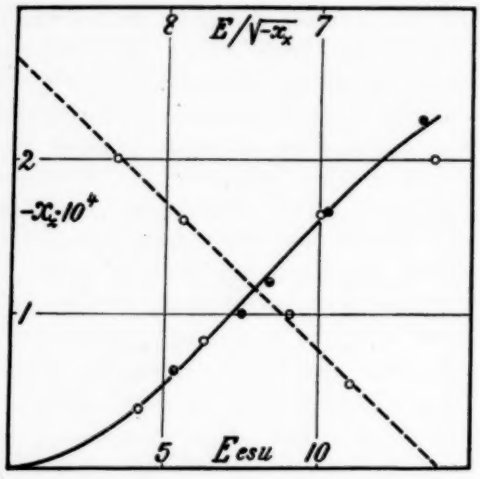

FIG. 2. The irreversible piezoelectric effect in Rochelle salt.

triclinic crystals, but they will be frequent in cubic crystals. The following consideration shows how they enter in the photoelasticity of cubic crystals.

According to the classical theory a pressure P normal to a cube face produces a birefringence

$$\delta(n_x-n_y)=\tfrac{1}{2}n^3(p_{11}-p_{12})(s_{11}-s_{12})P, \qquad (9)$$

where p_{ik}'s are the elasto-optical constants and s_{ik}'s are elastic compliance coefficients. This equation is modified by morphic effects which take into account the fact that the cubic crystal becomes tetragonal under the influence of the pressure. For a tetragonal crystal the photoelastic equation for pressure along the tetragonal axis is

$$\delta(n_x-n_y)=\tfrac{1}{2}n^3[(p_{11}-p_{21})s_{11}-(p_{22}+p_{23}-2p_{12})s_{12}]P.$$

The relations $p_{11}=p_{22}$ and $p_{12}=p_{21}=p_{23}$, which are valid for the undeformed cubic crystal, will not hold in the deformed crystal. Instead $(p_{11}-p_{21})$ must differ from $(p_{22}+p_{23}-2p_{12})$ by a quantity proportional to the pressure P. The photoelastic effect in a cubic crystal follows, therefore, a law of the form

$$\delta(n_x-n_y)=AP+BP^2. \qquad (10)$$

Maris,[9] and more recently Kidani,[10] have indeed shown that Eq. (10) is in better agreement with the observation than the classical law (9). The quadratic term BP^2 is of morphic origin and cannot be considered as an ordinary higher order effect, because the measurements of the change of refraction by a hydrostatic pressure, which creates no symmetry changes, show no deviations from the linear law.

It appears likely that morphic effects may play a role in many fields of crystal physics. The morphic effects are smaller than the linear effects, but they seem to be larger than the ordinary quadratic effects. We shall not attempt to develop here a general theory of the morphic effects but limit our consideration to their influence on the properties of Rochelle salt.

THE QUADRATIC PIEZOELECTRIC EFFECT AND THE ANOMALOUS THERMAL EXPANSION OF ROCHELLE SALT

Since the elastic properties of a crystal are given by a tensor of the same kind as that describing its optical properties, the equations for the piezoelectric effect have the same structure as those for the electro-optical phenomena. The equations for the piezoelectric effect in Rochelle salt for a field E_x are therefore similar to Eqs. (3), namely

$$-x_x=\varphi_1P_x^2, \quad -y_y=\varphi_2P_x^2, \quad -z_z=\varphi_3P_x^2, \qquad (11a)$$

$$-y_z=f_{14}P_x/c_{44}, \qquad z_x=x_y=0. \qquad (11b)$$

In addition to the linear effect, given by Eq. (11b), the field E_x will create a morphic effect resulting in three normal strains which cannot be reversed by inverting the direction of the field. Equations (11a) happen to be identical with those describing electrostriction. However, it should be noted that the conditions for the occurrence of the quadratic piezoelectric effect are different from those for electrostriction. The morphic piezoelectric effect occurs only if the shearing deformation y_z is not suppressed. The appearance of electrostriction is not dependent on this condition.

The existence of the quadratic piezoelectric effect has been verified in a preliminary experiment carried out in collaboration with Dr. H. T. Gerry. We measured with a Lippmann interferometer the change of length in the a direction of a Rochelle salt crystal when an electric field

[9] H. B. Maris, J. Opt. Soc. Am. **15**, 194 (1927).
[10] Y. Kidani, Proc. Phys.-Math. Soc. Japan **21**, 457 (1939).

E_x was applied. The change x_x was found to be a contraction and was independent of the direction of the field. The effect is many thousand times larger than any electrostrictive effect ever reported. Since it is a contraction it is impossible to account for it by heating effects due to Joule heat or to electrocaloric effects. The results obtained at a room temperature of 25.5°C are given by the full curve in Fig. 2. The field dependence of the quadratic piezoelectric effect is similar to that of the Kerr effect at the same temperature. By using the same arguments which lead to Eq. (6) one finds that above the Curie point the relation

$$E_x/(-x_x)^{\frac{1}{2}} = v(t-t_c) - wx_x \qquad (12)$$

should hold, where $v=1/C\varphi_1^{\frac{1}{2}}$, $w=B/\varphi_1^{\frac{1}{2}}$. The dotted curve in Fig. 2 shows indeed that Eq. (12) is satisfied and gives $v(t-t_c)=6\times10^2$, $w=1.3\times10^6$. The value of w/v^3 is again of the same order of magnitude as Q/R^3 and BC^3, but since the temperature of the crystal was not controlled we cannot give a reliable value of v. From w and B one estimates that $\varphi_1=1.2\times10^{-9}$ cm³/erg. No crystals suitable for the determination of φ_2 and φ_3 were available. The magnitude of the quadratic piezoelectric effect is surprisingly large. Near the Curie point a field of 3000 volt/cm creates a contraction of the same magnitude as that produced by a hydrostatic pressure of about 100 atmospheres. We are unable to understand how Körner[11] could fail to notice this effect.

The result of this experiment clarifies the origin of a series of effects in Rochelle salt. It shows that the quadratic electro-optical effect is, at least in part, of photoelastic origin, i.e., the birefringence is caused by the strains x_x, y_y, z_z. The order of magnitude and the sign of the Kerr effects are compatible with this explanation. The question, whether a part of the optical effects is due to the direct action of the field, can be answered only after the photoelastic properties of Rochelle salt have been studied.[12]

In the ferroelectric temperature range the spontaneous polarization P_x^0 will create spontaneous strains $-x_x^0=\varphi_1 P_x^{0^2}$, $-y_y=\varphi_2 P_x^{0^2}$, $-z_z=\varphi_3 P_x^{0^2}$, and, for fields E_x larger than the coercive field, the crystal should show a linear, but irreversible, piezoelectric effect given by equations of the form $-x_x=2\varphi_1 P_x^0 \kappa_1^0 E_x$. The spontaneous normal strains most probably give rise to an anomalous density variation of Rochelle salt at the Curie points. The available density measurements have not been carried out with sufficient accuracy to record this effect, but the existence of the spontaneous strain x_x^0 is confirmed by Hablützel's measurements[13] of the coefficient of linear thermal expansion in the a direction. The curve in the lower part of Fig. 3 presents Hablützel's data of $\alpha_x=dx_x/dt$. From this curve the dotted curve $x_x(t)$ in the upper part of the figure was evaluated by graphical integration. This curve is to be compared with the full drawn theoretical curve which is obtained by subtracting from the normal linear $x_x(t)$ variation the spontaneous contraction $x_x^0=\varphi_1 P_x^{0^2}$. The calculation of x_x^0 is based on the value $\varphi_1=1.2\times10^{-9}$ and the P_x^0 values in Table II of paper III. The agreement is better than could be expected from the accuracy of the data.

Hablützel also has measured the thermal expansion in a direction at 45° to the b and c

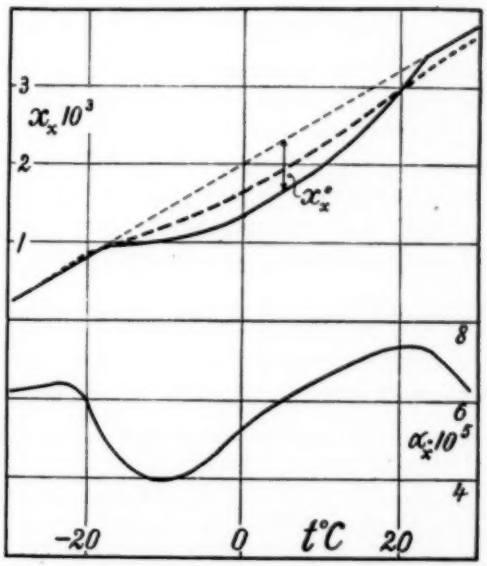

FIG. 3. The anomalous thermal expansion of Rochelle salt. Lower curve: Coefficient of thermal expansion, according to Hablützel. Upper curves: Thermal expansion according to theory (full curve) and experiment (dotted curve).

[11] H. Körner, Zeits. f. Physik **103**, 170 (1936).

[12] F. Pockels (reference 2) has measured 9 linear combinations of the photoelastic constants. Since Rochelle salt has 12 photoelastic constants, his work is not sufficient for the evaluation of all constants.

[13] J. Hablützel, Helv. Phys. Acta **8**, 499 (1935).

axes and found a curve of similar shape as for the expansion in the a direction. This result, which has been confirmed in recent measurements of Dr. Gerry, indicates that either one or both of the spontaneous strains y_y^0 and z_z^0 also are contractions. Gerry,[14] furthermore, finds that the anomalous expansion is different in the (011) and (0 −1 1) directions. This, of course, is due to the spontaneous shearing deformation y_z^0.

At the Curie points the crystal of Rochelle salt undergoes, therefore, more radical changes than has heretofore been realized. These changes correspond to three spontaneous normal strains which are proportional to $P_x^{0^2}$, and a shearing strain y_z^0 which is proportional to P_x^0. These strains reach maximum values between 10^{-4} and 10^{-3} at 5°C. The production of the normal strains gives an additional contribution to the change of the specific heat. The additional energy change is $\frac{1}{2}(c_{11}x_x^{0^2}+c_{22}y_y^{0^2}+c_{33}z_z^{0^2})$ and is proportional to $(P_x^0)^4$. The conclusions drawn in paper III are, therefore, still valid. While the shearing strain is responsible for the morphic effects and leads to the introduction of new elastic and dielectric constants, the normal strains will alter slightly the values of all "normal" constants of Rochelle salt. These effects are undoubtedly responsible for the change of the value and the temperature gradient of the resonance frequencies of the isolated crystal[15] at the Curie point, of the slight variations[16] of the dielectric constants ϵ_b and ϵ_c and the change of the intensities of certain x-ray reflections.[17] They justify our conclusion in paper III that the constants c_{44}, f_{14} and B suffer small changes at the Curie points.

The Transition of Rochelle Salt

The result of our discussions in papers II, III and IV may be summarized as follows: If the crystal of Rochelle salt were not piezoelectric it would show only a single transition point. The two Curie points and the large number of dielectric, piezoelectric, optical, caloric and thermal anomalies of the free crystal can all be explained on the basis of laws which are logical extensions of the laws of classical crystal physics. There remains, therefore, only the problem of understanding the nature of the transition of the clamped crystal. This transition is characterized by a high maximum of the dielectric constant, but the available evidence does not indicate any changes of the internal energy or of the structure. Figure 1 shows that the temperature gradient of the birefringence is altered but there is no sudden change of the optical constants. These peculiarities indicate that the transition can involve only a change of the position or of the dynamics of the protons of either the OH groups or the water of crystallization. The transition may be similar to those in HBr, HI, H_2S, PH_3.[18] It differs, however, from the modifications of these crystals by the fact that the transition of Rochelle salt produces no change of the specific heat. To account for this we propose the hypothesis that the transition is suppressed, i.e., with decreasing temperature the crystal approaches a transition point without actually reaching it, because in the initial stages of the transition secondary effects are created which suppress the modification and the crystal remains in its original state because at lower temperature the protons have not sufficient energy to change their positions. The nature of the suppressing agent may possibly be explained as follows.

The calculation in paper II of the dielectric susceptibility of the clamped crystal takes into account only the shearing strains y_z but neglects the normal strains. To be sure, if a crystal could be clamped so that the shearing strains are suppressed, it would also show no morphic

[14] H. T. Gerry's measurements lead to somewhat smaller values of y_z^0 than those reported in paper II, but the investigation had to be interrupted when the crystal cracked. This investigation was carried out in the Laboratories for Physical Chemistry of the Institute. I am indebted to Dr. Gerry (now with the Solvay Process Company, Hopewell, Virginia) for the permission to use his data. In contrast to Gerry's and Hablützel's results, the measurements of I. Viguess, Phys. Rev. **48**, 198 (1935) indicate that y_y^0 and z_z^0 are expansions.

[15] W. P. Mason, Phys. Rev. **55**, 775 (1939); G. Mikhailov, Tech. Physik U.S.S.R. **3**, 652 (1936).

[16] J. Hablützel, Helv. Phys. Acta **12**, 489 (1939).

[17] H. Staub, Physik. Zeits. **34**, 292 (1933).

[18] These transitions, commonly ascribed to hindered rotation, are not fully understood. The fact that these crystals have two transition points suggests certain analogies with Rochelle salt. Whether they are justified could be ascertained by dielectric measurements on single crystals of these substances. Measurements on polycrystalline samples give insufficient information, because for Rochelle salt they show no Curie points. For a review of these transitions see A. Eucken, Zeits. f. Elektrochemie **45**, 126 (1939).

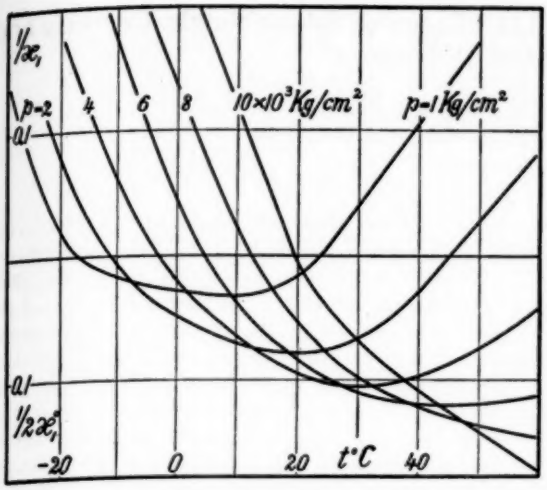

FIG. 4. Temperature dependence of the reciprocal susceptibility of Rochelle salt under hydrostatic pressure (according to the measurements of Bancroft).

effects and the normal strains would disappear. However, dielectric measurements on such a crystal would not lead to the theoretical $\chi_1(t)$ curve in Fig. 3, II. This curve applies to the experimentally unrealizable case of a crystal in which y_s is suppressed but in which the normal strains are those which occur in the free crystal. These normal strains, especially the spontaneous normal strains x_x^0, y_y^0, z_z^0, will certainly have considerable influence on the $\chi_1(t)$ curve. This follows from the investigations of Bancroft[19] who studied the influence of hydrostatic pressure on the $1/\kappa_1(t)$ curves of free crystals. Figure 4 is based on Bancroft's data. It shows, also, that at higher pressures the dielectric data can be represented by continuous curves without any discontinuities at the Curie points if one plots $1/\kappa_1(t)$ and $1/2\kappa_1^0(t)$, where κ_1 and κ_1^0 are the susceptibilities in the paraelectric and ferroelectric range, respectively. According to the results in paper II we are justified in assuming that the $\chi_1(t)$'s are parallel to those in Fig. 4, but the vertical displacement $\chi_1 - 1/\kappa_1$ will change with the pressure. Figure 4 shows that in the critical temperature range the slope of the $\chi_1(t)$ curves decreases and becomes negative, not only when the temperature is lowered at constant pressure, but also when the pressure is raised at constant temperature. Now, it is a characteristic feature of the $\chi_1(t)$ curve that, while it has a small curvature above the Curie point, its slope decreases rapidly as soon as the temperature drops below the upper Curie point. With further temperature decrease the slope becomes negative with the result that the critical condition $\chi_1 = 0$ is avoided. Since it is known that at least two of the normal strains are contractions they must influence the $\chi_1(t)$ curve in a manner similar to that produced by a hydrostatic pressure and it seems, therefore, natural to hold these strains responsible for the peculiar course of the $\chi_1(t)$ curve and for the suppression of the transition. If this hypothesis is correct we arrive at the following explanation of the properties of the free crystal of Rochelle salt. A rigid crystal, in which all strains are suppressed, would show a transition. Probably it would occur at about 18°C where the extrapolation of the $\chi_1(t)$ curve above the Curie point intersects the zero axis (Fig. 3, II). Because of the piezoelectric interaction the free crystal becomes spontaneously polarized and deformed before this transition temperature is reached, namely at the upper Curie point at about 24°C.[20] The elastic deformation, in particular the normal strains which are of morphic origin, prevent the occurrence of the transition and the crystal returns at lower temperatures to a state of low dielectric constant. During this process the free crystal must pass through a lower Curie point. For the other ferroelectric crystals, for which an anomaly of the specific heat has been observed, there is no reason to assume that the transition is suppressed, though the interaction and morphic effect should occur also in these crystals.

[19] D. Bancroft, Phys. Rev. **53**, 587 (1938).

[20] This temperature depends on the definition of the Curie point. Extrapolation of the measurements above the Curie point gives in almost all cases $t_c = 23$°C, but the maximum value of κ_1 occurs at 23.7°C. On the other hand, we find that the resonance frequencies of the foiled crystal have a minimum at 24.1°C. It is possible that this temperature differs in different crystals, depending on internal strains.

Photoelectric Work Functions of (100) and (111) Faces of Silver Single Crystals and Their Contact Potential Difference*

H. E. FARNSWORTH, *Brown University, Providence, Rhode Island*†
RALPH P. WINCH,‡ *Williams College, Williamstown, Massachusetts*

(Received July 9, 1940)

The work functions of the (100) and (111) faces of silver single crystals have been determined photoelectrically by the Fowler method of analysis, and were compared with the contact potential difference measured by the Kelvin null method. The equilibrium value of the work function for the (100) face is 4.81 ± 0.01 ev, and that for the (111) face is 4.75 ± 0.01 ev. These values were obtained after heating for more than 2000 hours at various temperatures up to visible red heat. The gas pressure in the tube during the final stages of outgassing was between 1 and 3×10^{-8} mm Hg with the crystals hot. Values of the measured contact potential difference obtained at frequent intervals during the outgassing agreed with the differences of the photoelectric work functions to within ± 0.01 volt. After these equilibrium values were obtained the crystals became contaminated by an unidentified impurity from heated tantalum with the result that the photoelectric data no longer agreed with the Fowler theoretical curve or with the measured contact potential difference. The apparatus permitted deposition of silver from the vapor state onto the crystal faces, after two previous distillations of the silver had been made to eliminate gas effects. Presence of the contamination referred to above complicated the results following deposition, but evidence is presented to show that the deposited silver gave a more gas-free surface than heating alone. The rate of return of gas to the surface following the deposit was determined by a comparison of the experimental results with a theory presented by Emslie. The results are explained by postulating that long heating of the crystals produced a stable gas configuration of a monomolecular layer on their faces, and that deposition of a gas-free layer of silver produced a surface free of most, if not all, of this layer of gas. The work function of the gas-free surface is 0.09 ± 0.03 volt less than that of the underlying structure previous to deposit.

INTRODUCTION

IT is now rather generally accepted that the work function of a metal single crystal is a function of the crystal face which forms the surface boundary. During the past several years various experimenters[1] have attacked this problem. Except for the fact that the specimen under investigation must be in the form of a single crystal, the methods employed are the same as those formerly used on polycrystalline specimens. While the photoelectric and thermionic methods should yield absolute values of work function under proper experimental conditions, a measurement of the contact potential difference furnishes values for the differences in work functions so that if the work function of one face is known, one can obtain by this method values for any other faces which can be prepared. Although it has been experimentally established for polycrystalline surfaces that the difference in photoelectric work functions is equal to the contact potential difference,[2] this has not been done previously for two different faces of the same single crystal. It is, therefore, of some importance to test this relationship for single-crystal surfaces.

A comparison could be made between the values obtained subsequent to prolonged heating of the crystals and those subsequent to a freshly evaporated film. Previous observations[3] indicate that a deposited layer forms on the surface of a crystal of the same material in a single lattice with the same orientation as the underlying crystal. Although completely reliable results on the deposited film were not obtained because of contamination, some interesting observations were made.

CRYSTALS

The silver crystals were cut and etched with one large plane surface parallel to a desired set

* Preliminary report, Phys. Rev. **56**, 1067 (1939).

† Experiments performed at Brown University.

‡ This author is indebted to the Class of 1900 Fund of Williams College for grants which made participation in this work possible.

[1] For example: B. A. Rose, Phys. Rev. **44**, 585 (1933); N. Underwood, *ibid.* **47**, 502 (1935); R. P. Johnson and W. Shockley, *ibid.* **49**, 436 (1936); C. E. Mendenhall and C. F. DeVoe, *ibid.* **51**, 346 (1937); S. T. Martin, *ibid.* **56**, 947 (1939); M. H. Nichols, *ibid.* **57**, 297 (1940).

[2] G. N. Glasoe, Phys. Rev. **38**, 1490 (1931); P. A. Anderson, *ibid.* **54**, 753 (1938).

[3] H. E. Farnsworth, Phys. Rev. **43**, 904 (1933); **49**, 605 (1936).

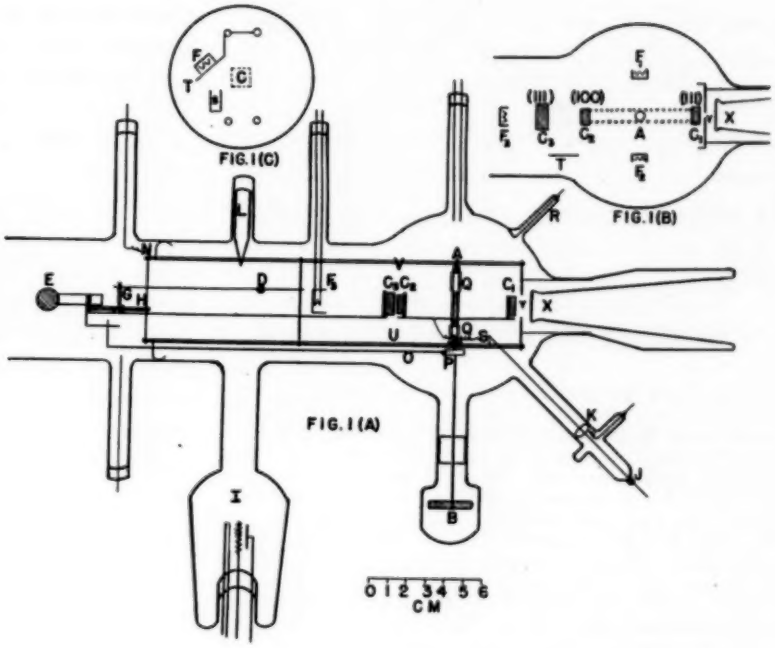

FIG. 1. Schematic diagram of the research tube. (A) is a vertical section along the axis of the tube, (B) is a horizontal section along the same axis, and (C) is a vertical section at right angles to the axis in the plane UV of (A). The inside of the bulb was covered with a thin conducting layer of tungsten. Iron armatures E and B were sealed in Pyrex envelopes.

of crystal planes. The method of cutting and preparing the crystals has been described previously.[4] In the present case it was found that smoother etched surfaces were obtained if the crystals were placed in hot distilled water before dipping in the HNO_3 etching solution. The crystal with the (100) face was approximately $1.0\times1.1\times0.4$ cm and the crystals with (111) faces were approximately $0.9\times0.95\times0.4$ cm and $1.4\times1.2\times0.5$ cm with the prepared faces on the surfaces of largest area.

Apparatus and Procedure

The arrangement was such that either of two different crystal faces could be brought opposite the quartz window X, Fig. 1(A), for photoelectric readings, by the rotation of an external electromagnet acting on the iron armature B attached to the vertical axle A. Q denotes quartz insulation. The mounting of the crystals was similar to that described by Underwood.[1] The crystals C_1 and C_2, when in front of the filaments F_1 and F_2, could be outgassed by electron bombardment. Molybdenum shields were placed at several positions in the tube to condense evaporated metal, and all bombarding filaments were surrounded by molybdenum shields except on one side.

The contact potential difference (referred to hereafter as CPD) was measured by the Kelvin null method with a Compton type quadrant electrometer. For this measurement a third crystal C_3 with a (111) face was mounted on a sliding mechanism operated by an external electromagnet acting on the iron armature E. The sensitivity was such that the CPD could be measured to within ±0.002 volt. When one of the rotor crystals was in position for photoelectric measurements, the other was accurately aligned with the slider crystal for CPD measurements. A special mechanism assured alignment of the crystals when measurements were made, and prevented the slider crystal from coming forward and striking the rotor crystal for any position of the latter. The minimum spacing between a rotor crystal face C_1 or C_2, and the slider crystal face C_3 was controlled by the spacer bar G, Fig. 1(A) and was normally about 0.25 mm.

Figure 1(C) shows the evaporator arrangement for depositing a film of silver on the faces of the silver crystals. The tantalum cup s which contained previously distilled silver was heated by electron bombardment (filament not shown). The tantalum plate T, which received some silver from s, could be similarly heated to deposit

[4] H. E. Farnsworth, Phys. Rev. **40**, 699 (1932).

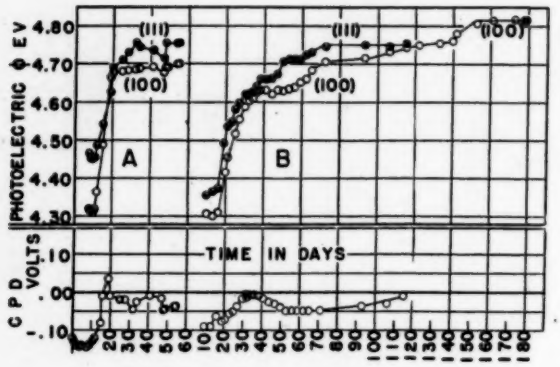

FIG. 2. Work functions, determined by Fowler[6] method, and CPD's as a function of elapsed time in days. Both crystals were heated continuously except for (1) times required during observations, (2) in case of (111) rotor crystal, a period between the 32nd and 47th days of experiment *A*, (3) in case of (100) rotor crystal, a period between the 41st and 47th day. Total heating time for (100) crystal during experiment *B* is 2639 hours. Total heating time for (111) crystal during experiment *B* is 1634 hours. While the (111) crystal remained at room temperature from the 32nd to the 47th day in experiment *A*, ϕ_{111} decreased only 0.04 ev. Similarly, while the (100) crystal remained at room temperature from the 41st to the 47th day the decrease in ϕ_{100} was 0.015 ev. This fatigue effect was even less in the later stages of outgassing. The sign of the CPD is taken as positive when the (100) face has the higher work function.

silver on the crystals.[5] During deposition on *T* the positions of the crystals were such that no silver from *s* could reach the crystal faces. Both *s* and *T* were preheated in an auxiliary vacuum tube. In the later stages of the experiment and before making final deposits on the crystals, the plate *T* was heated 1040 hours at temperatures up to 1400°C and the cup *s* 1340 hours at temperatures up to about 900°C at which temperature silver evaporated copiously from the cup. The first few deposits on *T* were driven off before exposing the crystal faces.

Prior to assembly of the tube, all parts were cleaned chemically and were outgassed by induction heating in an auxiliary vacuum. The assembly was carried out in a dust-free, dry room, and all parts were touched only by clean tools. Masks were worn to prevent contamination of the parts by the breath.

The Pyrex tube was connected with $1\frac{1}{4}$" Pyrex tubing to a vacuum system consisting of two oil diffusion pumps in series backed by a Cenco Hyvac. Two large traps in series separated the tube from the diffusion pumps, and a third trap separated the diffusion and backing pumps. The traps were cooled by solid carbon dioxide in acetone. This same vacuum system has been used previously in this laboratory to evacuate the tube used for low speed electron diffraction. No evidence of contamination from pump oil vapors was obtained in diffraction studies with low speed electrons of less than 50 ev energy. No grease or wax joints were on the research tube side of the traps. The research tube was left attached to the pumps throughout the experiment since it was deemed inadvisable to use any getter, such as barium, whose vapor might condense on the crystal faces and completely alter their work functions.

The residual gas pressure in the tube was measured with an ionization gauge *I*, Fig. 1(A). During all measurements, except the very early ones, this was from 1 to 3×10^{-8} mm Hg, and most of the time it was near the lower limit. In the early stages, the outgassing was conducted at a rate such that the pressure remained below 5×10^{-7} mm Hg after the second baking of the tube. In the final stages the pressure was independent of the temperature of the crystals.

A General Electric quartz capillary high pressure mercury arc served as a light source for photoelectric readings. A Bausch and Lomb quartz single monochromator, with the source and lenses, was mounted on a rotating table so that it could be turned to throw the image of the exit slit on the crystal face or on the receiver of a vacuum thermopile for measurement of the light intensity. Monochromator slit widths of 0.2 mm or less were used for all readings. Since the sensitivity of the thermopile was found to change slowly, with time, a calibration with standard lamp was made during each set of readings. An amplifier with a General Electric FP-54 Pliotron tube measured the photocurrents. The Fowler method[6] was used to determine the work functions.

Although tests of the monochromator showed the presence of some scattered light, this was found to affect only the observations very close to the long wave limit. In using the Fowler

[5] Some early results obtained by us (Phys. Rev. **53**, 935 (1938)) show that it is not sufficient to simply melt the silver in a vacuum, and then distill it onto the surface to be tested.

[6] R. H. Fowler, Phys. Rev. **38**, 45 (1931).

method a deviation of the observations near the long wave limit due to scattered light is easily detected, and allowance can be made for it.

Results and Discussion

Silver crystals outgassed by heating

Figure 2 shows the experimental values of work functions (hereafter referred to as ϕ) and CPD's as a function of elapsed time in days. Actual heating times are given in the caption. Experiment *A* was terminated after 55 days because a short circuit developed in the tube. Then, before obtaining curve *B*, the tube was dismantled for alterations; all three crystals were resurfaced and etched, after which the tube was reassembled and evacuated as soon as possible. It is to be noted that, except at the very beginning of three of the curves, the values of ϕ increase with outgassing and decrease very slightly when exposed to very low gas pressures for long periods of time. Most of the photoelectric readings were taken immediately after the crystals had cooled to room temperature, although ϕ changed only very slowly with time after heating so that during several hours there was no observable change.

In experiment *A* the (100) crystal never reached its equilibrium ϕ, but in *B* it reached this value of 4.81 ± 0.01 ev after 2283 hours of heating at various temperatures up to visible red heat. An additional heating for 356 hours did not change this value further. After the crystal had subsequently remained at room temperature for 2130 hours (not shown in Fig. 2) while measurements of another type were being made, ϕ_{100} decreased to 4.65 ev. Following this, 218 hours of heating brought ϕ_{100} back to the equilibrium value of 4.81 ev which was not altered by some further heating.

An equilibrium value of 4.75 ± 0.01 ev was obtained for ϕ for the (111) face in both experiments. In experiment *B* this value was attained after 1227 hours of heating, and was not altered by 407 hours of additional heating. This crystal had been outgassed in a previous experiment so it attained its equilibrium value in a much shorter time than did the (100) crystal which was somewhat larger and had not been outgassed previously.

It is to be noted that the observations on CPD, shown in the lower part of Fig. 2, check with few exceptions with the corresponding differences in photoelectric ϕ's within ± 0.01 volt. This and the fact that the experimental results are in agreement with the Fowler curve as shown below indicate that throughout the outgassing process ϕ is uniform over the surface.

Observations were made on *I* (the photocurrent per unit light intensity) as a function of elapsed time immediately after the crystals had been heated, and before they had reached room temperature. The results obtained were similar to those shown by Mendenhall and DeVoe[1] in their Fig. 2 except that our change with time was not as great. Their explanation of this change was based on the assumption that the heating of the crystal produced a gas-free surface, and that the change with time after heating was due to gas returning to the surface. There is undoubtedly some temperature dependence which has not been taken into account. Our results are consistent with the assumption that the change is entirely due to the changing temperature of the crystal as it cools to room temperature.

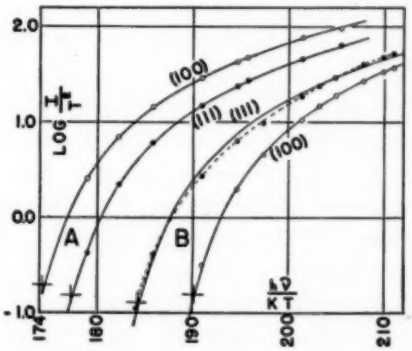

Fig. 3. Typical Fowler plots. *A*—Experimental points obtained before outgassing was completed. *B*—Results for (100) crystal after reaching equilibrium, and for (111) crystal after being contaminated. Solid curves are Fowler theoretical, and all points are experimental.

In Fig. 3 the pair of curves marked *A* show typical Fowler plots from which the values of ϕ were determined for Fig. 2. The solid curves are theoretical, and the points are experimental.

From the sample pair of curves marked *A* in Fig. 3, ϕ of the (111) face was found to be 4.490 ev, and that for the (100) face 4.413 ev

giving a difference of -0.077 ev. Under these same conditions the CPD of the (111) with respect to the (100) was measured to be -0.076 volt. These particular values check better than is to be expected from the errors in matching the experimental points to the Fowler curves.

Effects of contamination

At the point where the (111) curve ends in experiment *B*, Fig. 2, it is believed that the (111) crystal became slightly contaminated while heating the tantalum plate *T*, Fig. 1, near it. The crystal was in such a position that no contamination could go directly from *T* onto the face of the crystal, but it could go onto the edge of the crystal and migrate around onto the face[7] with subsequent heating. Calculations, based on the results of D. Langmuir and L. Malter[8] on the rate of evaporation of tantalum, showed that the contamination could not be caused by evaporated tantalum at the temperature to which the plate had then been heated (about 1000°C at the hottest place).[9] This contamination on the (111) face caused a decrease in ϕ, and a deviation of the experimental results from the Fowler theoretical curve. An example is shown for this (111) face in *B*, Fig. 3. As before, the solid curve is the Fowler theoretical curve, and a dotted curve has been drawn through the experimental points. The accompanying curve in this figure for the (100) face was obtained at the same time and shows a good fit of the experimental points to the theoretical curve, indicating that the (100) face had not been affected. Incidentally this is a plot of results obtained after the (100) face had reached its equilibrium ϕ of 4.81 ev. The difference of the ϕ's came out to be 0.147 ev while the measured CPD was 0.073 volt. While there is some choice in locating an average fit of the points to the theoretical curve for the (111) face, the above difference is greater than is permitted by this choice. Pairs of curves of the type shown in *B*, Fig. 2 were reproduced a great many times while the (111) face was contaminated and, since the results from the (100) face always fitted the theoretical curve while the results from the (111) face failed to fit in the manner shown, this result is not due to experimental error.[10] In fact, smaller deviations from the theoretical curve than those shown were found to be real in the early stages of contamination. The deviations were of the order which have been ignored by some observers in fitting results to a Fowler curve.

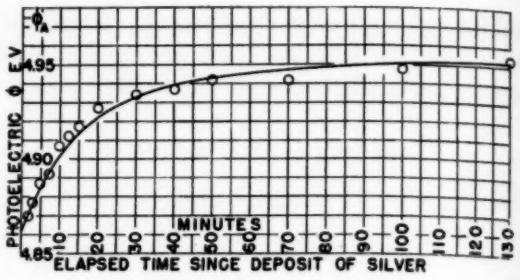

FIG. 4. A comparison of Emslie's theoretical curve with our experimental points for the change of ϕ with time after deposit of silver on the complex structure. The face underlying this complex structure was a (100).

Calculations by Emslie[11] show that an assumption of patches with different values of ϕ from that of the silver will modify the Fowler theoretical curve in the manner shown by the experimental points for the (111) face, but because of two arbitrary constants the formulation is unsatisfactory as a means of determining the relative areas and ϕ's of the patches.

After the part of experiment *B* previously

[7] There is abundant evidence for such migration, e.g., J. D. Cockcroft, Proc. Roy. Soc. **119**, 308 (1928).

[8] D. B. Langmuir and L. Malter, Phys. Rev. **55**, 748 (1939).

[9] Spectroscopic tests made at the National Bureau of Standards did not reveal the nature of the contamination. Photographs of the electron diffraction pattern from the crystal surfaces were also kindly made for us by L. H. Germer. Although the pattern showed some faint extra rings, we have been unable to identify the substance producing them. The visual appearance of the crystal surfaces when removed from the tube was as good or better than it was when they were first prepared.

[10] Measurements were made of the reflectivity of the two crystal faces in the ultraviolet to determine any differences which might affect the photoelectric results. The arrangement was such that light from the monochromator, after reflection from the crystal faces in the experimental tube, emerged through the quartz window and was then reflected by an aluminum mirror onto the molybdenum surface of a photo-cell. This photo-cell was chosen because of its smooth sensitivity curve in the ultraviolet. The photocell was calibrated before and after the reflectivity measurements. The results showed that any difference in the reflectivities of the two crystal faces was less than experimental error, and too small to account for differences in the measured photoelectric characteristics. Also, the reflectivity changed very little with wave-length over the range used in the experiment, so that no correction for such a change was necessary.

[11] Private communication.

described, the (100) crystal face was exposed to the tantalum plate T while at 1050°C at the hottest place. An exposure of 110 minutes caused a deviation of the results from the theoretical curve similar to that for the (111) face but less pronounced. A few more such exposures made this still more evident.

It was hoped, at the outset of the experiment, that the same equilibrium ϕ could be obtained for the two (111) faces in the tube so that they would show no CPD. Because the (111) slider crystal was larger than the (111) rotor, and had not been outgassed previously, a much longer heating time would have been required to reach its equilibrium ϕ, but before this time had elapsed the (111) rotor became contaminated. However, the fact that the same equilibrium value of ϕ_{111} was obtained in two different experiments (between which the (111) crystal was resurfaced) indicates that the failure to reach the above objective is not significant.

Deposition of silver on the crystal faces

Deposition of silver on the (100) crystal face caused ϕ to decrease abruptly from the value ϕ_A, Fig. 4. This was followed immediately (while the crystal was at room temperature) by an increase in ϕ. A typical deposition was made by heating the silver-coated tantalum plate for 100 seconds at a power input of 7.9 watts which maintained a temperature of about 930°C at the center and 750°C at the edges. Calculations indicate that about 1500 ± 1000 atomic layers of silver were deposited on the crystal surface.

The experimental values represented by circles, Fig. 4, were obtained in the following manner. Readings on five different wave-lengths were taken rapidly in rotation as a function of time after the deposit was completed.[12] A series of plots of $\log I/T^2$ against elapsed time was then made for these wave-lengths. These curves gave the values of $\log I/T^2$ at any given instant of time, and Fowler plots were then drawn to obtain the values of ϕ. Beyond the figure, ϕ continued to increase slowly for about 24 hours, reaching ϕ_A at the end of that time. The total increase in ϕ following six different deposits is given by 0.09 ± 0.03 ev. The vertical shifts, obtained in matching the experimental plots to the Fowler theoretical curve, were the same (-0.62 ± 0.02) for all of the ϕ determinations shown in Fig. 4. This shows that ϕ was changing without a change in the so-called "photoelectric efficiency."

These results are explained on the assumption that a monomolecular layer of gas exists on the surface before the deposit, and that the deposited silver produces a nearly gas-free surface which has a lower ϕ than a surface with a monomolecular layer. The change of ϕ with time after the deposit may be accounted for by condensation of gas from the residual gas in the tube. Figure 4 shows one theoretical curve calculated by A. G. Emslie.[13] A constant residual gas pressure was assumed. It will be noted that a smooth curve drawn through the experimental points would rise more rapidly at first and less rapidly thereafter than does the theoretical curve. This difference would be expected if the gas pressure in the tube were increased slightly during the deposition process and then decreased again with time after deposit, instead of remaining constant as postulated in obtaining the curve. The pressure increase during deposit was so small that it was hardly detectable on the ionization gauge, and could not have been more than about 2×10^{-9} mm Hg, but this appears to be enough to account for the above difference.

On removal from the research tube, the crystal faces were studied by high speed electron diffraction,[9] and the diffraction pattern from the (100) face was found to be very complex. It resembles to some extent but is much more complicated than the abnormal pattern obtained by Goche and Wilman[14] from a silver film condensed on a heated rocksalt cleavage-face in vacuum. They attribute their pattern to the presence of more than one set of crystal planes which are parallel to the rocksalt surface. It is believed that the contamination which collected on the crystal face after obtaining the results shown in Fig. 2, and prior to the first deposit of silver, caused the deposited silver to grow in

[12] The first observation was obtained 80 to 90 seconds after the deposit was completed. The time intervals between the next several successive readings were also 80 to 90 seconds, as timed with a stopwatch.

[13] Private communication.

[14] O. Goche and H. Wilman, Proc. Phys. Soc. 51, 648 (1939).

this complex structure. This structure, once started, probably continued even though the contamination soon became completely covered. Tests made in the latter part of the experiment seemed to indicate that contamination was no longer coming from the tantalum plate T. As an added precaution T was kept coated with a heavy layer of silver, and the time of deposit was limited to 100 seconds after which T was again coated with silver prior to the next deposit. The high ϕ shown in Fig. 4 is attributed to this complex structure, and is not considered to be characteristic of the (100) face. Since the (111) and (100) planes are the most densely populated ones in the face-centered lattice, the high ϕ may be due to the predominance of a less densely populated plane such as the (110).

Deposits were also made on the (111) rotor face with results similar to those shown in Fig. 4 for the (100) face. However, a detailed comparison cannot be made since the filament F_2 used for heating the (111) crystal burned out shortly after the end of the summary curve shown in Fig. 2(B), thus preventing the same procedure as used with the (100) crystal. A single deposit of silver on the (111) face caused its photoelectric readings to fit the Fowler theoretical curve over a range of 400A, showing that the patch work on the surface had been covered and that a uniform surface then existed. The absolute value of ϕ after making several deposits, thick enough to be opaque, was several tenths of a volt less than the high value shown in Fig. 4. This emphasizes that ϕ for a deposited metal film is greatly influenced by the underlying structure, so that a determination of ϕ for such a film, even when thick enough to be opaque, has no significance without a knowledge of the influence of the backing. Cashman[15] has arrived at a similar conclusion.

The initial deposit of silver on the (100) face produced a larger decrease in ϕ than any observed subsequently, and the rise in ϕ after the deposit was considerably less than the decrease due to the deposit. In no other case was the rise after deposit less than the decrease due to the deposit. (The thickness of the silver layer deposited on the crystal face in all cases was nearly the same.) This result and the following ones in this paragraph are not entirely clear in their interpretation, but it is believed that the presence of the contamination and the beginning of the complex structure growth are responsible. Several deposits subsequent to the first caused a small decrease in ϕ followed by a rise which was greater than the decrease. A small amount of heating of the crystal at this stage produced a remarkable rise in ϕ. For example, after a total of four deposits of silver had been placed on the (100) face, the crystal was heated for 10 minutes at about 500°C or less. This resulted in an increase of 0.06 ev in ϕ. Further heating caused ϕ to rise less and less rapidly until finally long continued heating produced no further change in ϕ. Deposits and heating were used in alternation until an equilibrium was reached such as that shown in Fig. 4 where the ϕ after deposit came back to, but not beyond, its value before deposit, and heating after the deposit produced no change in ϕ. It is believed that the complex structure grew when a deposit was placed on the crystal, and also when the crystal was heated until finally this structure reached a stable value. After this, silver grew during its deposit with the orientation of the underlying surface, and heating after the deposit caused no further growth. When this state was reached the only result of the deposit was to produce a more gas-free surface. The last step in the whole experiment was to place a deposit of silver on the (100) crystal so that when it was removed and studied by electron diffraction it had a fresh deposit of silver which had not been heated subsequently.

Some of the results used by Emslie in his paper were taken before this stable value of the complex structure was reached and some after, showing that his same explanation of the accumulation of gas on the surface after the deposit can be used throughout.

Comparison of results

The equilibrium values of the ϕ's obtained here, i.e., $\phi_{100}=4.81\pm0.01$ ev and $\phi_{111}=4.75\pm0.01$ ev, may be compared with 4.74 ± 0.03 ev obtained by one of us[16] for a thin filament of

[15] R. J. Cashman, Phys. Rev. **54**, 971 (1938).

[16] R. P. Winch, Phys. Rev. **37**, 1269 (1931); R. H. Fowler, *ibid.* **38**, 45 (1931). In Winch's experiment a mercury diffusion pump was used and the vacuum system included two traps, cooled with liquid air, between the research tube and the pumps.

polycrystalline silver which had been heated for 1200 hours. This heating included short intervals at temperatures as high as 850°C where evaporation is rapid. These repeated flashings of polycrystalline silver at 850°C caused no change in ϕ so it is reasonable to assume that higher temperature heating of the crystals would only ruin the faces without freeing the crystals further of their surface gas.

From a measurement of the CPD between barium and silver, and ϕ of barium obtained by Cashman,[15] Anderson[2,17,18] obtained 4.46 ± 0.05 ev for ϕ of polycrystalline silver deposited on a barium-on-glass surface from the vapor state, after first making observations on the barium. It seems probable to us that this value is too low, because of the presence of the barium. Although the whole tube was immersed in liquid air, local heating may have caused some of the barium to diffuse through the silver film as it formed. The fact that he obtained ten times as much variation from one film to another for silver as for barium may be due to varying amounts of barium on the surface of the silver films as well as to the structural differences which he mentions.

Anderson[18] obtained 0.12 ± 0.01 volt CPD between polycrystalline silver deposited on glass and the (100) face of a silver crystal formed by depositing silver on a rocksalt cleavage plane, with the (100) face having the higher ϕ. This experiment is not subject to the above criticism. If we add this value to Winch's value of 4.74 ±0.03 ev for polycrystalline silver, we obtain 4.86 ev, in agreement with our equilibrium value of 4.81 ± 0.01 ev for the (100) face.

Conclusions

We believe that $\phi_{100}=4.81$ ev and $\phi_{111}=4.75$ ev are the best values that can be obtained for silver crystals by heating alone since the crystals would etch rapidly if heated to appreciably higher temperatures than those employed here. The measured CPD between the crystal faces agrees with the difference of their ϕ's as long as the photoelectric data for both crystals agree with the Fowler theory. It is to be noted that ϕ_{111} is less than ϕ_{100} for silver as was also found to be the case for copper,[19] although the difference of 0.06 ev for silver is considerably less than the corresponding difference of 0.46 ev for copper.

The evidence from this experiment indicates that, as gas leaves the surface of a silver crystal, ϕ increases until a monomolecular layer of gas remains, and that removal of the last monomolecular layer of gas causes a decrease in ϕ. The above values of ϕ are thought to be characteristic of these faces when they are covered by a monomolecular layer of gas which cannot be removed by heating alone. This postulate and our evidence from the deposition of a gas-free layer of silver on a complex structure covering the crystal face indicate that ϕ is decreased by 0.09 ± 0.03 ev when the last monomolecular layer of gas is removed. There is uncertainty as to the influence of the underlying surface on this numerical value and hence the values for ϕ_{111} and ϕ_{100} quoted above have not been corrected for the presence of the monomolecular gas layer.

The results show that a slight amount of unknown contamination, which causes a non-uniform surface, may be detected photoelectrically by the deviation of the experimental results from the Fowler theoretical curve and by the failure of CPD to agree with the difference in the values of ϕ. Such slight amounts of contamination may be missed when CPD measurements alone are being made.

For the lower melting point metals, a more gas-free surface may be obtained by deposition of samples properly distilled in vacuum than by heating alone. However, ϕ for a film even though opaque may depend to a large extent on the backing. This makes it necessary to determine this dependence before any absolute values of ϕ for deposited films may be determined.

We have had the assistance of Mr. W. E. Johnson with the numerous calculations required.

[17] P. A. Anderson, Phys. Rev. **49**, 320 (1936).
[18] P. A. Anderson, Phys. Rev. **56**, 850A (1939).
[19] H. E. Farnsworth and B. A. Rose, Proc. Nat. Acad. **19**, 777 (1933).

Anomalous Scattering of Neutrons by Helium. (II)

H. STAUB AND H. TATEL*
Stanford University, Palo Alto, California
(Received September 3, 1940)

The anomalous scattering of neutrons by helium at neutron energies around 1 Mev has been investigated more closely. The backward scattering cross section shows a peak of 0.4 Mev half-width and indicates a doublet structure with a splitting of about 0.3 Mev. The absolute value of the ratio of the scattering cross sections of helium and hydrogen at 2.5-Mev neutron energy was redetermined and found to be considerably smaller than given in a previous investigation. This lowers the absolute values of the resonance scattering cross section given previously. The new values, however, are still consistent with the assumption that the resonance level is a P level. The measurements are found to be in agreement with the dispersion theory. The present experiments do not fix the sign of the splitting, although there is some indication that the doublet is normal.

INTRODUCTION

STAUB and Stephens[1] (hereafter referred to as I) have shown that the backward scattering cross section of He for neutrons of about 1 Mev energy shows a strong anomaly, caused by a virtual level of He^5 which is unstable by 0.8 Mev against disintegration into a neutron and an alpha-particle. The existence of this level was discovered by Williams, Shepherd and Haxby,[2] who investigated the reaction

$$_3Li^7+{}_1H^2\rightarrow{}_2He^5+{}_2He^4.$$

From the maximum observed ratio of the forward scattering cross section and the fact that the width of the level is some hundred kilovolts, Staub and Stephens[1] concluded that the level of He^5 involved must be a P level.

Since He^5 certainly represents a rather simple nuclear configuration it seemed desirable to carry on further investigation to obtain more information about the shape of the anomalous cross section curve, particularly since Staub and Stephens measured only two points close to the maximum. Furthermore, it seemed to be of considerable interest to investigate whether or not a splitting of the two levels, could be observed for values of the total angular momentum $J=\frac{3}{2}$ and $J=\frac{1}{2}$, respectively. Indication of a splitting was given by Gaerttner, Pardue and Streib.[3] Their results, however, were not analyzed according to the theoretical formulas and, therefore, did not present conclusive evidence.

The previous experiment (I) was carried out with almost monochromatic neutrons from the line spectrum of the Be (d, n) reaction. The neutron energy could be slightly changed by varying the bombarding energy of the deuterons. In the present experiment a continuous neutron spectrum was used, thus making it possible to investigate the scattering cross section in detail between 0.5 and 2 Mev. The continuous spectrum was produced by allowing the monochromatic neutrons of 2.5 Mev energy from the $d(d, n)$ reaction to strike a paraffin howitzer of suitable shape, in which they were slowed down by elastic scattering. The howitzer had a cylindrical shape with a coaxial conical opening, the common axis passing through the center of the target of the neutron generator and the center of the cloud chamber (Fig. 1). For a neutron point source the angle of the conical hole determines the maximum energy of the continuous neutron spectrum. This angle was 27°, hence the spectrum extended to about 2 Mev. The outer radius of the howitzer was 5.7 cm, its thickness 4.5 cm. Neutrons which are scattered so as to have about 1 Mev after scattering are produced in an effective layer of paraffin of about 5 cm and have to pass through about 3 cm to emerge. An estimate shows that, for this kind of a howitzer, the number of neutrons per 0.1 Mev energy interval is about 2 percent of the total

* Now at Physics Department, University of Michigan, Ann Arbor, Michigan.

[1] H. Staub and W. E. Stephens, Phys. Rev. **55**, 131 (1939).

[2] J. H. Williams, W. G. Shepherd, R. O. Haxby, Phys. Rev. **52**, 390 (1937).

[3] E. R. Gaerttner, L. A. Pardue and J. F. Streib, Phys. Rev. **56**, 856 (1939).

number observed in the undisplaced group at 2.5 Mev. The conical opening of the howitzer is important for two reasons: First, it allows, with or without the howitzer, the same number of neutrons of 2.5 Mev energy to strike the recording instrument. Secondly, it facilitates the emission of the low energy neutrons by reducing the amount of paraffin through which they have to pass. Since the howitzer as a whole represents the neutron source, its dimensions have to be kept small enough to insure a sufficiently small uncertainty in the origin of the observed neutrons. This, in turn, requires that the density of hydrogen in the howitzer material be as great as possible. This was obtained by turning the howitzer from a solid block of bubble-free paraffin.

The neutron source used in this experiment was a *dd* neutron generator operated at 170 kv and similar to a generator previously described by one of us.[4] Since the ion current was turned on only during the short time of sensitivity of the cloud chamber, a heavy ice target cooled with a mixture of dry ice and alcohol proved to be very satisfactory. The arrangement of the howitzer requires a small target spot, the diameter of which was limited by suitable diaphragms to $\frac{3}{4}''$ (19 mm). The maximum obtainable ion current was about 200 μa. Since the ion source was of the high voltage type[5] it is estimated that about 60 percent of the ions were atomic. The total yield of neutrons was equivalent to that from 10 g of Ra+Be. The ion source was easily timed by letting the cloud-chamber mechanism operate a relay which controlled the primary current of the high voltage for the ion source.

An automatic cloud chamber of the diaphragm type was used for recording the neutrons. It had an effective diameter of 13.4 cm and a depth of 2.6 cm. Its center was 50 cm from the target and 108 cm above the floor, in order to reduce the excessive recording of neutrons scattered from there. For the hydrogen experiments the chamber was filled with methane at a pressure of 6 lb. above atmospheric, having a stopping power of about 1.4. For He a pressure of 1 lb. above atmospheric was used, the stopping power being about 0.26.

[4] E. Baldinger, P. Huber and H. Staub, Helv. Phys. Acta 11, 245 (1938).
[5] F. A. Heiyn, Philips Tech. Rev. **3**, 339 (1938).

Experiments

To obtain the ratio of the backward scattering cross sections of He and H the neutron spectrum was recorded, once with a helium- and once with a methane-filled cloud chamber, according to the technique developed by Bonner and Brubaker.[6] Stereoscopic pictures of the recoil tracks were taken by simultaneously photographing the direct image and one reflected on a surface aluminized mirror. Only tracks within an angle of $\pm 8°$ with respect to the direction of the incident neutron were measured. The ratio of the scattering cross section is then simply obtained as the ratio of the numbers of observed helium and hydrogen recoils in each energy interval. This ratio, however, has to be multiplied by a constant depending on the total number of neutrons hitting the chamber in either one of the experiments. The value of this constant is determined by the ratio of the intensities of the group of 2.5-Mev neutrons in either one of the two experiments, provided that the ratio of the cross section of helium and hydrogen is known. The absolute value of the backward scattering cross section finally is obtained from the theoretically known value of the hydrogen cross section.

Preliminary experiments had revealed that without any paraffin in the neighborhood of the target, the neutron spectrum still shows an

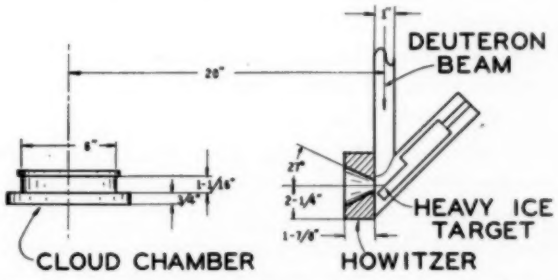

FIG. 1. Arrangement of chamber, target and howitzer.

appreciable low energy tail which consists mainly of neutrons scattered from the surrounding walls and the floor. Since these neutrons have random directions, they produce recoils of various energies in the direction of measurement. This fact makes it necessary to subtract this background from the two spectra taken with the paraffin howitzer in place. The background

[6] T. W. Bonner and W. M. Brubaker, Phys. Rev. **47**, 910 (1935).

measurements were taken with a carbon howitzer in place of the paraffin. This howitzer was geometrically identical with the one of paraffin and contained the same number of carbon atoms. Such an arrangement was chosen because it may well be that the distribution of the background recoils is affected by elastic scattering of the carbon in the paraffin. This can hardly be the case for the hydrogen in the howitzer, however, since every neutron scattered by the hydrogen

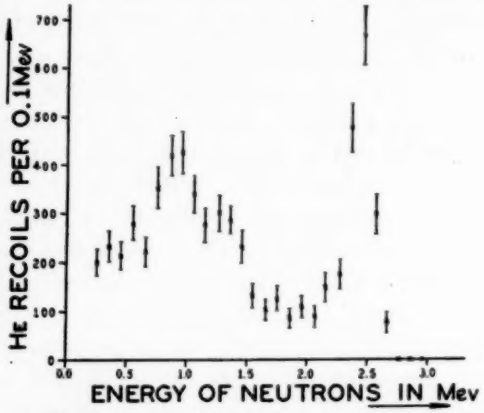

FIG. 2. Corrected number-energy curve of the He recoils in 0.1-Mev intervals as observed with the paraffin howitzer in front of the target.

has to undergo a large deflection in order to be scattered back by the floor, thus losing practically its whole energy. Moreover, the carbon may easily scatter additional neutrons of the monochromatic 2.5-Mev group into the cloud chamber which would affect the monitor intensity of the 2.5-Mev group.

In this experiment the following cloud-chamber pictures were taken: with He and the paraffin howitzer, 3500 pictures, yielding 635 measured tracks within the correct angle; with the carbon howitzer, 3750 pictures containing 499 tracks; with methane, 3000 pictures, with each of the howitzers yielding 1082 and 1168 tracks, respectively.

Considerable care was taken in measuring the tracks. Since the source of neutrons subtends an angle of 6.5°, the angle with respect to the direction to the target center within which a track has to be located to be measured, was chosen to be ±8°. The uncertainty of the recoil angle is therefore 14.5° and hence the uncertainty of the neutron energy is 6.5 percent. The pictures were always carefully examined so that short tracks were not missed. Since the interesting energy region corresponds to a track length in the interval from about 0.9 to 3.8 cm in case of He, and from 0.5 to 11.4 cm in methane, one has to correct the results for the decreasing chance that a track will have its entire length visible in the chamber as its length increases. In the previous work this correction did not substantially affect the result. In the present case, however, the result depends largely on this correction, requiring, therefore, a more accurate formula. A simple calculation shows that in order to take the finite depth of the chamber and the finite distance from the neutron source into account one has to multiply the expression given in (I) by the two factors

$$(1-4l\sin\vartheta_0/3\pi h)\cdot(1-l/2D),$$

where l is the apparent track length, ϑ_0 the maximum allowed angle of the recoils with respect to the horizontal plane of symmetry of the chamber, h its depth, and D the distance of its center from the target. The first of these two factors arises from the decreasing chance of a track within ±8° to the horizontal to have its entire length within the depth of the chamber. The second factor is due to the fact that the incident neutrons are not parallel because the source (assumed to be point-like) has a finite distance from the chamber. These two factors have to be multiplied with the expression given in (I) which was derived by assuming parallel incidence of the neutrons, large depth of the chamber, and a negligibly small angular spread of the recoils. Thus the expression by which the observed number of tracks of length l has to be divided is

$$K=(1/\pi)[2\sin^{-1}(1-l^2/4r^2)^{\frac{1}{2}}-(l/r)\times(1-l^2/4r^2)^{\frac{1}{2}}]\cdot(1-4l\sin\vartheta_0/3\pi h)\cdot(1-l/2D),$$

where r is the radius of the cloud chamber. It was frequently checked on the cloud-chamber pictures, by measuring nonhorizontal tracks, that the full depth of the chamber was always sensitive. The stopping power of the gas was determined by the extrapolated integral number range curve of the homogeneous group. Bonner's[7] Q value of 3.28 Mev for the dd reaction was used with the correction given by Livingston and

[7] T. W. Bonner, Phys. Rev. **53**, 711 (1938).

Bethe.[8] By means of the range-energy relation given by Livingston and Bethe and corrected for protons according to Parkinson, Herb, Bellamy and Hudson[9] and for α-particles by Holloway and Livingston,[10] the results were converted into equal energy intervals.

After completion of the resonance experiments the absolute values of the helium backward scattering cross section were determined in the above-mentioned way by using the value 1.4 for the ratio of the cross section of helium and hydrogen at 2.5 Mev as determined in (I). A comparison with the theory, however, revealed that these values were much too large even if one assumed zero splitting and a very low value of the potential scattering. As the experimental value of the hydrogen cross section at this energy is very close to the theoretical one, the discrepancy must have been caused by the value of the ratio at 2.5 Mev. The present results indicate that the influence of the resonance level is still appreciable at 2.5 Mev causing a strong angular anisotropy of the scattering. As discussed later there is indeed a strong increase of low energy recoils at 2.5 Mev. The technique used in (I) is rather insensitive to angular anisotropy. The result obtained in this way is, therefore, probably rather the average ratio of the scattering cross sections of helium and hydrogen than the value for the backward direction. It seemed, therefore, desirable to repeat this measurement with a different technique. For this purpose the cloud chamber was filled with a known mixture of the gases. The observed number of recoils in the forward direction of each kind then gives directly the value of the ratio. This simple procedure involves, however, a serious difficulty because the ranges of protons of 2.5 Mev and α-particles of $(16/25)\times 2.5$ Mev $=1.6$ Mev are enormously different. This can be avoided by measuring first the scattering cross section ratio of helium and deuterium and then of deuterium and hydrogen, since deuterons of $(8/9)\times 2.5$ Mev $=2.22$ Mev have only about half the range of protons of 2.5 Mev. For these experiments the same cloud chamber at the same distance was used and the tracks measured in the same way as before. First the chamber was filled with 1.590 atmos. helium of 96 percent purity (the rest being oxygen and nitrogen) and 0.795 atmos. of deuterium of 99.5 percent purity ($\frac{1}{2}$ percent hydrogen). A small amount of argon was added to increase the stopping power. Water was used as a liquid in order to avoid an excessive number of protons. The mean ranges of the particles are in this case 8.15 and 1.12 cm, respectively. For the second experiment 0.791 atmos. of deuterium were mixed with 0.825 atmos. of ordinary tank hydrogen (purity assumed to be 100 percent) and 0.9 atmos. of argon added. Again, pure water was used as liquid and since, in this experiment, the hydrogen of the water contributes to the recoils, the temperature of the cloud-chamber gas was always carefully measured and the water vapor taken into account. The ranges of the particles were 8.57 and 4.5 cm. The evaluation was made in the same way as before; in particular the same track length corrections were applied. The fact that the density of the tracks is different for the three kinds of particles should not involve any serious errors

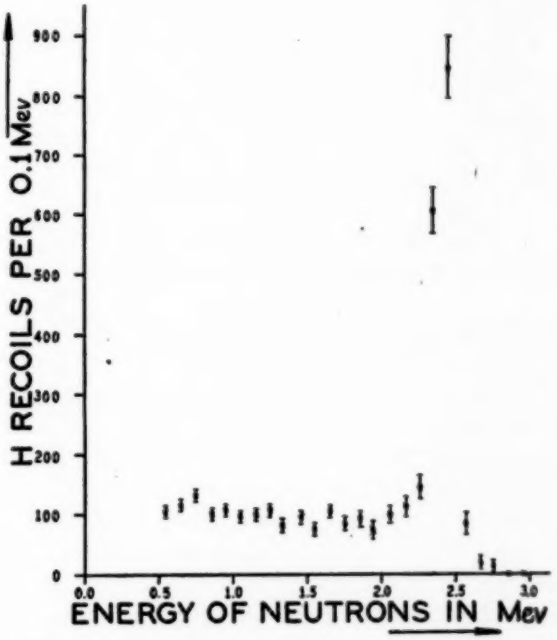

FIG. 3. Corrected number-energy curve of the H recoils in 0.1-Mev intervals as observed with the paraffin howitzer in front of the target.

[8] M. S. Livingston and H. A. Bethe, Rev. Mod. Phys. **9**, 245 (1937).
[9] D. B. Parkinson, R. G. Herb, J. C. Bellamy and C. M. Hudson, Phys. Rev. **52**, 75 (1937).
[10] M. S. Holloway and M. S. Livingston, Phys. Rev. **54**, 18 (1938).

by omitting fainter tracks, since in every case the specific ionization is still so high that no individual droplets can be observed and furthermore because recoils only originate during a time which is probably much shorter than the time of sensitivity of the chamber.

Results

Figures 2 and 3 show the results of the measurements of the spectrum with helium and

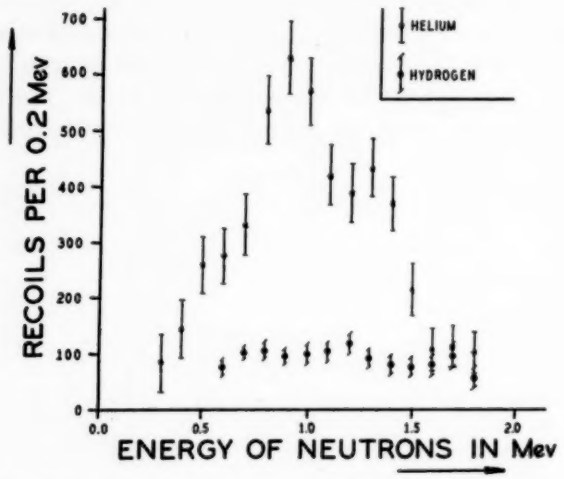

Fig. 4. The difference curves of helium and hydrogen in 0.2-Mev overlapping intervals.

methane, respectively, in the cloud chamber and the paraffin howitzer at the target. The anomalous cross section of He produces a marked and rather wide peak which indicates clearly a doublet structure, whereas the methane spectrum has no irregularities exceeding the statistical error. The scale of the two figures is such as to give the same intensity to the homogeneous group. The width of this line is in very good agreement with the calculated value[8] thus proving that no extraneous instrumental width has been introduced.

The measurements with the carbon howitzer show the same shape for the homogeneous line. For methane, the measurements indicate that about 50 percent of the observed recoils in the low energy region are due to the presence of the paraffin. The number of neutrons per 0.1-Mev interval is then about 1.7 percent of the total number of neutrons in the homogeneous group, in agreement with the calculation for this howitzer. For He the background is the same at 1.7 Mev but about twice as big at 1 Mev as the methane background. This indicates that part of the neutrons scattered from the surroundings have lost an appreciable fraction of their original energy and therefore show up more in He, because of its increased scattering cross section. No indication of the homogeneous group at 0.9 Mev found by Bonner[7] is present. With both gases the background is rather uniform, increasing slightly towards small energies. It may be pointed out that most of the background neutrons are not scattered on the cloud chamber, for in that case the background would be appreciably changed by substituting the carbon howitzer for the paraffin. Preliminary experiments had definitely shown that the number of slow neutrons emerging from the paraffin increased relative to the background when the chamber was placed closer to the target. This indicates that the scattering on the cloud chamber can only be a fraction of that due to the surroundings. The two difference spectra in helium and in methane are represented in Fig. 4. They were obtained after adjusting the intensity of the homogeneous group to one common value. The probable errors do not contain the contribution due to the uncertainty in the multiplicative constant used for matching to equal intensity because this error affects every point of the difference in the same way.

The cloud-chamber pictures taken with the gas mixtures for the determination of the absolute value of the ratio of the backward scattering cross sections at 2.5 Mev yielded two distribution curves with distinct groups from which only a small background had to be subtracted. Their mean ranges determined according to Livingston and Bethe[8] were in excellent agreement with the calculated ones. 3000 pictures taken with the helium-deuterium mixture yielded 398 α-particles and 330 deuterons in the $\pm 8°$ forward direction. After correcting for track length, the ratio of helium to deuterium backward scattering cross section becomes 0.409 ± 0.03. The second set of 3000 pictures taken with the hydrogen-deuterium mixture contained 413 deuterons and 129 protons. The ratio of the backward scattering cross sections becomes thus 1.307 ± 0.110. Hence the ratio of the backward scattering cross sections of

helium and hydrogen is 0.534 ± 0.06. This value is considerably lower than the one found previously (I) which was 1.41. The new value, however, is in agreement with a more recent measurement by Ladenburg[11] who used an ionization chamber and observed a differential number-energy distribution. This value is 0.65 ± 0.13.

With the value of the ratio at 2.5 Mev, the absolute value of the ratios at the lower energies is determined. To compare the present results with the theory, one has to obtain the helium scattering cross section. Experimental data on the hydrogen cross section around 1 Mev neutron energy are not available. Thus one has to rely on the theoretical formula of Wigner and Bethe[12]

$$\sigma_H=\frac{4\pi\hbar^2}{M}\left[\frac{3}{4}\frac{1+\alpha_0 r}{E_0+\tfrac{1}{2}E}+\frac{1}{4}\frac{1+\alpha_1 r}{E_1+\tfrac{1}{2}E}\right];$$

$$\alpha_1=\frac{(ME_0)^{\frac{1}{2}}}{\hbar};\quad \alpha_1=\frac{(ME_1)^{\frac{1}{2}}}{\hbar}.$$

In this formula the values given by Zinn, Seely and Cohen,[13] *viz.*:
$r=2.8\cdot10^{-13}$ cm; $E_0=2.17$ Mev; $E_1=0.066$ Mev were used. According to their measurements the experimental value at 2.88 Mev disagrees only by about 5 percent from the theoretical value whose parameters are chosen in agreement with the results of the proton-proton scattering and the scattering cross section of thermal neutrons. Whether the formula is correct at 1 Mev may be questionable, since several measurements[14] give values which are lower than required by the above formula. Such a large deviation would affect the present results. It is furthermore assumed that the neutron-proton scattering is isotropic in the center of gravity system. Because of the finite dimensions of the source, the recoils measured within $\pm8°$ extend, on the average, over a region from -12 to $+12°$ in the laboratory system. The hydrogen cross section within this solid angle is given by

$$\sigma_H'=2\int_0^{12°}\sigma_H\sin\vartheta_r\cos\vartheta_r d\vartheta_r=0.0432\sigma_H.$$

where σ_H is the total hydrogen cross section, ϑ_r the angle of the recoil proton and the incident neutron in the laboratory system.

The experimental results obtained in this way for the backward helium scattering cross section ($\pm12°$) are represented in Fig. 5 in 0.2-Mev overlapping energy intervals. The points at 1.0 and 1.2 Mev include the previous measurements (I) after readjusting them to the new value at 2.5 Mev, since they were in agreement within the statistical errors with the present values. The resonance peak shows a half-width of about 0.4 Mev and indicates clearly a structure with a separation of about 0.3 Mev. It may be mentioned that the same structure has been obtained

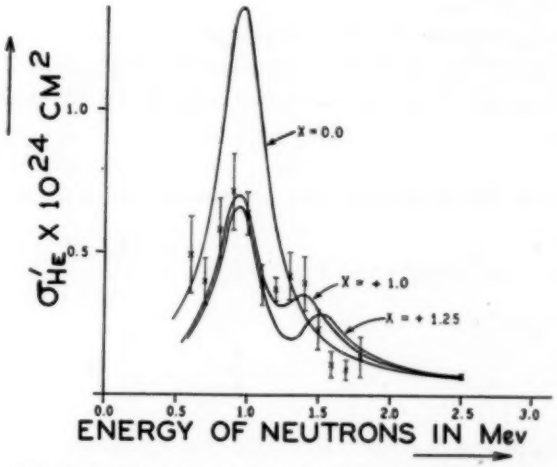

FIG. 5. The backward scattering cross section of helium for a solid angle of $\pm12°$ of the recoils in the laboratory system and inverted splitting. Curves calculated according to formula (2) with $\Gamma=0.4$ Mev, $E_{3/2}=0.95$ Mev, $\sigma_0=0.7\times10^{-24}$ cm^2, $\delta_0>0$, $x=0.0$; $+1.0$; $+1.25$. Points represent observed values in 0.2-Mev overlapping intervals.

in two independent preliminary experiments with entirely different paraffin howitzers. As already mentioned, the present data are consistent with the ones published in (I) provided the new calibrating value at 2.5 Mev is taken into account. The only exception is the point at 0.5 Mev the accuracy of which, as stated in (I), is quite small. The measurements recently published by Hudspeth and Dunlap[15] are also in

[11] We are very much indebted to Professor Ladenburg for communication of his results prior to publication.
[12] See, for example, J. Schwinger and E. Teller, Phys. Rev. **52**, 286 (1937).
[13] W. H. Zinn, S. Seely and V. W. Cohen, Phys. Rev. **56**, 260 (1939).
[14] E. Amaldi, D. Bocciarelli, F. Rasetti and G. C. Trabacchi, Phys. Rev. **56**, 881 (1939). T. Goloborodko and A. Leipunski, Phys. Rev. **56**, 891 (1939); M. Goldhaber, Nature **137**, 824 (1936); W. E. Good and G. Scharf-Goldhaber, Phys. Rev. **58**, 89 (1940).
[15] E. Hudspeth and H. Dunlap, Phys. Rev. **57**, 971 (1940).

agreement with the present results. The fact that their data lack the indication of a structure is obviously due to the smaller number of recoils which they observed. The results of Bonner and Hudspeth[16] cannot be compared, since they refer to the total scattering cross section.

Discussion of the Results

It may first be pointed out that although the absolute values of the helium cross section have been considerably lowered by the newly determined smaller value at 2.5 Mev, the height of the resonance peak is still larger than the highest possible value for an S resonance level. If one assumes the potential and resonance scattering to be caused only by an S wave, the scattering cross section for the observed solid angle would be:

$$\sigma_{\mathrm{He}}' \leq 0.0432 \cdot 4\pi\lambda^2 = 0.182 \cdot 10^{-24} \text{ cm}^2,$$

which is about one-fourth of the observed value.

The complete expression for the resonance scattering of neutrons in helium, taking potential scattering and a finite splitting of the two P levels into account has been given by Bloch[17] (see following article). It is given by

$$\frac{d\sigma_{\mathrm{He}}}{d\omega} = \lambda^2 \left\{ \left| \sin\delta_0 + e^{-i\delta_0} \left(\frac{\Gamma}{E_{3/2} - E - \frac{1}{2}i\Gamma} + \frac{1}{2} \frac{\Gamma}{E_{1/2} - E - \frac{1}{2}i\Gamma} \right) \cos\Theta \right|^2 + \tfrac{1}{4} \sin^2\Theta \left| \frac{\Gamma}{E_{3/2} - E - \frac{1}{2}i\Gamma} - \frac{\Gamma}{E_{1/2} - E - \frac{1}{2}i\Gamma} \right|^2 \right\}. \quad (1)$$

For comparison, the above expression has to be integrated over a solid angle of the recoil α-particles of $\pm 12°$ in the laboratory system. The angle of the recoil ϑ_r in the laboratory system is related to the angle Θ of the scattered neutron in the center of gravity system by:

$$\vartheta_r = \tfrac{1}{2}(\pi - \Theta).$$

Thus the backward scattering cross section for the recoil within $\pm 12°$ becomes:

$$\sigma_{\mathrm{He}}' = \lambda^2 \left\{ 0.0432 \sin^2\delta_0 + 1.49 \frac{[(\epsilon-x)^2+1] + 2[(\epsilon+x)^2+1] - 8x^2/3}{[(\epsilon-x)^2+1] \cdot [(\epsilon+x)^2+1]} + \frac{0.132 \cdot 4x^2/3}{[(\epsilon-x)^2+1][(\epsilon+x)^2+1]} - 1.040 \sin\delta_0 \cos\delta_0 \left[\frac{2(\epsilon-x)}{1+(\epsilon-x)^2} + \frac{\epsilon+x}{1+(\epsilon+x)^2} \right] - 1.040 \sin^2\delta_0 \left[\frac{2}{1+(\epsilon-x)^2} + \frac{1}{1+(\epsilon+x)^2} \right] \right\}, \quad (2)$$

where ϵ and x have the following meaning:

$$\epsilon = \frac{2}{\Gamma} \left(\frac{E_{3/2} + E_{1/2}}{2} - E \right); \quad x = \frac{E_{3/2} - E_{1/2}}{\Gamma}.$$

Therefore, positive values of x mean an inverted doublet, negative values a normal one. $E_{3/2}$, $E_{1/2}$, Γ are the energies of the two P levels and their width, which is assumed to be constant over the resonance region, in either center of gravity or laboratory system; λ is the wavelength of the neutron in the center of gravity system. The four parameters $E_{3/2}$, δ_0, x and Γ have to be chosen so as to be in agreement with the experimental facts. It is assumed that the pure "potential scattering" $4\pi\lambda^2 \sin^2\delta_0 = \sigma_0$ is constant over the resonance region and has a value which is comparable to that determined by Carroll and Dunning[18] for thermal neutrons, viz.:

$$\sigma_0 = 1.5 \times 10^{-24} \text{ cm}^2.$$

The analysis was carried out for positive and negative values of sin δ corresponding to values: 0.0, 0.7, 1.5×10^{-24} cm^2 for σ_0. The width Γ was

[16] T. W. Bonner and E. Hudspeth, Phys. Rev. **57**, 1188 (1940).

[17] F. Bloch, Phys. Rev. **58**, 829 (1940), formula (48).

[18] H. Carroll and J. R. Dunning, Phys. Rev. **54**, 541 (1938).

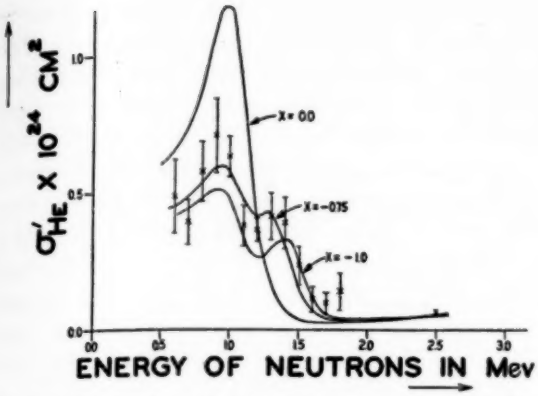

FIG. 6. The backward scattering cross section of helium for a solid angle of $\pm 12°$ of the recoils in the laboratory system and normal splitting. Curves calculated according to formula (2) with: $\Gamma=0.4$ Mev, $E_{1/2}=1.05$ Mev; $\sigma_0=1.5\times10^{-24}$ cm^2, $\delta_0<0$, $x=0.0$; -0.75; -1.0.

chosen to be 0.4 Mev for the neutrons in the laboratory system and the values of $E_{1/2}$ or $E_{3/2}$ so that the maximum of the curve occurred at 0.95 Mev. This was done for various positive and negative values of the splitting x.

The position of the experimental points would, of course, suggest that the splitting is positive since the more intense peak occurs at lower energies. In fact one finds a well fitting theoretical curve with the following values of the parameters:

$$x=+1.0^{+0.31}_{-0.20};\quad E_{3/2}=0.95\text{ Mev};\quad E_{1/2}=1.35\text{ Mev};$$
$$\Gamma=0.4\text{ Mev};\quad \sigma_0=0.7\times10^{-24}\text{ cm}^2.$$

This curve is represented in Fig. 5 together with two curves corresponding to $x=0.5$ and $x=1.25$, respectively, and the same values of σ_0, $E_{3/2}$ and Γ. It is evident that both structure and height of the resonance peak are distinctly in agreement within their statistical errors for $x=+1.0$. This would, therefore, indicate that if the doublet is inverted the splitting would be $0.4^{+0.12}_{-0.08}$ Mev for the neutrons in the laboratory system.[19] For the two states of He^5 one obtains the corresponding energies by multiplying by $m_{He}/(m_{He}+m_n)$

$$E_{3/2}=0.76\text{ Mev};\quad E_{1/2}=1.08\text{ Mev};$$
$$\Delta E=0.32^{+0.10}_{-0.06}\text{ Mev};\quad \Gamma(He^5)=0.32\text{ Mev}$$

where $E_{3/2}$ and $E_{1/2}$ represent the energies above a separated α-particle and a neutron. The probable errors are estimated from the statistical errors indicated in the figure and the systematic errors arising from matching the four measurements determining the points to the same intensity of the 2.5-Mev line. The theoretical curve was not integrated over 0.2 Mev, since this would not substantially affect its shape.

If one chooses the negative sign of the phase, the curve looks entirely different. In fact, the interference term in formula (2) which is proportional to $\sin\delta_0\cos\delta_0$ and changes its sign with δ, tends, in the case of negative phase, to lower the value of σ_{He}' on the high energy side and to increase it on the low energy side. For positive values of x and negative values of δ the curve shows scarcely any structure.

This influence of one of the interference terms suggests, therefore, that it may be possible that the doublet is normal. If one chooses negative values of the phase and of x, it may happen that for sufficiently large σ_0 the apparent intensities are reversed. This is shown in Fig. 6. A well fitting curve is again obtained with

$$x=-0.75\pm^{+0.19}_{-0.25};\quad E_{1/2}=1.05\text{ Mev};$$
$$E_{3/2}=1.35\text{ Mev};\quad \Gamma=0.4\text{ Mev};$$
$$\sigma_0=1.5\times10^{-24}\text{ cm}^2.$$

The corresponding values for He^5 would be

$$E_{1/2}=0.84\text{ Mev};\quad E_{3/2}=1.08\text{ Mev};$$
$$\Gamma(He^5)=0.32\text{ Mev};\quad \Delta E=0.24^{+0.06}_{-0.08}\text{ Mev}.$$

The width $\Gamma(He^5)$ which is found from the present results may be checked against the experiments of William, Shepherd and Haxby[2] on the reaction:

$$_3Li^7+{}_1H^2\rightarrow{}_2He^5+{}_2He^4.$$

The observed group of α-particles has a width of $\Gamma_\alpha=0.14$ Mev. In order to obtain[20] from Γ_α the width $\Gamma(He^5)$, one has to observe that

$$\Gamma(He^5)=(1+m_\alpha/m(He^5))\Gamma_\alpha=0.25\text{ Mev}$$

which is in good agreement with the present value of 0.32 Mev.

[19] Compare previous results given in Phys. Rev. **57**, 936 (1940).

[20] It may be noted that the statement given in (I) that $\Gamma_\alpha=\Gamma(He^5)$ is, of course, erroneous.

The analysis of the experimental data shows that it is not possible within the present accuracy to decide whether the two states of He^5 form a normal or an inverted doublet. However, it is evident that the sign of the splitting is related to the sign of the phase of the S potential scattering. A normal doublet requires a negative phase and vice versa. An investigation of the angular distribution of the helium recoils produced by resonance neutrons would quite easily show the sign of the phase and hence of the splitting. The present cloud-chamber data which are taken with nonmonochromatic neutrons do not allow this procedure. If one assumes that δ does not change its sign between 1 and 2.5 Mev one may obtain its sign according to a suggestion of Ladenburg from measurements of the angular distribution of the recoils at 2.5 Mev. This distribution was found by Ladenburg, Barschall and Kanner[21] to be highly anisotropic, showing a rapid increase of the number of recoils toward small scattering angles of the neutrons. This increase was believed (I) to arise from a small number of slow neutrons in the spectrum of the *dd* reaction. The recent measurements of Ladenburg, Barschall and Kanner show clearly that the anisotropy is not caused by slow neutrons. The steep rise of the recoils with small scattering angles of the neutrons can be explained at least partly by the fact, that at 2.5 Mev there is still a considerable amplitude of the P resonance wave interfering with the S potential wave. One obtains an increase of low energy recoils only if one assumes a negative phase. A positive phase would produce a decrease of the low energy recoils. This would, therefore, indicate that if one assumes that δ does not change its sign between 1 and 2.5 Mev, the He^5 doublet is normal.

Theoretically the doublet structure of He^5 has been investigated by Dancoff.[22] His results show that a doublet caused by the relativistic Thomas force would be inverted but would show a splitting of only some kev. A splitting of several hundred kev as observed can be obtained by calculating the second-order spin-orbit interaction due to the tensor forces. Dancoff showed that in this case the doublet should be normal.

In conclusion, we wish to express our gratitude to Dr. F. Bloch and Dr. N. Bradbury for much helpful discussion and advice during the course of this experiment.

[21] We are very much indebted to Professor Ladenburg for the kind communication of his results before publication and the discussion of this point.

[22] S. M. Dancoff, Phys. Rev. **56**, 384 (1939).

Theory of the Resonance Scattering of Protons and Neutrons on Helium

F. Bloch
Stanford University, Palo Alto, California
(Received September 3, 1940)

A treatment of the general dispersion problem is presented in which the wave function, describing a resonance process appears as a monochromatic Fourier component of a wave packet, which is built in such a way that it represents for $t>0$ the decay of a compound state and for $t<0$ the building up of the same compound state. The method is applied to the resonance P scattering of protons and neutrons on helium.

THE existence of an unstable p state of He^5 and Li^5 and the correlated anomalies[1] in the scattering cross sections of protons and neutrons on He^4 represent a particularly interesting case of nuclear dispersion. It seems worth while to work out this case separately both for its simplicity and for the fact that here the finer features of the theory, arising from two levels with a splitting comparable to their width and from the interference of the so-called "potential scattering" with the resonance scattering are essential in the discussion of the experiments.

1. The Dispersion Formula

The general theory of nuclear dispersion has been well worked out by several authors.[2] Among these the treatment of Kapur and Peierls deserves special attention insofar as it requires a minimum of assumptions, the compound state of the system being introduced merely by the condition that at sufficient distance one will observe only out-going but no incoming waves. Their general results, however, become simple and useful, without a detailed knowledge of the system, only if one assumes further that the compound state has a long life.

We want to indicate a simple derivation of the dispersion formula where this assumption is introduced from the beginning, thus allowing the usual methods of perturbation theory, but where we start from the very existence of the compound state without any further assumption as do Kapur and Peierls. Particularly we want to abandon the unnecessary restriction that all nuclear processes which do not show resonance are to be described as potential scattering, i.e., are caused by forces acting solely on the incident particle. It is indeed noteworthy that the distinction between resonance and nonresonance processes is merely an approximate one, to be made only so long as the compound state has a comparatively long lifetime.* While for certain states of one and the same dynamical system this condition may be fulfilled, it will generally turn out that for others, particularly the states with higher energy, this distinction becomes entirely impracticable. In the study of resonance processes one is only interested, however, in the anomalies occurring within a certain small range of energies and it is quite sufficient to examine specially only those compound states which lie close to or within that range. We can and shall choose the number of these states to be finite, since, as we shall see below, it is by no means necessary that the eigenfunctions describing them form a complete set.

Let us consider a dynamical system consisting of certain nuclear particles. These particles may be any heavy nuclear fragments or even light quanta, electrons, neutrinos or mesotrons. If one could find the rigorous stationary solutions of the wave-mechanical problem they could obviously be classified into those which are energetically stable and those which are not. The stable solutions would be described by wave functions which vanish if any one of the particles

[1] See the preceding paper of H. Staub and H. Tatel; also W. P. Heydenburg and N. F. Ramsey, Phys. Rev. **57**, 106 (1940).

[2] G. Breit and E. Wigner, Phys. Rev. **49**, 519 (1936); H. A. Bethe and G. Placzek, *ibid.* **51**, 450 (1937); H. A. Bethe, Rev. Mod. Phys. **9**, 69 (1937); F. Kalckar, J. R. Oppenheimer and R. Serber, Phys. Rev. **52**, 273 (1937); P. L. Kapur and R. Peierls, Proc. Roy. Soc. **A166**, 277 (1938); A. Siegert, Phys. Rev. **56**, 750 (1939).

* *Note added in proof.*—This point is also emphasized in a recent paper by G. Breit, Phys. Rev. **58**, 506 (1940).

is moved to infinite distance from any other, while the unstable ones could be written asymptotically (i.e., for large distances of certain particles from a remaining residual nucleus) as a product of a free solution of that particle times a wave function, describing the residual nucleus. In the idealized limit of infinitely long lifetimes of certain compound states there will now be a degeneracy between some of the unstable states which, by proper linear combinations, will yield new states of the same energy whose wave functions have the same asymptotic behavior as those of the energetically stable states, i.e., to vanish, as any one of the particles is infinitely removed from any other. A finite number of such metastable states, obtained in the way just described, we shall denote by a subscript $r (r=1, 2\cdots n)$ and their wave functions by φ_r. Besides these states r there will of course still be an infinite set of states, to be described by the subscript s, whose wave functions φ_s have the asymptotic behavior generally characteristic of unstable solutions.

Omitting the energetically stable solutions, we can then write the wave function describing our system in this limit in the form

$$\psi=\sum_r c_r e^{-iE_r t/\hbar}+\sum_s c_s e^{-iE_s t/\hbar}, \tag{1}$$

where the quantities c_r and c_s are arbitrary constants.

The rigorous time-dependent Schrödinger equation which ψ has to satisfy, will now imply that these quantities are generally no longer constants, but depend on the time in a way which, without further restrictions but merely by an appropriate choice of the states r and s is described by the equations

$$-(\hbar/i)\dot{c}_r=\sum_s V_{rs}e^{i(E_r-E_s)t/\hbar}, \tag{2a}$$

$$-(\hbar/i)\dot{c}_s=\sum_r V_{sr}e^{i(E_s-E_r)t/\hbar} \tag{2b}$$

with $V_{rs}=V_{sr}^*$. It is not necessary and generally not even possible to know the quantities V_{rs} nor any "small perturbation" V of which they may be considered to be the matrix elements.

As in the theory of spontaneous emission of radiation, one can show that there exist n characteristic solutions of Eqs. (2) which after a sufficient time $t\gg T$ take the form

$$c^+{}_{r\rho}=e^{-i(E_\rho-E_r-\frac{1}{2}i\Gamma_\rho)t/\hbar}d^+{}_{r\rho}, \tag{3a}$$

$$c^+{}_{s\rho}=\sum_r V_{sr}\frac{e^{-i(E_\rho-E_s-\frac{1}{2}i\Gamma_\rho)t/\hbar}-1}{E_\rho-E_s-\frac{1}{2}i\Gamma_\rho}d^+{}_{r\rho}; \tag{3b}$$

$$\rho=1, 2\cdots n,$$

where the quantities $d^+{}_{r\rho}$ are constants, satisfying the system of homogeneous equations

$$(E_\rho-\tfrac{1}{2}i\Gamma_\rho)d^+{}_{r\rho}=\sum_{r'}(H_{rr'}-\tfrac{1}{2}i\Gamma_{rr'})d^+{}_{r'\rho}; \tag{4}$$

$$r=1, 2\cdots n$$

with the n complex eigenvalues

$$E_\rho-\tfrac{1}{2}i\Gamma_\rho. \tag{5}$$

The index ρ of the quantities c_r and c_s indicates that they refer to a special solution of (4) representing the compound state ρ and the $+$ sign indicates that this solution is valid for sufficiently large positive times.

Equation (3a) represents the exponential decay of the compound state ρ with lifetime $\hbar/\Gamma_\rho$ and Eq. (3b) the corresponding building up of the "free particle states" s.

Both the hermitian matrices $H_{rr'}$ and $\Gamma_{rr'}$ in (4) are to be derived from the matrix function

$$F_{rr'}(E_s)=2\pi\sum_\sigma V_{r\sigma}(E_s)V^*{}_{r'\sigma}(E_s)P_\sigma(E_s), \tag{6}$$

where instead of the subscript s we have used the energy E_s of the state s and another subscript σ which may be necessary for its complete characterization; the number of states lying between E_s and E_s+dE_s is given by $P_\sigma(E_s)dE_s$.

The limits of validity of Eqs. (3) are also determined by (6); let E_0 be the amount by which E_s has to vary in order that $F_{rr'}$ varies in the neighborhood of the values E_ρ by its own order of magnitude. E_0 will largely depend on the kinds of processes under consideration. If the outgoing particles are neutrons of not too high energies so that the main variation in $F_{rr'}$ arises from $P_\sigma(E_s)$ one will have to choose E_0 of the order of magnitude of the kinetic energy of the neutrons. In the presence of a Coulomb barrier E_0 may have to be chosen considerably smaller and for energies comparable to the nuclear bind-

ing energy E_0 will be of the order of these binding forces since in both these latter cases the quantity $V_{r\sigma}V^*_{r'\sigma}$ will be the determining factor.

Equations (3) can now claim validity if the two conditions

$$t \gg T = h/E_0; \quad \Gamma_\rho \ll E_0 \quad (7) \text{ and } (8)$$

are satisfied. Relation (8) expresses the main assumption which underlies the perturbation treatment, namely that the lifetime h/Γ_ρ of the compound state ρ be large compared to the characteristic time $T = h/E_0$.

From the solutions (3) we can obtain a somewhat more general solution of Eqs. (2) in the form

$$c^+_r = \sum_\rho K^+_\rho c^+_{r\rho}, \tag{9a}$$

$$c^+_s = \sum_\rho K^+_\rho c^+_{s\rho} \tag{9b}$$

with arbitrary constants K_ρ^+. Although (9) is valid only for $t \gg T$ we can investigate the form it will take if we integrate Eqs. (2) backward to negative times t. First we remark that the quantities c_r and c_s satisfy the same Eqs. (2) as c_r^* and c_s^* if V_{rs} is replaced by $V^*_{rs} = V_{sr}$ and t by $-t$. We thus obtain n further solutions of Eqs. (2), valid for $-t \gg T$ which, in analogy to (3), take the form

$$c^-_{r\rho} = e^{-i(E_\rho - E_r + \frac{1}{2}i\Gamma_\rho)t/\hbar} d^-_{r\rho}, \tag{10a}$$

$$c^-_{s\rho} = \sum_r V_{sr} \frac{e^{-i(E_\rho - E_s + \frac{1}{2}i\Gamma_\rho)t/\hbar} - 1}{E_\rho - E_s + \frac{1}{2}i\Gamma_\rho} d^-_{r\rho} \tag{10b}$$

with

$$(E_\rho + \tfrac{1}{2}i\Gamma_\rho) d^-_{r\rho} = \sum_{r'} (H_{rr'} + \tfrac{1}{2}i\Gamma_{rr'}) d^-_{r'\rho}. \tag{11}$$

Again condition (8) has to be satisfied and the $-$ sign indicates that (10) claims validity for sufficiently large negative times. Equations (4) and (11) lead to the same eigenvalues E_ρ and Γ_ρ since $H_{rr'} = H^*_{r'r}$ and $\Gamma_{rr'} = \Gamma^*_{r'r}$ so that the conjugate complex of (11) differs from (4) merely by the interchange of rows and columns of the matrix $H_{rr'} - \frac{1}{2}i\Gamma_{rr'}$ and thus leaves its complex eigenvalues $E_\rho - \frac{1}{2}i\Gamma_\rho$ unaltered. We further note that with proper normalization of the constants $d_{r\rho}$ (4) and the conjugate complex of (11) lead immediately to the relation

$$\sum_r d^+_{r\rho} d^*_{r\rho'} = \delta_{\rho\rho'}. \tag{12}$$

Finally we can write in analogy to (9)

$$c^-_r = \sum_\rho K^-_\rho c^-_{r\rho}, \tag{13a}$$

$$c^-_s = \sum_\rho K^-_\rho c^-_{s\rho} \tag{13b}$$

with n more constants K_ρ^-.

In order that (9) and (13) join on to the same solution at $t = 0$ it can be shown under the condition (8) that there must exist the n relations

$$\sum_r K^+_\rho d^+_{r\rho} = \sum_r K^-_\rho d^-_{r\rho}; \quad r = 1, 2 \cdots n, \tag{14}$$

between the constants K_ρ^+ and K_ρ^- so that through (12) one set of constants can be expressed in terms of the other. Equations (10) evidently describe the manner in which a compound state ρ is built up for negative times which for positive times decays according to Eqs. (3).

Substituting (9) and (13) into (1) we now obtain two wave-functions ψ^+ and ψ^- which, except for higher order terms in Γ_ρ/E_0 express correctly one and the same solution ψ of the time-dependent Schrödinger equation for positive and negative times, respectively. For the dispersion problem we are interested in a stationary solution corresponding to a given energy E of the total system which we obtain from ψ by Fourier analysis in the form

$$\chi(E) = \int_{-\infty}^{+\infty} e^{iEt/\hbar} \psi(t) dt. \tag{15}$$

Furthermore we only need the asymptotic form $\chi^\tau(E)$ which (15) will assume as any particle Q is far removed from the residual nucleus. We shall denote by R, θ, Φ the polar coordinates of the particle Q relative to the center of gravity of the system and by τ a system of quantum numbers, characterizing the internal state of Q and the remaining nucleus as R approaches infinity. Before we can write down the definite expression for $\chi^\tau(E)$ we have to define the corresponding asymptotic forms of the functions φ_s, used in (1) since these only will contribute to χ.

Including the case where both particle Q and remaining nucleus are charged we then can write asymptotically

$$\varphi_s \rightarrow \varphi^r{}_s(E_s) = \frac{1}{R}\sum_{l,m}\left[a^r{}_{\sigma,l,m}(E_s)e^{i(kR-\frac{1}{2}l\pi+\eta_l-\alpha\log 2kR)} + b^r{}_{\sigma,l,m}(E_s)e^{-i(kR-\frac{1}{2}l\pi+\eta_l-\alpha\log 2kR)}\right]Y_l^m(\theta,\Phi), \quad (16)$$

where the functions Y_l^m are spherical harmonics, normalized to 4π on the sphere. Here again we have characterized the state s by its energy E_s and by an additional set of quantum numbers σ. The quantities $a^r{}_{\sigma,l,m}$ and $b^r{}_{\sigma,l,m}$ depend on all dynamical variables except R,θ and Φ. If $v=v(E_s)$ is the relative velocity of particle Q and remaining nucleus, corresponding to the total energy E_s of the system we have

$$k = mv/\hbar = k(E_s) \quad (17)$$

with m as the effective mass of particle Q. Further it is

$$\alpha = e_R e_Q/\hbar v = \alpha(E_s), \quad (18)$$

e_R and e_Q being the charges of remaining nucleus R and particle Q, respectively, and finally it is

$$\eta_l = \arg\left[(l+i\alpha)!\right] = \eta_l(E_s). \quad (19)$$

With (1), (9), (13) and (16) we then obtain from (15) asymptotically

$$\chi^r(E,R,\theta,\Phi) = -\frac{2\pi\hbar}{R}\sum_{r,\rho,\sigma,l,m}\left[K_\rho{}^+ d^+{}_{r\rho}a^r{}_{\sigma,l,m}(E)\frac{e^{i(kR-\frac{1}{2}l\pi+\eta_l-\alpha\log 2kR)}}{E_\rho - E - \frac{1}{2}i\Gamma_\rho}\right.$$
$$\left. + K_\rho{}^- d^-{}_{r\rho}b^r{}_{\sigma,l,m}(E)\frac{e^{-i(kR-\frac{1}{2}l\pi+\eta_l-\alpha\log 2kR)}}{E_\rho - E + \frac{1}{2}i\Gamma_\rho}\right]V_{\sigma r}(E)P_\sigma(E)\,Y_l^m(\theta,\Phi). \quad (20)$$

This can be written in a more convenient form by using the relations (14). Writing as an abbreviation

$$S_\sigma{}^\pm(E) = -2\pi\hbar\sum_{r\rho}P_\sigma(E)\,V_{\sigma r}(E)d^+{}_{r\rho}\frac{K_\rho{}^\pm}{E_\rho - E \mp \frac{1}{2}i\Gamma_\rho}, \quad (21)$$

we have

$$\chi^r(E,R,\theta,\Phi) = \frac{1}{R}\sum_{\sigma,l,m}\left[S_\sigma{}^+(E)a^r{}_{\sigma,l,m}(E)e^{i(kR-\frac{1}{2}l\pi+\eta_l-2\log 2kR)}\right.$$
$$\left. + S_\sigma{}^-(E)b^r{}_{\sigma,l,m}(E)e^{-i(kR-\frac{1}{2}l\pi+\eta_l-2\log 2kR)}\right]Y_l^m(\theta,\Phi), \quad (22)$$

where the quantities $S_\sigma{}^+$ and $S_\sigma{}^-$ are related by

$$S_\sigma{}^+(E) = S_\sigma{}^-(E) + i\sum_{\rho\sigma'}\frac{\Gamma_{\rho;\sigma\sigma'}(E)}{E_\rho - E - \frac{1}{2}i\Gamma_\rho}S^-{}_{\sigma'}(E) \quad (23)$$

with

$$\Gamma_{\rho;\sigma\sigma'}(E) = 2\pi\sum_{rr'}\bar{d}^*{}_{r'\rho}V_{r'\sigma'}(E)P_\sigma(E)\,V_{\sigma r}(E)d^+{}_{r\rho}. \quad (24)$$

Equation (22) may properly be called the general dispersion formula, since it contains all those features in the asymptotic form of the wave-function which are caused by long life compound states. Comparing (22) with the functions $\varphi_\sigma{}^r(E)$ of (16) we see that the compound states establish essentially a changed relation between the amplitudes of incoming and outgoing particle waves which is described by the relations (23) between the quantities $S_\sigma{}^+$ and $S_\sigma{}^-$. Besides the energies E_ρ and widths Γ_ρ of the compound states there enter in (23) the quantities $\Gamma_{\rho;\,\sigma\sigma'}(E)$ which over a range of the energy E, small compared to E_0 may be replaced by constants. These values are not quite inde-

pendent of the matrices $H_{rr'}$ and $\Gamma_{rr'}$ from which E_ρ, Γ_ρ and $d^{\pm}{}_{r\rho}$ are derived through the equations (4) and (11). Indeed in this range, from (6)

$$\Gamma_{rr'}=F_{rr'}(E)=2\pi\sum_\sigma V_{r\sigma}(E)V_{\sigma r'}(E)P_\sigma(E), \tag{25}$$

so that we have

$$\sum_\sigma \Gamma_{\rho;\sigma\sigma}=\sum_{rr'}\bar{d}^{*}_{r'\rho}\Gamma_{rr'}d^{+}{}_{r\rho}. \tag{24a}$$

It seems to us that the closed form (22) forms a most convenient basis for the discussion of dispersion problems and we shall now proceed to specialize it to the case in which we are interested.

2. Elastic Scattering of a Particle with Spin $\frac{1}{2}$ by a Nucleus with Spin Zero

The main simplifying feature here lies in the conservation of angular momentum. We shall assume that the incident wave represents a particle with spin $\frac{1}{2}$ [3] in the direction of incidence (z direction). We then have to consider only states of the total system for which j_z, the z component of the total angular momentum, has the value $\frac{1}{2}$. Assuming that the spin orbit coupling is small compared to the spacing of levels with different orbital momentum l of the compound state, so that a given value l is still a good quantum number we can for $j_z=\frac{1}{2}$ characterize a state s besides its energy E_s by its orbital momentum l and its total angular momentum $j=l\pm\frac{1}{2}$. It will be sufficient to replace the index σ in (16) by $l\pm\frac{1}{2}$, having it understood that at the same time the orbital momentum shall assume the value l.

It is then easily seen that

$$\varphi^{r}{}_{l+\frac{1}{2}}(E_s)=\frac{1}{R}A^{r}\sin\left(kR-\frac{l\pi}{2}+\eta_l+\delta_{l+\frac{1}{2}}-\alpha\log 2kR\right)\frac{1}{(2l^2+l)^{\frac{1}{2}}}$$
$$\times[[l(l+1)]^{\frac{1}{2}}Q_{\frac{1}{2}}Y_l^0(\theta,\Phi)+lQ_{-\frac{1}{2}}Y_l^1(\theta,\Phi)] \tag{26}$$

and

$$\varphi^{r}{}_{l-\frac{1}{2}}(E_s)=\frac{1}{R}A^{r}\sin\left(kR-\frac{l\pi}{2}+\eta_l+\delta_{l-\frac{1}{2}}-\alpha\log 2kR\right)\frac{1}{(2l^2+l)^{\frac{1}{2}}}$$
$$\times[lQ_{\frac{1}{2}}Y_l^0(\theta,\Phi)-[l(l+1)]^{\frac{1}{2}}Q_{-\frac{1}{2}}Y_l^1(\theta,\Phi)], \tag{27}$$

where $Q_{\pm\frac{1}{2}}$ represents a spin eigenfunction of the particle Q with spin orientation in the positive and negative z direction, respectively, and where A^r represents the wave function of the residual nucleus with spin zero. By comparison with (16) we obtain thus first from (26) and (27) the quantities a and b, entering in (22). They contain essentially the phases $\delta_{l\pm\frac{1}{2}}$ about which nothing can be said without knowing finer details of the interaction between particle Q and residual nucleus except that they will generally vary slowly with E.

It remains to determine the quantities $S_\sigma{}^{\pm}$ or $S^{\pm}{}_{l\pm\frac{1}{2}}$ in (22). If E lies close to the energy of a compound state with angular momentum l^* while all other compound states lie far away, we can for all values $l\neq l^*$ write

$$S^{+}{}_{l\pm\frac{1}{2}}=S^{-}{}_{l\pm\frac{1}{2}}=C_{l\pm\frac{1}{2}}e^{i(\eta_l+\delta_{l\pm\frac{1}{2}})}. \tag{28}$$

Since only states with equal angular momentum combine we obtain from (23) two separate equations for $S^{\pm}{}_{l+\frac{1}{2}}$ and $S^{\pm}{}_{l-\frac{1}{2}}$ which, using (24a) for $l=l^*$, can be written in the form

$$S^{+}{}_{l^*\pm\frac{1}{2}}=S^{-}{}_{l^*\pm\frac{1}{2}}\left(1+i\frac{\Gamma_{l^*\pm\frac{1}{2}}}{E_{l^*\pm\frac{1}{2}}-E-\frac{1}{2}i\Gamma_{l^*\pm\frac{1}{2}}}\right)=S^{-}{}_{l^*\pm\frac{1}{2}}\frac{E_{l^*\pm\frac{1}{2}}-E+\frac{1}{2}i\Gamma_{l^*\pm\frac{1}{2}}}{E_{l^*\pm\frac{1}{2}}-E-\frac{1}{2}i\Gamma_{l^*\pm\frac{1}{2}}}. \tag{29}$$

[3] All angular momenta are measured in units $\hbar=h/2\pi$.

Or with

$$\gamma_{l^*\pm\frac{1}{2}}=\arctan\frac{1}{2}\frac{\Gamma_{l^*\pm\frac{1}{2}}}{E_{l^*\pm\frac{1}{2}}-E-\frac{1}{2}i\Gamma_{l^*\pm\frac{1}{2}}}, \tag{30}$$

$$e^{-i\gamma_{l^*\pm\frac{1}{2}}}S^+_{l^*\pm\frac{1}{2}}=e^{i\gamma_{l^*\pm\frac{1}{2}}}S^-_{l^*\pm\frac{1}{2}}=C_{l^*\pm\frac{1}{2}}e^{i(\eta_{l^*}+\delta_{l^*\pm\frac{1}{2}})}. \tag{31}$$

Using (26), (27), (28), and (31) we can now write (22) in the form

$$\chi^\tau(E,R,\theta,\Phi)=\frac{A^\tau}{R}\sum_l\left\{C_{l+\frac{1}{2}}e^{i\beta_{l+\frac{1}{2}}}\sin\left(kR-\frac{l\pi}{2}+\beta_{l+\frac{1}{2}}-\alpha\log 2kR\right)\frac{1}{(2l^2+l)^{\frac{1}{2}}}[[l(l+1)]^{\frac{1}{2}}Q_{\frac{1}{2}}Y_l^0(\theta,\Phi)\right.$$
$$\left.+lQ_{-\frac{1}{2}}Y_l^1(\theta,\Phi)]+C_{l-\frac{1}{2}}e^{i\beta_{l-\frac{1}{2}}}\sin\left(kR-\frac{l\pi}{2}+\beta_{l-\frac{1}{2}}-\alpha\log 2kR\right)\frac{1}{(2l^2+l)^{\frac{1}{2}}}\right.$$
$$\left.\times[lQ_{\frac{1}{2}}Y_l^0(\theta,\Phi)-[l(l+1)]^{\frac{1}{2}}Q_{-\frac{1}{2}}Y_l^1(\theta,\Phi)]\right\}, \tag{32}$$

where we have introduced

$$\beta_{l\pm\frac{1}{2}}=\delta_{l\pm\frac{1}{2}}+\eta_l \quad \text{for} \quad l\neq l^* \tag{33a}$$

and

$$\beta_{l^*\pm\frac{1}{2}}=\delta_{l^*\pm\frac{1}{2}}+\gamma_{l^*\pm\frac{1}{2}}+\eta_{l^*} \tag{33b}$$

and where the energy dependent quantities η_l, $\delta_{l\pm\frac{1}{2}}$ and k are to be taken with those values which they assume for the energy E. We now have to determine the constants $C_{l\pm\frac{1}{2}}$ in (32) in such a way that the incoming spherical waves are those belonging asymptotically to a plane wave of the form

$$A^\tau e^{i[kZ+i\alpha\log k(R-Z)]}=\frac{1}{kR}A^\tau\sum_{l=0}^{\infty}(2l+1)^{\frac{1}{2}}i^l\sin\left(kR-\frac{l\pi}{2}-\alpha\log 2kR\right)Q_{\frac{1}{2}}Y_l^0(\theta,\Phi). \tag{34}$$

This means that

$$lC_{l+\frac{1}{2}}-[l(l+1)]^{\frac{1}{2}}C_{l-\frac{1}{2}}=0, \quad [l(l+1)]^{\frac{1}{2}}C_{l+\frac{1}{2}}+lC_{l-\frac{1}{2}}=(2l^2+l)^{\frac{1}{2}}(2l+1)^{\frac{1}{2}}i^l/k$$

or

$$C_{l+\frac{1}{2}}=(l+1)^{\frac{1}{2}}i^l/k; \quad C_{l-\frac{1}{2}}=l^{\frac{1}{2}}i^l/k. \tag{35a) and (35b)}$$

Substituting these values into (32) we find

$$\chi^\tau=\frac{A^\tau}{kR}\sum_l\frac{i^l}{(2l+1)^{\frac{1}{2}}}\{e^{i\beta_{l+\frac{1}{2}}}\sin(kR-\tfrac{1}{2}l\pi+\beta_{l+\frac{1}{2}}-\alpha\log 2kR)[(l+1)Q_{\frac{1}{2}}Y_l^0+[l(l+1)]^{\frac{1}{2}}Q_{-\frac{1}{2}}Y_l^1]$$
$$+e^{i\beta_{l-\frac{1}{2}}}\sin(kR-\tfrac{1}{2}l\pi+\beta_{l-\frac{1}{2}}-\alpha\log 2kR)[lQ_{\frac{1}{2}}Y_l^0-[l(l+1)]^{\frac{1}{2}}Q_{-\frac{1}{2}}Y_l^1]\}. \tag{36}$$

Subtracting (34) from (36) we obtain for the scattered wave

$$\chi_s=\frac{A^\tau}{kR}e^{i(kR-\alpha\log 2kR)}\left\{Q_{\frac{1}{2}}\sum_l\frac{1}{(2l+1)^{\frac{1}{2}}}[(l+1)e^{i\beta_{l+\frac{1}{2}}}\sin\beta_{l+\frac{1}{2}}+le^{i\beta_{l-\frac{1}{2}}}\sin\beta_{l-\frac{1}{2}}]Y_l^0\right.$$
$$\left.+Q_{-\frac{1}{2}}\sum_l\left(\frac{l(l+1)}{2l+1}\right)^{\frac{1}{2}}[e^{i\beta_{l+\frac{1}{2}}}\sin\beta_{l+\frac{1}{2}}-e^{i\beta_{l-\frac{1}{2}}}\sin\beta_{l-\frac{1}{2}}]Y_l^1\right\}. \tag{37}$$

The first part in the bracket of (37) represents those particles which have not altered the orientation of their spin in the scattering process, the second those which have reversed it. In the total

scattering cross section these two parts contribute incoherently and we thus find for the cross section per unit solid angle

$$\frac{dS}{d\omega}=\frac{1}{k^2}\left\{\left|\sum_l \frac{1}{(2l+1)^{\frac{1}{2}}}[(l+1)e^{i\beta_{l+\frac{1}{2}}}\sin\beta_{l+\frac{1}{2}}+le^{i\beta_{l-\frac{1}{2}}}\sin\beta_{l-\frac{1}{2}}]Y_l^0\right|^2\right.$$
$$\left.+\left|\sum_l\left(\frac{l(l+1)}{2l+1}\right)^{\frac{1}{2}}[e^{i\beta_{l+\frac{1}{2}}}\sin\beta_{l+\frac{1}{2}}-e^{i\beta_{l-\frac{1}{2}}}\sin\beta_{l-\frac{1}{2}}]Y_l'\right|^2\right\}. \quad (38)$$

It remains to further specialize this formula to the case where the compound state is a P state, i.e., where $l^*=1$ and to introduce those simplifications which seem likely to be valid in the case of the scattering of protons and neutrons on He^4. First of all, because of the smallness of spin-orbit forces we may assume that

$$\delta_{l+\frac{1}{2}}=\delta_{l-\frac{1}{2}}=\delta_l. \quad (39)$$

This means with Eq. (33a) that

$$\beta_{l+\frac{1}{2}}=\beta_{l-\frac{1}{2}}=\beta_l=\eta_l+\delta_l \quad \text{for} \quad l\neq l^*. \quad (40)$$

For $l=l^*$ this equation cannot be maintained to be valid since $\gamma_{l^*+\frac{1}{2}}$ and $\gamma_{l^*-\frac{1}{2}}$ will vary irregularly in the neighborhood of the two different values $E_{l^*+\frac{1}{2}}$ and $E_{l^*-\frac{1}{2}}$ of the energy E, respectively. However, the smallness of spin-orbit forces will allow one further simplification, namely, that we may set

$$\Gamma_{l^*+\frac{1}{2}}=\Gamma_{l^*-\frac{1}{2}}=\Gamma \quad (41)$$

In Eq. (30). Formula (38) may thus be simplified to

$$\frac{dS}{d\omega}=\left\{\left|f(\theta)+\frac{1}{2k}\frac{e^{2i(\eta_{l^*}+\delta_{l^*})}}{(2l^*+1)^{\frac{1}{2}}}\left[(l^*+1)\frac{\Gamma}{E_{l^*+\frac{1}{2}}-E-\frac{1}{2}i\Gamma}+l^*\frac{\Gamma}{E_{l^*-\frac{1}{2}}-E-\frac{1}{2}i\Gamma}\right]Y^0{}_{l^*}\right|^2\right.$$
$$\left.+\frac{1}{4k^2}\frac{l^*(l^*+1)}{2l^*+1}\left|\frac{\Gamma}{E_{l^*+\frac{1}{2}}-E-\frac{1}{2}i\Gamma}-\frac{\Gamma}{E_{l^*-\frac{1}{2}}-E-\frac{1}{2}i\Gamma}\right|^2|Y^1{}_{l^*}|^2\right\} \quad (42)$$

with

$$f(\theta)=\frac{1}{k}\sum_l(2l+1)^{\frac{1}{2}}e^{i(\eta_l+\delta_l)}\sin(\eta_l+\delta_l)Y_l^0(\theta) \quad (43)$$

and using (30) and (41)

$$e^{i(\eta_{l^*}+\delta_{l^*}+\gamma_{l^*\pm\frac{1}{2}})}\sin(\eta_{l^*}+\delta_{l^*}+\gamma_{l^*\pm\frac{1}{2}})-e^{i(\eta_{l^*}+\delta_{l^*})}\sin(\eta_{l^*}+\delta_{l^*})=e^{2i(\eta_{l^*}+\delta_{l^*})}\frac{\Gamma}{E_{l^*\pm\frac{1}{2}}-E-\frac{1}{2}i\Gamma}.$$

Specializing further to $l^*=1$ and using

$$Y_1^0=3^{\frac{1}{2}}\cos\theta, \quad Y_1^1=(3/2)^{\frac{1}{2}}e^{i\varphi}\sin\theta,$$

we obtain

$$\frac{dS}{d\omega}=\left|f(\theta)+\frac{1}{k}e^{2i(\eta_1+\delta_1)}\left(\frac{\Gamma}{E_{3/2}-E-\frac{1}{2}i\Gamma}+\frac{1}{2}\frac{\Gamma}{E_{1/2}-E-\frac{1}{2}i\Gamma}\right)\cos\theta\right|^2$$
$$+\frac{1}{4k^2}\left|\frac{\Gamma}{E_{3/2}-E-\frac{1}{2}i\Gamma}-\frac{\Gamma}{E_{1/2}-E-\frac{1}{2}i\Gamma}\right|^2\sin^2\theta. \quad (44)$$

This formula cannot be simplified any further without special assumptions about the function $f(\theta)$, or, according to (43) about the phases δ_l.

3. Scattering of Protons on Helium

We will here for simplicity assume, that for all values of l we may take $\delta_l=0$ so that all the non-resonant scattering is due to the Coulomb field; there may be course easily be a noticeable nuclear

"potential" scattering, particularly for $l=0$ and which, if necessary, could be taken account by taking in (43) $\delta_0 \neq 0$. Omitting this correction we obtain for $f(\theta)$ the well-known form which leads to the Rutherford scattering:

$$f(\theta) = -\frac{\alpha}{2k \sin^2 \theta/2} e^{i\alpha \log 2(1-\cos\theta)+2i\eta_0}. \tag{45}$$

Using with (19)

$$\eta_1 - \eta_0 = \arg \frac{(1+i\alpha)!}{(i\alpha)!} = \arg (1+i\alpha) = \arctan \alpha,$$

we obtain from (44)

$$\frac{dS}{d\omega} = \lambda^2 \left[\left| \frac{\alpha}{2 \sin^2 \theta/2} - e^{i[2 \arctan \alpha + \alpha \log 2(1-\cos\theta)]} \cos\theta \left(\frac{\Gamma}{E_{3/2}-E-\frac{1}{2}i\Gamma} + \frac{1}{2} \frac{\Gamma}{E_{1/2}-E-\frac{1}{2}i\Gamma} \right) \right|^2 \right.$$
$$\left. + \frac{\sin^2\theta}{4} \left| \frac{\Gamma}{E_{3/2}-E-\frac{1}{2}i\Gamma} - \frac{\Gamma}{E_{1/2}-E-\frac{1}{2}i\Gamma} \right|^2 \right\}. \tag{46}$$

Here we have written $1/k = \lambda$ and α stands according to (18) for $2e^2/\hbar v$, v being the velocity of the incident proton and $2\pi\lambda$ its wave-length in the system in which the center of gravity is at rest. It is evident from (46) that after subtraction of the pure Rutherford term $\alpha^2\lambda^2/4 \sin^4 \theta/2$ there still remains even for appreciable scattering angles θ and for protons of about 3 Mev ($\alpha = 0.18$) a noticeable influence of the Coulomb scattering, due to its interference with the resonance term. Particularly for $\theta < \pi/2$ this fact must be taken into account for any conclusion drawn from the scattering of protons on He^4 upon the existence of a compound P state of Li^5.

4. Scattering of Neutrons on Helium

Since in this case $\alpha = 0$ it follows from (19) that $\eta_l = 0$ for all values of l. Evidently we may not assume here that also all the phases δ_l are zero since otherwise according to (43) $f(\theta) = 0$ which would mean, that the scattering of neutrons on He^4 is caused entirely by resonance. It will, however, for the energies actually used be a good approximation to assume that only $\delta_0 \neq 0$. In this case we obtain from (43), since $Y_0^0(\theta) = 1$

$$f(\theta) = (1/k) e^{i\delta_0} \sin \delta_0 \tag{47}$$

and from (44)

$$\frac{dS}{dw} = \lambda^2 \left\{ \left| \sin \delta_0 + e^{i\delta_0} \left(\frac{\Gamma}{E_{3/2}-E-\frac{1}{2}i\Gamma} + \frac{1}{2} \frac{\Gamma}{E_{1/2}-E-\frac{1}{2}i\Gamma} \right) \cos\theta \right|^2 \right.$$
$$\left. + \frac{\sin^2\theta}{4} \left| \frac{\Gamma}{E_{3/2}-E-\frac{1}{2}i\Gamma} - \frac{\Gamma}{E_{1/2}-E-\frac{1}{2}i\Gamma} \right|^2 \right\}, \tag{48}$$

where we have again written $2\pi\lambda = 2\pi/k$ for the neutron wave-length in the system in which the center of gravity is at rest. The discussion of this formula is given in the preceding paper by H. Staub and H. Tatel.

Production of Mesotrons by Penetrating Non-Ionizing Rays

BRUNO ROSSI* AND VICTOR H. REGENER
Ryerson Physical Laboratory, The University of Chicago, Chicago, Illinois
(Received October 3, 1940)

IN an attempt to obtain information as to the nature of the secondary processes giving origin to the cosmic-ray mesotrons, an experiment has been recently performed at 4300 m above sea level (Mt. Evans, Colorado) with the counter arrangement schematically represented in Fig. 1. The 2 counters F and likewise the 5 counters A were connected in parallel. The counter battery A completely covered and extended beyond the solid angle subtended by counters B, C, D and E. By means of a circuit which will be described by one of us (V. H. R.) on a later occasion, the following events were simultaneously recorded: (1) fourfold coincidences ($BCDE$), (2) fourfold coincidences ($BCDE$) not accompanied by a pulse in any of counters A (anticoincidences ($BCDE$–A)), (3) fivefold coincidences ($BCDEF$), (4) fivefold coincidences ($BCDEF$) not accompanied by a pulse in any of counters A (anticoincidences ($BCDEF$–A)). Ten cm of lead were permanently placed in position S_1 and 5 cm of lead in position S_2, so that only particles penetrating 15 cm of lead could give rise to fourfold coincidences ($BCDE$). Measurements were taken with 5 additional centimeters of lead either in position R_1 or R_2 and with various absorbers in position Σ. The experimental results are summarized in Table I.

The anticoincidences ($BCDE$–A) recorded with 5 cm of lead in R_2 and no lead either in R_1 or in Σ are only 0.4 percent of the fourfold coincidences ($BCDE$). They represent a "zero effect" caused by lack of efficiency of the counter battery A, by chance coincidences, and possibly by scattering and by showers coming from the side, which discharge counters B, C, D and E without striking counters A. The last effect is probably responsible for the few anticoincidences ($BCDEF$–A) recorded in the same condition. By moving the lead from R_2 to R_1, when no absorber is present in Σ, the numbers of anticoincidences ($BCDE$–A) and ($BCDEF$–A) increase considerably. This result can be interpreted as indicating the existence of non-ionizing rays traversing the counter battery A un-

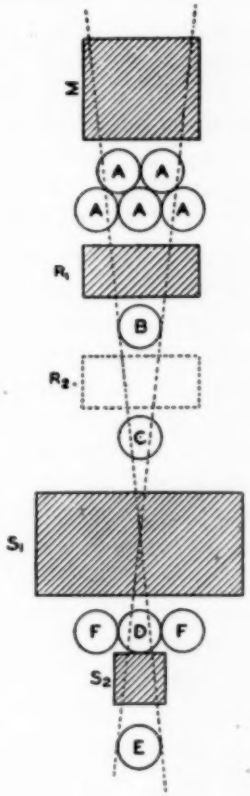

FIG. 1. Arrangement of counters.

* Now at Cornell University.

TABLE I. *Various coincidence and anticoincidence counts.*

EXPERIMENTAL CONDITION	TIME OF EXPER. (HOURS)	*BCDE*	*BCDE–A*	*BCDEF*	*BCDEF–A*
R_1=0, R_2=5 cm Pb, Σ=0	20.00	198±3.1	0.8 ±0.2	7.7±0.6	0.15
R_1=5 cm Pb, R_2=0, Σ=0	120.70	198±1.3	2.83±0.15	10.6±0.3	0.86±0.09
R_1=5 cm Pb, R_2=0, Σ= 2.5 cm Pb	108.38	192±1.4	2.37±0.15	10.1±0.3	0.75±0.08
R_1=5 cm Pb, R_2=0, Σ=10 cm Pb	127.06	176±1.2	1.75±0.12	8.8±0.3	0.68±0.07
R_1=5 cm Pb, R_2=0, Σ=20 cm Pb	24.00	162±2.7	1.75±0.27	8.5±0.6	0.71±0.17

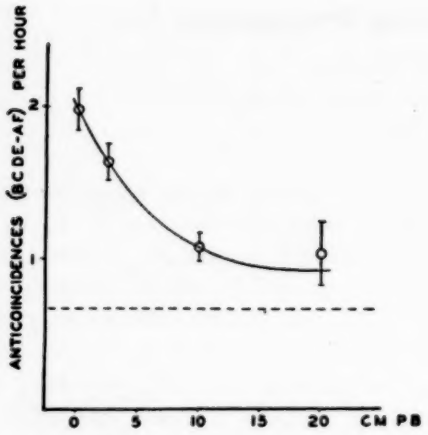

FIG. 2. Anticoincidence counts as a function of thickness of lead absorber.

detected and producing in R_1 ionizing penetrating particles (mesotrons), which discharge the counters underneath. A proof of the above interpretation is found in the fact that an absorber of sufficient thickness placed above counters A (position Σ) strongly reduces the number of anticoincidences ($BCDE$–A) recorded with lead in R_1. This is what one would expect if most of these anticoincidences are due to non-ionizing rays producing mesotrons in R_1. Indeed, a non-ionizing ray traversing Σ has a certain probability of generating a secondary ionizing particle which discharges A. In this case, no anticoincidence can be produced even if the non-ionizing ray survives the encounter. On the contrary, anticoincidences due to spurious phenomena like scattering, showers from the side, etc., should be equally frequent with and without the absorber Σ. The production of mesotrons by non-ionizing rays seems, thus, to be definitely established in agreement with results obtained by Schein and Wilson and by Schein, Jesse and Wollan in the high atmosphere.[1]

Valuable information on the nature of the mesotron producing rays is provided by the experimental data on the rate of decrease of anticoincidences with increasing thickness of the absorber Σ. In order to avoid anticoincidences due to side showers from being recorded, we shall consider only the coincidences ($BCDE$) unaccompanied by pulses either in counters A or in counters F (anticoincidences ($BCDE$–AF)). Side showers are unlikely to discharge counter D without hitting counters F.[2] The counting rate ($BCDE$–AF), which is equal to the difference between the counting rates ($BCDE$–A) and ($BCDEF$–A), is plotted against absorber thickness in Fig. 2. The dotted line represents the zero effect observed with $R_1=0$ and $R_2=5$ cm Pb. It appears that the non-ionizing mesotron producing rays have a large probability of traversing several centimeters of lead without generating secondary ionizing particles. In fact, about 10 cm of lead in Σ are needed to cut off most of the anticoincidences. This behavior is very different from that of photons, most of which materialize into electron pairs already in 1 cm of lead, as recently shown by Jánossy and Rossi.[3] We conclude that the non-ionizing rays which produce mesotrons are more penetrating than photons. They could be "neutrettos" (neutral mesotrons) or high energy neutrons. The last assumption would be in agreement with Johnson's arguments indicating protons as the primary origin of mesotrons.[4] Indeed, mesotron production by heavy particles could be accompanied by transitions from protonic to neutronic states and vice versa, so that the observed neutrons could arise from the transformation of primary protons.

The authors acknowledge with thanks the encouragement given to this research by Professor A. H. Compton.

[1] M. Schein and V. C. Wilson, Phys. Rev. **54**, 304 (1939); M. Schein, W. P. Jesse and E. O. Wollan, *ibid.* **57**, 847 (1940). Other observations of the same kind had been previously reported: see B. Rossi, Zeits. f. Physik **68**, 64 (1931); D. S. Hsiung, Phys. Rev. **46**, 653 (1934); H. Maass, Ann. d. Physik **27**, 507 (1936). However, it has been shown recently by Rossi, Jánossy, Rochester and Bound (this issue, p. 761) that the observed effects were caused by spurious phenomena rather than by mesotron production. This only partially applies to the results of F. R. Shonka [Phys. Rev. **55**, 24 (1939)].

[2] It is still uncertain, however, how many of the anticoincidences ($BCDEF$–A), which we disregard, are caused by side showers rather than by multiple production of mesotrons.

[3] L. Jánossy and B. Rossi, Proc. Roy. Soc. **175**, 88 (1940). The experimental method used is very similar to that described in the present note.

[4] T. H. Johnson, Rev. Mod. Phys. **11**, 208 (1939).

Velocity-Range Relation for Fission Fragments

N. BOHR, J. K. BØGGILD, K. J. BROSTRØM AND T. LAURITSEN
Institute for Theoretical Physics, University of Copenhagen, Copenhagen, Denmark
(Received September 3, 1940)

IN two recent notes[1,2] a number of features of the penetration of uranium fission fragments through matter as revealed by cloud-chamber photographs were discussed. In particular, it was pointed out that we have here to do with a velocity-range relation of a novel character which depends on the interplay between electron capture by the fragments over their entire range, and the ultimate stopping by nuclear collisions. It was also shown in this connection that the rapid fall of the total charge of the fragments with decreasing velocity implies that even a considerable difference in mass and charge of the nuclear fragments will have a relatively small effect on the total range of fragments emitted with the same momentum. Because of this fact, the preliminary study of the cloud-chamber tracks did not immediately indicate the presence of the two main groups of fragments which are shown so clearly in the chemical analysis of the fission products as well as in measurements of the total ionization produced by individual fragments.[3] A closer analysis of a large new body of material, however, gives definite evidence of the presence of two groups of tracks and yields at the same time some further information regarding the range-velocity relation.

This evidence is obtained partly from the measurement of the total ranges of a small number of selected tracks from thin uranium layers, and partly from the counting of branches at various parts of the range of a large number of tracks originating in thick uranium targets. The range measurements of twelve tracks, of which eight were members of pairs ejected in opposite directions and four were single tracks, yield two broad groups with 22- and 29-cm range in normal air. Because of the rather large straggling within each group, it is difficult, however, to draw quite certain conclusions on the basis of so few measurements. It is therefore fortunate that it is possible to obtain from a statistical analysis of the number of branches which are such a conspicuous feature of the tracks, still stronger evidence for the grouping. Because of the entirely fortuitous distribution of the branches, it is, of course, not possible to make any such separation on the basis of the branching of individual tracks, but, from the way in which the number of branches in a given portion of the range are distributed for a large number of tracks the grouping is quite evident.

If the probability for branching were the same for all tracks at a given distance from the end of the range, the number of branches with lengths within given limits in a certain portion of the track should be distributed according to the well-known law[4]

$$P(n)=\omega^n e^{-\omega}/n!,$$

where ω is the mean value of the number of branches in the interval considered and $P(n)$ is the expectation of the occurrence of just (n) branches in this interval. Actual measurements on several hundred tracks in argon gas gives the result that in the region of the track from 0.3 to 1.15 cm (normal air) from the end of the range, the mean value of the number of branches is about 2.2 and the proportion of tracks which have 0, 1, 2 and 3 branches are, respectively, 0.17, 0.25, 0.20 and 0.15, while the formula gives 0.11, 0.24, 0.27 and 0.20. From these figures, it is quite clear that the probability of branching for the different tracks is not the same. An almost perfect fit to the experimental values is obtained, however, if we assume that the tracks fall into two groups differing in their mean numbers of branches by a factor of three. A similar analysis of the branch distribution in the last 0.3 cm from the end of the range, gives a much closer fit with the formula holding for a single group, indicating that here the ratio between the mean values for the two groups of tracks is not far from one.

[1] K. J. Broström, J. K. Bøggild and T. Lauritsen, Phys. Rev. **58**, 651 (1940).
[2] N. Bohr, Phys. Rev. **58**, 654 (1940).
[3] Cf. L. Turner, Rev. Mod. Phys. **12**, 22 (1940).
[4] Cf. e.g. N. Bohr, Phil. Mag. **30**, 581 (1915).

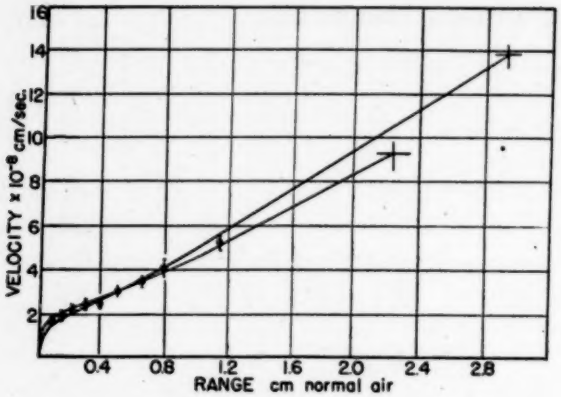

FIG. 1. Range-velocity relation for fission fragments.

Since the probability for energy transfer in nuclear collisions depends, apart from the velocity, simply on the charges and masses of the nuclei involved, the statistical analysis of the branch distribution along the tracks offers a direct means of obtaining the average range-velocity relation for the fission fragments, provided the range-energy relation of the particles giving rise to the branches is known. Because of the large uncertainty of these relations for the low energies involved, and the difficulty of the identification of the branches in the photographs, the velocity determinations so obtained are not reliable in absolute measure, but their relative values give useful information about the general course of the range-velocity relation and they give a strong support for the conclusions previously drawn from direct measurements by individual large branches.[1]

The evidence regarding the range-velocity relation for the fission fragments derived from the material discussed is embodied in Fig. 1. The two curves correspond to the two main groups having different ranges and different initial velocities. These velocities are calculated assuming a mass ratio of 2 : 3 for the two nuclear fragments ejected with a total kinetic energy of 160 Mev.[5] The attribution of the shorter range to the heavier particle follows directly from the general character of the curves for the higher velocities, where the course is nearly linear and the slopes should not differ greatly for the two groups of fragments. The shape of the curves for the lower velocities is determined from the branch counts. The points indicated in the figure give on a suitable scale the mean velocities in this region, derived from the number of branches within given limits of length in various intervals of the range.

Since the steep descent at the end of the range must be ascribed to the effect of numerous nuclear collisions,[2] the velocity of the heavy fragment should be the higher in this region, as is also indicated from the study of the branch distribution. In fact, the probability of branching due to nuclear collision is proportional to (Z^2/V^2), where Z is the charge number and V is the velocity; the close equality of the average number of branches for the two groups in this region therefore implies that the effect of the charge difference is partially neutralized by the difference in velocity. On the other hand, the large difference for the groups in the average number of branches at greater distances from the end of the range is a clear indication that here the velocity of the lighter fragment is the greater. In this region, the rate of decrease of momentum is approximately the same for the two types of fragments as would be expected from the general theoretical arguments. Still, this rate appears to be somewhat larger for the heavier particle, pointing to a slightly higher net charge for the same velocity, as is also consistent with the looser binding of the outer electrons in an atom of greater atomic number.

The various points discussed in this note will be more closely considered in the two forthcoming papers in the *Communications of the Copenhagen Academy* to which reference has already been made in our earlier articles.

[5] Because of an arithmetical error in the estimate of the average initial velocities of the fragments, the curve of Fig. 3 in the earlier note was drawn too high. This correction does not, however, alter the conclusions regarding the general character of the curve.

LETTERS TO THE EDITOR

Prompt publication of brief reports of important discoveries in physics may be secured by addressing them to this department. Closing dates for this department are, for the first issue of the month, the eighteenth of the preceding month, for the second issue, the third of the month. Because of the late closing dates for the section no proof can be shown to authors. The Board of Editors does not hold itself responsible for the opinions expressed by the correspondents.

Communications should not in general exceed 600 words in length.

Acceleration of Electrons by Magnetic Induction

For some time it has been realized that it might be possible to make use of the electromotive force induced by a changing magnetic flux to accelerate charged particles traveling in an orbit around the changing flux. Although previous attempts to accelerate electrons by this means have been unsuccessful,[1,2] careful examination showed that it should be possible to get good magnetic focusing by the proper arrangement of a magnetic field to guide the electrons around the changing flux and that if the rate of change of flux within the orbit were sufficiently high it would be possible to capture electrons in usable orbits and that vacuum requirements should not be difficult to satisfy.

It seemed feasible to attempt the experiment with a 600-cycle per second magnetic field, since a sufficiently high rate of change of flux would be obtained and since it seemed that it would not be necessary to have a vacuum better than 10^{-6} millimeter of mercury in the acceleration chamber, in spite of the fact that at this frequency the length of the electron path would be of the order of 10^7 centimeters.

To hold the electrons in the acceleration chamber for such a long path it is necessary to fulfill the condition that $\phi=2\pi R_0^2 H$, where ϕ is the flux enclosed by the orbit and H is the magnetic field at the orbit which causes the electrons to travel in a circle of radius R_0. When this condition is satisfied, the electron orbit neither shrinks nor expands, and the electrons can be accelerated by increasing ϕ and H together.

A laminated electromagnet with pole faces 8 inches in diameter, which satisfied all the necessary conditions, was constructed. The stable orbit was shrunk from R_0 toward the position of a tungsten target by causing saturation of the portion of the magnetic circuit which supplied the flux through the center of the orbit. X-rays produced by the impact of the electrons upon the target showed that the accelerator operated, and a lead collimator in front of a Geiger-Müller counter showed that the only portion of the acceleration chamber from which x-rays came was the target.

By taking the sweep voltage for an oscillograph from a coil surrounding the core of the magnet and putting the pulses from the Geiger-Müller counter circuit on the vertical deflection plates, the phase of the magnetic field at which the electrons struck the target could be determined. It was possible to hold the electrons in the acceleration chamber for one-fourth of a cycle during which the magnetic field changed from a low value to its maximum. Conservative estimates of the magnetic field at the target when the electrons strike it indicated that the energy of the electrons was about 2.2 Mev. This estimate was substantiated by a comparison of the absorption of the x-rays in lead with published data on the absorption of x-rays produced by 2-million-volt electrons.[3] After filtering the x-rays from the accelerator through about 1.8 cm of lead, their absorption coefficient is 0.57 cm^{-1}. A correction had to be made for scattering of x-rays from the magnet yoke. Since the absorption coefficient for x-rays produced by 2.0-Mev electrons is 0.62 cm^{-1}, the electrons in the new accelerator must have reached about 2.35-Mev energy before striking the target. The absorption measurements were taken with Lauritsen electroscopes, and calibration of the electroscopes showed that the intensity of the radiation was greater than the intensity of the gamma-rays from 10 millicuries of radium.

Of several suggestions which have been made for naming the apparatus, induction accelerator seems to be the shortest descriptive one.

It has been a great help to be able to discuss the theoretical aspects of the accelerator with Professor R. Serber and Professor H. M. Mott-Smith.

D. W. KERST

University of Illinois,
Urbana, Illinois,
October 15, 1940.

[1] Wideröe, Archiv f. Elektrotechnik **21**, 400 (1938).
[2] E. T. S. Walton, Proc. Camb. Phil. Soc. **25**, 469 (1929).
[3] D. L. Northrup and L. C. Van Atta, Am. J. Roentgenology and Radium Therapy **41**, 633 (1939).

Effect of an Eclipse on Cosmic Rays

A cable message received from Professor G. Wataghin of the University of Sao Paulo states that Messrs. Monteux, Occhialini and Santos have established the existence of an effect of an eclipse on cosmic rays. He adds that observation of the penetrating rays made by Santos and himself underground showed that their behavior was different from that of the total radiation.

We shall await with interest further details with regard to the nature and magnitude of this observed effect, which has heretofore been sought without success.

ARTHUR H. COMPTON

Ryerson Physical Laboratory,
University of Chicago,
Chicago, Illinois,
October 4, 1940.

Fresnel Diffraction of Electrons as a Contour Phenomenon in Electron Supermicroscope Images

Early in 1939 a qualitative investigation into the effect on electron microscope images of chromatic aberration predicted and demonstrated the existence of a characteristic contour at the image of the line of separation of two areas of the specimen, having widely different atomic mass thicknesses.[1] A little later Borries and Ruska[2] described similar contours which they explained as having been caused by variations in the spherical aberration of the objective for different regions of the specimen. It is now known that both effects are present in electron microscope images, their relative importance depending on the magnitude of the angular aperture of the illuminator, the physical angular aperture of the objective, and on the nature of the specimen. R. Rebsch[3] has established theoretically that the contours caused by spherical aberration do not diminish the resolving power of the microscope as deduced from its ability to separate the images of closely adjoining edges or particles.

During the past three months extensive tests have been carried out on the resolving power of the most recent RCA electron microscope, designed by the author under the supervision of Dr. V. K. Zworykin and in collaboration with A. W. Vance and J. M. Morgan. While a complete description of this instrument will be published shortly, it is pertinent to mention here that the stability of the electrical supplies and the freedom of the electron-optical system from extraneous electrical and mechanical effects is such that it is possible to make exposures of as long as 30 minutes with image disturbances of less than 10A. Precise focusing obtained photographically and the use of illumination of angular aperture less than 10^{-5} radian has been made possible by this development.

Photographs taken under these conditions have shown a new type of contour which, in appearance, is similar to the diffraction effects observed in the light microscope. Figure 1 shows such a contour as it appeared at the edge of the image of a thin filament of synthetic rubber suspended across the specimen holder opening. The over-all linear magnification was 500,000 times. As the physical aperture of the objective used was 6×10^{-3} radian, the possibility of the observed maxima and minima being due to an aperture diffraction defect is precluded by the magnitude of the separation of the fringes. A more probable explanation is that the phenomenon is a case of Fresnel diffraction by a straight edge where the fringes have been made visible and spread out in the image by the action of the spherical aberration of the objective.

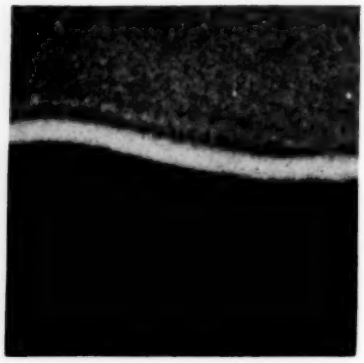

FIG. 1. Electron microscope image of the edge of a thin filament showing multiple fringes in the contour. Electronic magnification 15,000, enlarged to 500,000.

FIG. 2. Electron microscope image of thin film of synthetic rubber showing the fineness of detail. Electronic magnification 15,000, enlarged to 500,000.

By passage through a lens with large spherical aberration, successive wave fronts, which originate in the diffraction (coherent scattering) at the edge of the specimen, are distorted so that at the image plane in the position of best focus they cover an appreciable area on either side of the geometrical position of the image of the edge. Moreover, owing to the strong spherical aberration, the curvature of such wave fronts is not very different from that of the wave fronts which traverse unhindered the clear space adjacent to the specimen, and which, after passing through the approximate focus of the lens, form the image of the clear space next to the image of the specimen. Thus it is possible for interferences between these two sets of wave fronts to occur in the image plane. Owing to the fact that the two sets of wave fronts are almost parallel near the image of the geometrical edge of the specimen, and have nearly equal curvatures, the fringes are spread over relatively large distances. It is now suggested that such fringes may be used as a criterion for testing the magnitude of the spherical aberration of electron microscope objectives.

Figure 2, which is another section of the same negative enlarged to the same magnification, illustrates the absence of noticeable contours where the differences in scattering power of the particles observed are slight. The *separating* power of the electron microscope with its present adjustment is estimated to lie in the range 20–30A.

JAMES HILLIER

Research Laboratories,
RCA Manufacturing Company,
Camden, New Jersey,
October 7, 1940.

[1] J. Hillier, Can. J. Research **A17**, 64–69 (1939).
[2] B. v. Borries and E. Ruska, Naturwiss. **27**, 281–292 (1939).
[3] R. Rebsch, Ann. d. Physik **31**, 551–560 (1938).

A Long-Lived Isotope of Yttrium

In samples of strontium bombarded with 16-million-volt deuterons from the Berkeley 60-inch cyclotron in order to produce radioactive strontium for biological investigations, we separated a long-lived (about 100 days) radioactive yttrium having interesting properties. This isotope has been independently observed by L. A. DuBridge and J. Marshall[1] from strontium bombardment with protons. If their assignment is correct it would be Y^{86} produced by a $1d-2n$ reaction from Sr^{86}. It emits a penetrating gamma-radiation and practically no beta-radiation harder than 300 kev. No experiment capable of detecting softer beta-rays has yet been done. The absorption curve in Cu, Pb and Fe of yttrium and radium gamma-rays, filtered through 2 cm of lead, are almost identical. E. Segrè and the writer have observed that the yttrium gamma-radiation is capable of producing photo-neutrons in beryllium. The photo-neutrons, slowed in paraffin, were detected by the radioactivity induced in rhodium.

The yield is about 12 milligrams radium equivalent for 1000 microampere hours of 16-million-volt deuterons (about 10 hours of the Berkeley 60-inch cyclotron) when strontium oxide is bombarded, as compared with 6 millicuries of Sr^{89}. Since radioactive strontium has been produced in large quantities for therapeutic purposes, an appreciable amount of long-lived yttrium has been made available (about 25 milligrams radium equivalent). Figure 1 shows that this isotope should be suitable for industrial radiography. The upper picture shows an iron clamp partially covered with a piece of iron, two inches thick. The gamma-radiation is sufficiently penetrating so that the clamp appears clearly in both cases, whether it is or is not covered with the iron plate. The lower picture shows an electric motor. Because of its long life and its penetrating gamma-radiation, this radioactive yttrium is, among the artificial radioactive elements known at the present time, the most likely to be substituted for radium, but it must be considered at the present time merely as a by-product of the radio-strontium preparation as it is, as yet, appreciably more expensive than radium for a like dose of gamma-radiation.

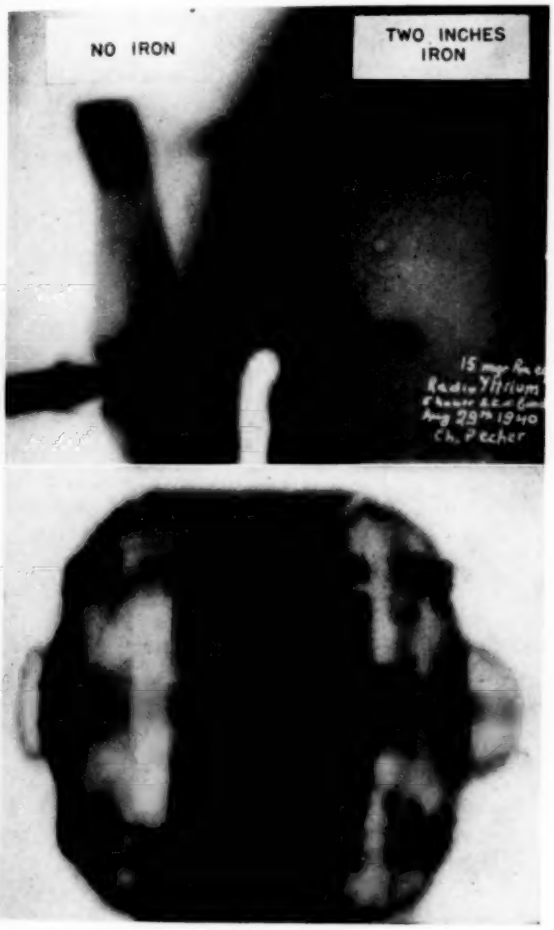

FIG. 1. Gamma-ray radiographs with radioactive yttrium.

CHARLES PECHER*
William H. Crocker Radiation Laboratory,
University of California,
Berkeley, California,
October 14, 1940.

[1] L. A. DuBridge and J. Marshall, Phys. Rev. **58**, 7 (1940).
* Fellow of the Belgian-American Education Foundation.

The Ratio of e, c, and h

The problem of expressing e in terms of c and h splits up in two separate questions. First, if the electronic particle is characterized by its rest energy mc^2 and by a basic time a/c (a="radius") then how large is the product $mc\cdot a\cdot\hbar^{-1}=\mu$? The answer of quantum theory[1] is that μ is the smallest root of the equation $2\pi\mu[y_0(\mu)]^2=1$, namely $\mu=0.02985037$. Second, how large is a, or if we write $a=\gamma e^2/mc^2$, how large is γ? With μ and γ known, Sommerfeld's constant α would be $\alpha=e^2/c\hbar=\mu/\gamma$. The value of γ can be obtained from the consideration that mc^2 and a/c shall be measurable by one and the same fundamental process characterizing the particle. Since mc^2 is the creation energy, a/c must be related to the time duration of a creation process, which in its turn depends on the magnitude of the scattering cross section of the particle for light. Therefore we tentatively identify $a^2\pi$ with the universal scattering cross section $\phi=8\pi e^4/3m^2c^4$ of Thomson which yields $\gamma=(8/3)^{\frac{1}{2}}$. This value is too small, however. The creation cross section must be larger. Now, if we identify $a^2\pi$ with $2\pi\phi$ rather than ϕ, that is, if we put $\gamma=(2\pi 8/3)^{\frac{1}{2}}$ then we obtain for α^{-1} the value $137.1273\cdots$ in perfect agreement with the best experimental evidence.[2] This result cannot be accidental since the value of μ was obtained *a priori*, and physical considerations tell us that $a^2\pi$ must be closely related to Thomson's ϕ. Only the factor 2π is introduced *a posteriori*. We therefore think that our α-formula is the correct one, but the physical origin of the factor 2π is not yet clear. A simple *classical* theory of the creation is needed similar to Thomson's *classical* theory of the scattering.

ALFRED LANDÉ
Ohio State University,
Columbus, Ohio,
October 16, 1940.

[1] A. Landé, J. Frank. Inst. **229**, 768 (1940).
[2] F. G. Dunnington, Rev. Mod. Phys. **11**, 65 (1939); R. T. Birge, Phys. Rev. **58**, 658 (1940).

The Absorption of Cosmic Rays in Lead at a Depth of 1000 m Water Equivalent

In a previous experiment[1] the absorption of cosmic rays was measured in the coal mines of Dorog at a depth of 957 m water equivalent. For these measurements we used a threefold coincidence telescope. The thickness of the interposed lead layer was at first gradually increased between the central and bottom tube, and only after this thickness had attained 50 cm was the additional lead placed between the upper and central tube also. When similar absorption measurements are made at sea level, as is well known, the intensity sinks rapidly as far as 15 cm Pb and then decreases slowly. In contrast to this at 957 m water equivalent depth we have found[2] that although in the beginning the intensity decreases rapidly as far as 10 cm Pb, this decrease is then succeeded for a greater thickness of lead by an increase of the intensity, which may reach 90 percent of the initial intensity. A second decrease was observable only when the additional lead was placed between the two upper tubes. For the interpretation of this new type of absorption we must assume—as already pointed out in our first paper—that at such great depth only non-ionizing radiation is able to penetrate, which reveals itself by producing ionizing secondary rays along its path. To be able to account for the minimum of the intensity at 10 cm Pb we must assume that the range of the particles emerging from clay or brick layer above the apparatus is shorter, about 10 cm Pb, than the range of the particles produced in the lead, which may be estimated to 25 cm Pb.

Since September 1939, during a period covering 7000 hours, we have been performing similar absorption measurements at a different place in the same mine, at a depth of 941 m water equivalent. The only difference between the apparatus employed at present and that used in the investigations of 1938 is, that at present we place the same amount of lead between the upper and central tube as between the central and bottom tube in every position, and that in 1938 we had 2.5 cm Pb above the upper tube instead of which we now use 70 cm of wood. The results are represented in Fig. 1. We may remark that here the decrease of intensity up to 10 cm Pb followed by an increase of intensity is again observable. We should like to point out that this second measurement performed at a different place in the mine and more than a year later than the first investigation establishes sufficient evidence for the existence of the minimum at 10 cm Pb. But in Fig. 1 we see a second very sharp decrease with subsequent increase of the intensity between 37 and 47 cm Pb. In order to secure equally well-established evidence for this second minimum, we have several times measured the intensity of the radiation in the minimum and in its neighborhood. In Fig. 2 these results are reproduced. We may remark that the three different curves agree well with each other; the sharp fall of the intensity is found in every case at 42 cm Pb. At every thickness of lead where measurements were several times repeated the values of the intensity found on different occasions lay between the limits of their probable error, even at 42 cm Pb when more than 8 months had elapsed between the first and the last determination.

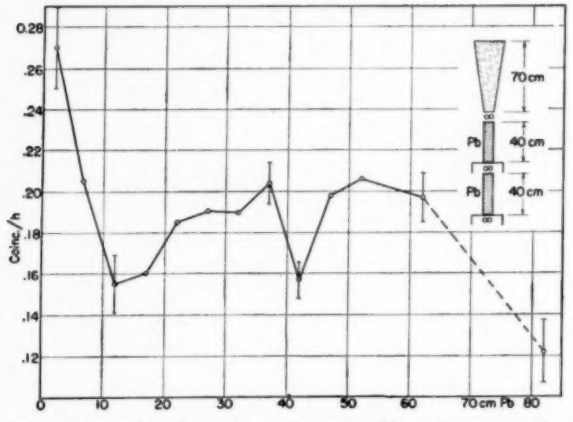

FIG. 1. Absorption of cosmic rays in lead at 941 m water equivalent depth with 70 cm of wood above the apparatus. The vertical lines represent the probable errors of the measurements.

We may also be able to explain this absorption in a qualitative manner with the same assumption made in connection with the curve found in 1938, namely, that at such great depth only a non-ionizing radiation is present,

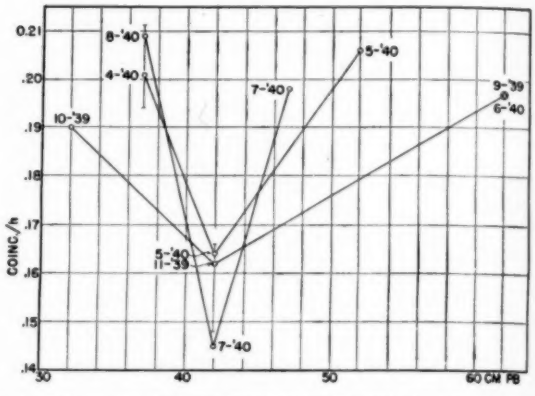

FIG. 2. Minimum of the intensity at 42 cm Pb with the dates when the measurements were performed.

which produces ionizing secondaries with 10 cm Pb range in the clay or brick layer and ionizing secondaries with 25 cm Pb range in lead. With these assumptions we can expect from numerical calculations two intensity maxima, one at 25 cm Pb and a somewhat higher one at 50 cm Pb, with a flat minimum between the two. In order to account for the sharp fall of the intensity at 42 cm Pb we must further assume that in wood another kind of more penetrating particles with well-defined ranges of 40 cm Pb is created. This would also enable us to explain the intensity decrease found at 82 cm Pb. Since the number of the H nuclei is rather abundant in wood it does not seem too far-reaching to postulate that these rays with 40 cm Pb range are perhaps protons, whereas the rays created in clay or lead might rather be of mesotronic nature.

In conclusion the writers wish to express their thanks to Councilor Dr. S. Schmidt and to Manager K. Roth of the Salgótarjáni Coal Mine Company for permitting us to execute experiments in the mines of Dorog, as well as to the engineers of the Company for their kind help. The

experiments were performed with the financial support of the Széchenyi Scientific Society, the Hungarian Council for Natural Science and the Hungarian Academy of Science.

J. BARNÓTHY
M. FORRÓ

Institute for Experimental Physics,
University,
Budapest,
September 27, 1940.

[1] J. Barnóthy and M. Forró, Phys. Rev. **55**, 870 (1939).
[2] See Fig. 2 of the cited article.

The Second Law of Thermodynamics and Irreversible Processes

The two papers by Eckart in the *Physical Review* for August first permit a simple interpretation which amounts to an extension of the second law.

The conventional statement of the second law, when applied to irreversible processes, is that the entropy of an isolated system increases whenever an irreversible process occurs within it. No attempt is made to evaluate how much the increase of entropy may be under such circumstances, and in fact the precise evaluation of irreversible increases of entropy has always been considered to be beyond the power of methods thermodynamic in spirit, and to be rather the proper subject of statistical mechanics or kinetic theory. This accepted impotence of thermodynamics has always struck me as a surprising thing. It would seem that thermodynamics ought to be able to handle any system that is causally determined from the macroscopic point of view, that is, any system which can be adequately described in terms of operations with macroscopic instruments. This means that whenever the readings of the macroscopic instruments are repeated the future behavior of the system as measured with those same instruments repeats. The readings of the macroscopic instruments should then become the parameters for a complete treatment, thermodynamic in an extended even if not in the classical sense. Of course there are many processes which are so complicated that they cannot be adequately described in terms of a number of macroscopic variables small enough to be manageable, as in the efflux of a jet of gas from a nozzle, and it is not to be expected that systems in which apparent irreversibility thus arises from intractable complication will be completely amenable to any treatment. But there are many systems in which irreversible processes occur which are completely describable in terms of a few macroscopic parameters, and such systems should be amenable to an exact treatment, including an exact evaluation of the increase of entropy. Examples of such completely describable irreversible processes are: conduction of heat down a temperature gradient, development of Joulean heat when an electrical current flows against resistance; development of frictional heat when one solid rubs on another or in the interior of a viscous liquid; and when there is diffusion down a concentration gradient.

Sometime ago I proposed that a plausible extension of the second law to such completely defined irreversible processes was to postulate that whenever such a process occurs a corresponding characteristic increase of entropy occurs. Thus when an electric current i flows against a resistance r at absolute temperature θ there is an increase of entropy per unit time of i^2r/θ, and when the amount of heat Q drops by conduction through a temperature range $\Delta\theta$ there is a similar increase of entropy of $Q\Delta\theta/\theta^2$. I applied the equations to thermoelectric phenomena, and showed how the equations of Kelvin could be derived without illegitimately neglecting the irreversible aspects of the phenomena, as had been necessary in all previous treatments. In my book, *The Thermodynamics of Electrical Phenomena in Metals*, several other applications were given, particularly to deducing a relation between the Nernst and the Ettingshausen coefficients. I have also discussed the matter in a forthcoming book on the foundations of thermodynamics.

It is the purpose of this note to point out that Professor Eckart's equations can be written exactly in accord with this postulate of the extended second law. In general one must have: (increase of entropy in the region within a closed surface) plus (entropy which has flowed out of the region across the surface) equals (entropy generated by irreversible processes within the surface). The last term (entropy generated by irreversible processes within the surface) should be capable of precise formulation when the irreversible processes are well defined. Such is the fact in the cases considered by Professor Eckart. In his first paper the irreversible processes are thermal conduction and viscous motion of a fluid. His Eq. (15) on page 269 is:

$$(d/dt)\int\int\int_S m\eta d\tau+\int\int_S (1/\theta)\mathbf{q}\cdot d\sigma = \int\int\int_S \{[k(\nabla\theta)^2]/\theta^2+[(\mathfrak{p}\cdot\nabla)\cdot\mathbf{V}]/\theta\}d\tau.$$

In this equation the first term on the left is recognizably the increase in unit time of the entropy of the material within the surface S, the second term is the outward flow of entropy across the surface, the first term in the integrand on the right is the rate of increase of entropy due to irreversible thermal conduction within the region and the second is the increase of entropy due to frictional generation of heat in the viscously moving liquid. The latter is obviously the general expression for the characteristic rate of entropy increase in a moving liquid, and the first is the same as the expression I had already used, $Q\Delta\theta/\theta^2$. In Professor Eckart's second paper, Eq. (26) on page 272 contains the additional terms for the characteristic increase of entropy when there is diffusion in general. Professor Eckart has pointed out to me in correspondence that the expression for the increase of entropy due to diffusion is not separable into the sum of a term due to diffusion down a concentration gradient and another due to diffusion down a temperature gradient, but the two diffusion effects are cross connected. This suggests the necessity for detailed working out of the entropy increases, which is what Professor Eckart has essentially done, and by methods entirely macroscopic. That it can be done, constitutes the justification for the proposed extended formulation of the second law.

P. W. BRIDGMAN

Research Laboratory of Physics,
Harvard University,
Cambridge, Massachusetts,
October 3, 1940.

Short-Lived Radioactivities of $_{14}Si^{27}$, $_{16}S^{31}$, and $_{18}A^{35}$

In an attempt to extend the well-known series of radioactive elements characterized by the formula $Z-N=1$, the following new reactions have been observed:

Reaction	Half-life
$_{12}Mg^{24}(\alpha, n)_{14}Si^{27}$	4.92 sec.
$_{14}Si^{28}(\alpha, n)_{16}S^{31}$	3.18 sec.[1]
$_{16}S^{32}(\alpha, n)_{18}A^{35}$	1.91 sec.

These reactions were produced by 16-Mev alpha-particles. Because of the short lifetimes the bombardments were performed outside of the cyclotron thus reducing the bombarding energy by a 0.6-mil aluminum window. The bombardment time varied from one to three seconds in an alpha-beam of about 0.05 microampere.

Since these periods are too short to identify chemically one must rely for their correct assignment on: (1) the fact that from simple theoretical considerations[2] it is expected that Si^{27}, S^{31} and A^{35} should be short-lived positron emitters; (2) the relative abundance of the stable isotopes of the elements bombarded; and (3) the elimination of possible radioactive isotopes by their known half-lives.

Si^{27} when produced by alpha-bombardment had previously been incorrectly assigned a half-life of 6.7 minutes; this was shown to be incorrect by Bethe and Henderson.[3] The Rochester groups[4] and more recently the Princeton group[5] have obtained this radioactive isotope by using high energy protons on aluminum. The half-life obtained by the latter group agrees well with that obtained by us.

The half-lives given above have been measured by means of a multiple scale Geiger counter circuit. The dial readings of the mechanical counter are photographically recorded at regular time intervals of $\frac{1}{2}$ or 1 second. Every point used in the determination of the half-lives had at least 50,000 counts and data were taken for a sufficiently long time so that any longer periods as well as the background could be subtracted out. The activities showed an exponential decay over at least three lifetimes.

Energy measurements of the positrons emitted are in progress.

L. D. P. KING
D. R. ELLIOTT

Purdue University,
West Lafayette, Indiana,
October 10, 1940.

[1] Dr. Van Voorhis has informed us that the Rochester group using protons on phosphorus has obtained S^{31} with a half-life similar to that obtained by us.
[2] E. Wigner, Phys. Rev. **56**, 512 (1939).
[3] H. A. Bethe and W. J. Henderson, Phys. Rev. **56**, 1060 (1939).
[4] G. Kuerti and S. N. Van Voorhis, Phys. Rev. **56**, 614 (1939).
[5] Barkas, Creutz, Delsasso, Sutton and White, Phys. Rev. **58**, 38 (1940).